DETECTION OF DYSAUTONOMIA IN SPINAL CORD INJURY THROUGH NON-INVASIVE MULTI-MODAL SENSING AND MACHINE LEARNING

by

Shruthi Suresh

A Dissertation

Submitted to the Faculty of Purdue University

In Partial Fulfillment of the Requirements for the degree of

Doctor of Philosophy

Weldon School of Biomedical Engineering

West Lafayette, Indiana

December 2020

THE PURDUE UNIVERSITY GRADUATE SCHOOL
STATEMENT OF COMMITTEE APPROVAL

Dr. Bradley S. Duerstock, Chair
Weldon School of Biomedical Engineering
School of Industrial Engineering

Dr. Riyi Shi
Weldon School of Biomedical Engineering
Department of of Basic Medical Sciences

Dr. Andrew O. Brightman
Weldon School of Biomedical Engineering

Dr. Guang Lin
Department of Mathematics

Dr. Thomas H. Everett IV
Krannert Department of Cardiology
IU School of Medicine

Approved by:
Dr. George Wodicka

ACKNOWLEDGMENTS

Thank you Dr. Duerstock for your faith in this research. Thank you to my committee members Dr. Riyi Shi, Dr. Andrew O. Brightman, Dr. Thomas H. Everette and Dr. Guang Lin for their guidance. Thank you, Ana De La Torre, Dr. Ting Zhang, Mandira Marambe, Aditya Shanghavi for having my back in the IAS lab. I would like to thank the members of CPR-Jennifer Crodian, Dr. Siyuan Sun, Sunny Zhang, Seth Herr, Edmond Rogers, Dr. Jianming Li, Bhavani Gopalakrishnan, Michael Walls and Megan Saenger. Thank you to Dr. Elwood Walls and Dr. Edward Bartlett for their feedback and inputs during sensor development.

Thank you, Dr. Peng-Sheng Chen and Johnson Wong, for your guidance in helping me understand how to analyze and interpret the skin nerve activity signals. Special thanks to Dr. Amanda Darbyshire, Sarah Raymer and Carol Dowell for all the guidance and training that I required to ensure the rats survived. Thank you to all the rats that are in Rat Heaven right now for their contribution to this work. Thank you, David Newton and Chang Cheng, for all the help with data processing and feature selection.

Thank you to my undergraduate helpers Zada Anderson and Misael Rodriguez for their assistance with data collection from the rats and assisting me with acclimating the rats and caring for them post-injury! Thank you to my amazing friends Dr. Jackie Cha, Glebys Gonsalez, Dr. Ketharini S. Kumar, Kavya Cherukuri and Pravallika Kollipara.

Thank you to my husband Shanmugam MPl, my brother Ashwin Suresh, my amazing parents Suresh Vembu and Saraswathi Suresh and my in-laws Alamelu MPl and Muruga Palaniappan for their love, support and prayers through it all.

TABLE OF CONTENTS

LIST OF FIGURES

LIST OF TABLES

ABSTRACT

Dysautonomia is the dysfunction of the Autonomic Nervous System (ANS) that frequently occurs in individuals with spinal cord injuries (SCI), stroke, diabetes, or Parkinson's disease. Dysautonomia after SCI that results in tetraplegia most commonly presents as autonomic dysreflexia (AD). AD can be triggered by different stimuli below the level of injury resulting in paroxysmal hypertension. If not properly managed, AD can have severe clinical consequences, leading to stroke and potentially death. AD is currently detected in-clinic through continuous monitoring of blood pressure using a cuff-based system. However, existing techniques are time-consuming, obtrusive, lack automated detection capabilities, and have low temporal resolution. Thus, a wearable diagnostic tool was developed that could detect the onset of AD using non-invasive physiological sensors through repeatable machine learning and data science techniques.

This work presents a novel, multimodal system that can quantitatively characterize and distinguish unique signatures of AD. We used rodent models of SCI to detect finer temporal changes in the sympathetic and parasympathetic branches of the ANS due to AD. Signal processing and feature selection techniques were used to determine five features which were most significant to characterizing AD. This allowed us to characterize a concomitant increase in sympathetic activity followed by an increase in vagal activity during the onset of AD. Additionally, we used the unique signature to train a neural network to detect the onset of AD with an accuracy of 93.4%. We developed a model that can distinguish between reactions of sympathetic hyperactivity due to different stimulus triggers above and below the level of injury. The system could serve as a complementary tool to the clinically accepted gold standard of determining AD using solely blood pressure, providing a method for universally detecting the onset of AD and discriminating the different triggers for sympathetic stress for improved management of AD in individuals with SCI.

1 INTRODUCTION

1.1 The Autonomic Nervous System

The mammalian nervous system has evolved to become a unique system which can perform a number of complex thought processes and actions. It receives millions of bits of information every minute from various sensory nerves and organs and integrates them to determine the responses to be made by the body [1]. The nervous system consists of the Central Nervous System (CNS), with over 100 billion neurons including those in the brain and spinal cord, and the Peripheral Nervous System (PNS), which connects the CNS to every other part of the body. The PNS can be further divided into the somatic nervous system, which is associated with voluntary control of body movements through skeletal muscles, and the autonomic nervous system (ANS), which is associated with involuntarily regulating bodily functions [2]. The ANS is largely responsible for involuntarily maintaining internal physiologic homeostasis [3]. The ANS functions as a reflex circuit and uses sensory feedback from the organs to modify and adapt the output of the ANS to adjust the physiological state of the body [2]. It helps to control arterial pressure, gastrointestinal motility, urinary bladder emptying, thermoregulation and various other activities. The ANS can rapidly modify the intensity and speed of visceral functions such as heart rate[3], [4]. The ANS comprises of two antagonistic sets of nerves, the sympathetic and the parasympathetic nervous system, which innervate three major types of muscle (cardiac muscle, smooth muscle and the glands) and various effector organs (Figure 1). The activity of each organ innervated by the sympathetic and parasympathetic nerve fibers depends on the interaction and balance between the signals from both systems[5], also known as the sympatho-vagal balance.

The activation of the sympathetic nervous system (SNS) leads to reactions of alarm, often referred to as the “fight or flight” response. The most obvious phenomena of SNS activation include pupil dilation, piloerection (‘goosebumps’), sweating, increased cardiac activity in the form of increased blood pressure (BP) and heart rate (HR), and inhibition of the urinary and genital functions[4]. Sympathetic nerves originate in the vertebral column and are located in the thoracolumbar spinal cord (T1-L2 segments).

The parasympathetic nervous system (PSNS) is related to functions of protection and conservation, often known as the “rest or digest” responses. It works in direct contrast with the SNS and regulates the functioning of visceral organs such as the liver, kidney and heart. Stimulation of the PSNS leads to pupillary constriction, decreased heart rate, promoted digestion, urinary activity and genital activity. The PSNS, also known as the vagal system, originates from the craniosacral region and innervates the thoracic and abdominal regions of the body through the vagus nerve, which contains 75% of all the parasympathetic nerves fibers

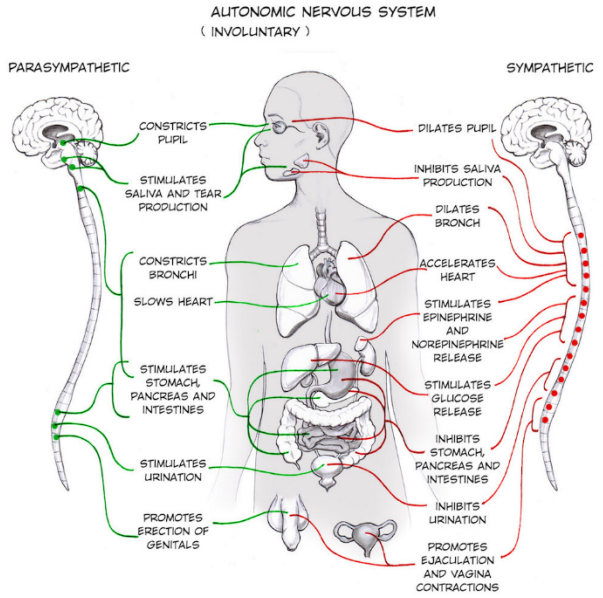

Figure 1: Innervation of the ANS- including the sympathetic and parasympathetic nervous system.

The ANS primarily regulates the functions of the cardiovascular and sudomotor systems. The sympatho-vagal interaction allows control of the HR and BP of an individual. The sympathetic nerves control vasomotor tone and cardiac output, which are directly proportional to the arterial BP and stimulation of the SNS results in an increase in HR and BP. In contrast, stimulation of the PSNS leads to a lowering of HR and BP [6]. Due to the influence of the ANS on the cardiovascular function, the evaluation of cardiovascular measures such as heart rate variability and fluctuations in BP allow clinicians to develop a better understanding and diagnosis of ANS function. In addition, the ANS regulates sudomotor function and ensures thermoregulation[7]. The eccrine sweat glands are innervated by nerves from the hypothalamus and thoracolumbar segments of the spinal cord.

1.2 Dysautonomia: Dysfunction of the Autonomic Nervous System

Dysfunction of the ANS, commonly referred to as dysautonomia, is an umbrella term for several medical conditions which lead to malfunctioning of the ANS. Dysautonomia often gives rise to impaired control of cardiovascular activity including regulation of blood pressure (BP) and heart rate (HR), impaired bowel, bladder and gastrointestinal function, and impaired thermoregulation[8]. Dysautonomia ranges from transient episodes to progressive ANS dysfunction resulting from spinal cord injury (SCI), Parkinson's disease (PD), diabetes and stroke [9]–[11]. Dysautonomia is correlated with poor rehabilitation outcomes, significant reduction in the quality of life, and in severe cases, increased morbidity or mortality[12], [13]. Diseases which lead to dysautonomia often affect different components of the central autonomic network, pre- and post-ganglionic neurons and their target organs. Symptoms include fluctuations in BP, abnormal heart rates, gastroparesis, anhidrosis, blurred vision and in severe cases, death[14]. In some cases the signs of dysautonomia can be subjectively disabling and uncomfortable, but in some diseases, dysautonomia can make the prognosis of the disease unfavorable[15].

Dysautonomia in PD has been recognized since the original description of the disease by James Parkinson in 1817[16]. Almost a third of all individuals with PD experience symptoms of dysautonomia[17], although a wide variation has been found in studies which report prevalence of dysautonomia in PD ranging from 5% to almost 90% [18]–[21]. This may be due to the wide variation of the presentation of dysautonomia in individuals with PD. Dysautonomia may be caused by the presence of Lewy bodies in the autonomic regulatory regions including the hypothalamus, SNS and PSNS [22]–[24]. Until recently symptoms of dysautonomia were attributed as side-effects of anti-parkinsonian drugs such as Levadopa, but recent studies have identified that dysautonomia is part of the disease process itself [21], [24].

In most cases, dysautonomia occurs as a secondary health condition in diseases such as spinal cord injuries (SCI)[25], stroke[10], [26], and diabetes[27]. In diabetes, dysautonomia is among the least recognized and understood complications[28]. Cardiovascular autonomic neuropathy (CAN) is one of the most common manifestations of dysautonomia [29], [30] and is caused by damage to the autonomic nerve fibers which innervate the heart and blood vessels.

CAN causes resting tachycardia, postural hypotension, orthostatic hypotension and myocardial infarctions. CAN was reported in 16.8% of all individuals with type 1 diabetes and 22.1% of individuals with type 2 diabetes[31]. While it is possible to identify early stages of CAN with careful measurement of autonomic function, it is the significant cause of morbidity and mortality associated with sudden death[15], [26]. Dysautonomia is caused by the metabolic disorders of diabetes which lead to widespread damage to the ANS, including a metabolic insult to the nerve fibers causing nitrosative stress which damages endothelium and neurons[32], [33]. Lastly, cerebrovascular diseases such as stroke affect crucial control sites for autonomic function including the insular cortex, amygdala and lateral hypothalamus[34]. The insular cortex is an important cortical area in the middle cerebral artery which controls sympathetically and parasympathetically mediated cardiovascular regulation[35]–[37]. The insult to the insular cortex leads to more severe cardiovascular presentations of dysautonomia in stroke.

Gastrointestinal disturbances due to dysautonomia are also common and severely disabling. Gastrointestinal dysfunction in the form of dysphagia occurs in almost 80% of patients with PD during the course of the disease[38] and in 50% of patients with acute stroke. Constipation and difficult defecation are the most-common gastrointestinal symptoms among PD patients[39]. Other gastrointestinal manifestations of dysautonomia include swallowing problems such as drooling, motility disorders, gastroparesis, constipation, vomiting and diarrhea[20], [23], [38], [40], [41]. In diabetics, gastrointestinal disturbances are more common in patients who have been diagnosed for long periods of time with poorly controlled blood glucose level but are frequently overlooked and left untreated [42]. Control of blood glucose levels in diabetics often leads to an improvement of the gastric motor dysfunction

Over 70 million people worldwide live with various forms of dysautonomia [14] and while there is currently no cure for dysautonomia, a variety of treatments are available for the symptoms caused by the disorder. Alternately, treatments of the underlying disease which cause dysautonomia can also help with symptom management. While some treatments are available to improve quality of life through medications and lifestyle changes/adaptations, many patients with dysautonomia experience disabling symptoms which significantly reduce their quality of life. Despite the prevalence of dysautonomia, a lack of awareness amongst the public and within

the medical profession often leads to a delayed diagnosis for most patients, sometimes even several years[24]. This leads to the need for a reliable recognition of the signs of dysautonomia through quantitative analysis tools. However, there is currently a lack of simple techniques which can detect anomalies in the functioning of the ANS early.

1.3 Dysautonomia in Individuals with Spinal Cord Injuries

In the United States, there are currently 280,000 individuals who live with a diagnosis of SCI with an incidence rate of approximately 64 cases per million population [43]. Young adults are often the age group with the highest risk of SCIs and individuals with SCI often fall between 18 and 30 years of age. High level SCIs have a considerable impact on the lives of the individuals who are injured as well as their families. Despite the low incidence of SCIs compared to health conditions such as heart disease and stroke, persons with SCI are most likely to live with paralysis and other consequences of SCI for longer periods of time [44]. The most frequent age of injury is 19 and with a near normal life expectancy of individuals with chronic SCI due to advances in medicine in the past few decades. The economic consequences and impacts on the quality of life of living with a SCI are substantial. For an individual with tetraplegia, estimated yearly direct costs such as healthcare and living expenses, and indirect costs including loss of wages, fringe benefits and productivity are $1.1 million and $0.8 million per individual, respectively [45].

In addition to the severe medical risks during acute management of SCI, there is a life-long risk of secondary health complications. Every year 30-50% of persons with SCI are re-hospitalized due to secondary health complications. Post SCI health conditions include skin pressure sores, urinary tract infections, orthostatic hypotension, deep vein thrombosis and most frequently, autonomic dysreflexia (AD), which occurs in almost 70% of the SCI population [46]–[48]. After SCI in the cervical or high thoracic vertebral regions parasympathetic control is often preserved after the injury; however, there is a lack of supraspinal control of the SNS leading to profound effects of SNS dysfunction[49], [50]. Due to the disproportionate activity of the SNS and the PSNS in SCI, there is a loss of synergy between the two systems resulting in dysautonomia.

Autonomic dysreflexia (AD) and orthostatic hypotension (OH), are two of the most common manifestations of dysautonomia. AD leads to uncontrolled systolic hypertension over 200mm Hg [51], [52] in individuals with SCI. It is a potentially life threatening syndrome caused by hyperreflexia of the SNS and occurs in about 70% of individuals with an SCI above the sixth thoracic (T6) level of the spine[53], [54]. AD is initiated by irritation or noxious stimuli below the level of injury or triggers with 85% of cases of AD being triggered by urinary tract infections or impacted bowels [55], [56]. Other AD triggers include pressure sores below the level of injury, restrictive clothing, wounds, exercise, or sexual function[57]. AD causes debilitating symptoms including pounding headaches, acute anxiety, chills, blurred vision, flushing, and sweating above the level of injury [58]. If left untreated, AD can cause a dangerous increase in blood pressure that can lead to possible cerebral hemorrhage and even death [59], [60]. In a study of life-threatening instances of AD, 22% of cases resulted in death [61].

1.4 Relevance of Dysautonomia Detection

Late stages of dysautonomia also increases the cost of care for individuals and has a significant negative impact on the quality of life, with an estimated 25-50% of diabetic patients with symptomatic dysautonomia dying within 5-10 years of diagnosis[12], [13], [43], [47], [48]. There is a need to recognize the importance of dysautonomia in individuals and identify methods to improve management of symptoms. Similarly, recognition of the various autonomic abnormalities of PD is important to ensure that effective treatment may be available which can measurably improve quality of life for individuals with PD. This makes the detection of autonomic function early on in the disease states is crucial for improvement of quality of life of individuals with disease states and their caregivers.

The severity of stroke has also been associated with autonomic function, wherein more severe strokes lead to a progressive loss of overall autonomic modulation, decline in parasympathetic tone, and progressive shift toward sympathetic dominance[34], [62]. Diagnosis of dysautonomia early post-stroke can be used as an indicator for stroke severity[63] allowing necessary therapeutic interventions to be provided. Moreover, dysautonomia has also been associated with increased in-hospital neurological complications[63] and adverse clinical outcomes[64] such as cardiac complications, hyperglycemia, immune depression, sleep

disordered breathing, and malignant edema[65]–[68]. While ANS function can gradually return to normal range within six months post-stroke, in several cases there is no improvement in the ANS function in patients with atypical, definite or severe autonomic dysfunction two months to a year after ischemic stroke[69], [70]. Thus, earlier diagnosis of dysautonomia can offer valuable insights to clinicians regarding decisions made about prognosis and the subsequent therapy[71]. Similarly, autonomic function has also been used as clinical predictive biomarkers for severity of PD[72]–[75], and regular testing of autonomic function could allow therapeutic interventions to slow the progression of the disease.

The majority of patients with stroke experience incomplete recovery of motor deficits despite having received some type of rehabilitation, with up to 60% having impaired manual dexterity six months following the stroke[76]. Likewise, in patients with SCI, approximately half of the motor recovery occurs within the first two months after the injury and is assumed to be complete two years after the injury[77]. Quantitative measurements of dysautonomia form the groundwork for successive treatment of various stroke-related autonomic disorders[78], [79], making determination of dysautonomia to gauge somatomotor-sympathetic coordination early in the rehabilitation process critical to successful recovery of locomotor function.

1.5 Current Methods of Dysautonomia Detection

Several diagnostic tools have been adopted in routine clinical evaluation and include both invasive and non-invasive tests. Since cardiovascular dysfunction is one of most common manifestations of dysautonomia, several clinical tests are based on the evaluation of cardiovascular reflexes to triggering maneuvers. These include stimuli which raise BP and mainly activate the sympathetic outflow. Among the batteries of tests, the Ewing battery is the most popular and commonly used in diagnosis of autonomic function and comprises deep breathing, orthostatic testing, and Valsalva maneuver[80].

1.5.1 Cardiovascular testing

The Valsalva maneuver allows an evaluation of the baroreceptor sensitivity and the body's ability to compensate for changes in the amount of blood that returns to the heart. The

maneuver is performed by asking the subject to blow into a tube to maintain a column of mercury at 40mm Hg for 15 seconds and measuring the ECG response[81]–[83]. The changes in the BP and thoracic pressure during the activity can be divided into four phases (**Error! Reference source not found.**). The Valsalva ratio is derived from the longest RR interval in phase IV divided by the shortest RR interval in phase II and at the very beginning of phase III. The ratio reflects parasympathetic activity and a value lower than 1.21 is considered abnormal [84], [85], often requiring further evaluation of the healthy, able-bodied participant.

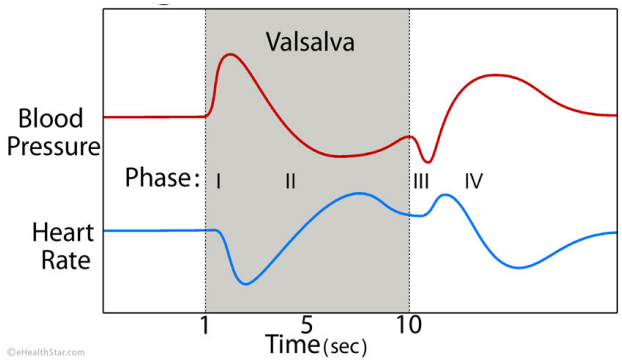

Figure 2: Blood pressure and heart rate during the Valsalva maneuver. In phase II, blood pressure normally increases from its lowest, and in phase IV blood pressure overshoots baseline prior to the maneuver.

The Valsalva maneuver can also reliably assess sympathetic function by measuring changes in heart rate and blood pressure through several repetitions of the test and the rate of return to baseline values. However, the test can be intrusive, and results are affected by age, sex, body position and medications[79]. Moreover, individuals with stroke, SCI and PD may not have the mobility required to perform the maneuver.

Several tests use electrocardiogram (ECG) measurements, and a common measure is the fluctuation of the mean interval between two R waves on the ECG (RR interval). Heart Rate Variability (HRV) provides a measure of the RR interval which is a resulting factor of the sympatho-vagal interaction[81], [86], [87]. Due to the ability to non-invasively determine HRV through ECG measurements, it has recently become a popular clinical methodology to detect dysautonomia[81], [88]. ECG based evaluation of HRV can be performed through frequency and time-based domain analyses as well as non-linear techniques. The analysis is often based on 24 hour Holter recordings or on shorter ECG recordings ranging from 0.5 to 5 minutes[89]. Time

domain analyses of HRV from ECG recordings have the widest application in routine clinical evaluation. Parameters such as the SDNN, derived from measurements of the standard deviation of the Normal to Normal (NN) intervals, square root of the mean of the sum of the squares of differences between adjacent NN interval (RMSSD), and the percentage difference between adjacent NN intervals that are greater than 50 ms (pNN50) allow determination of the function of the ANS[88]–[91]. The SDNN reflects overall variability but RMSSD and pNN50 predominantly reflect the parasympathetic modulation of the heart, which often decreases due to dysautonomia. However, the various time-domain based HRV parameters do not reflect the sympathetic modulation of the heart.

Frequency based analysis of the HRV through Fast Fourier transformation (FFT) separates the frequency components of the HRV into three major components: high frequency (HF) ranging from 0.15-0.4Hz, low frequency (LF) ranging from 0.04-0.15Hz, and very low frequency (VLF) which is below 0.04Hz. LF power is often interpreted as a measure of a combination of sympatho-vagal activity[91]–[93]. Other measures of sympatho-vagal balance include the LF/HF ratio[2], [81], wherein a higher ratio indicates an increased sympathetic activity, while a lower ratio indicates an increased parasympathetic activity[94], [95]. In a normal adult in resting conditions, the LF/HF ratio is between 1 and 2. While the powers of signal oscillations in the frequency-domain analyses are considered to reflect the sympatho-vagal influence, they cannot be considered an absolute measure of the SNS or PSNS outflow [96], [97]. There are also established correlations between the time and frequency domain analyses wherein pNN50 and RMSSD values correlate between themselves and HF power which reflect vagal activity [87], [95], [98].

HRV values vary significantly with age and are influenced by factors including body position, circadian rhythm, respiration, gender or diet[87], [88]. The clinical application of HRV assessment through time domain analyses are further limited by a lack of consensus on the most accurate HRV parameter for clinical use[99]. On the other hand, while frequency-domain analysis provides a better understanding of the sympatho-vagal balance, it is time consuming and requires long, nearly artifact free recordings as well as specific software and computer

techniques. These may not be readily available in the clinical setting to allow immediate diagnosis of dysautonomia.

1.5.2 Sudomotor testing

The testing of sudomotor function tests the cholinergic system of the ANS and reflects the function of small, unmyelinated fibers to determine any neuropathies in the small fibers[86]. Sudomotor testing is one of the earliest detectable neurologic abnormalities in dysautonomia and these tests may be abnormal in patients without any cardiovascular abnormalities[100].

Sympathetic skin response (SSR) is a measure of electrodermal activity and is based on the temporary change to electrical resistance due to stimuli which leads to a change in skin potential. SSR provides a surrogate measure of sympathetic cholinergic sudomotor function. To determine SSR, the potential difference between the skin over the front and back of the hand or foot is measured via surface electrodes[101]. The stimuli used are physiological (loud noise, flash, touch, inspiratory gasps) or electrical (peripheral nerve stimulation – median, tibial, peroneal, supraorbital nerve) and changes in SSR are measured. SSR is considered abnormal if amplitudes between the left and right side differ by at least 50% or if one of four limb responses is absent[102]. SSR measurements have also been used to determine dysautonomia in individuals with SCI with a relatively high accuracy[103], [104]. Despite being easy to perform, the technique requires an increasing stimulus intensity as the response habituates to allow continuous detection of ANS function, which often leads to discomfort.

1.5.3 Other testing methods

While sudomotor and cardiovascular measures are most commonly used in clinical settings, other symptoms of dysautonomia can also be used to assess the function of the ANS. Techniques such as video cinefluoroscopy[12], [100], endoscopy[105], [106], gastric emptying studies[107], [108] and intraluminal pressure recordings can be used to determine the impact of dysautonomia on the gastrointestinal system. Similarly, testing of the urinogenital system through techniques such as penile plethysmography[100], intracavernosal papaverine[100], and urodynamic studies[109] also provide an insight into the level of dysfunction of the ANS in

individuals. However, due to the invasive nature of these tests and the discomfort caused by them, they are more commonly used in research settings and less adopted by clinicians.

1.5.4 Gap in Autonomic Testing

While the various tests to detect autonomic function are built on well understood physiological basis, they are often difficult, time consuming and require specific instruments and personnel with a great deal of training and experience[81], [110]. Multiple factors influence autonomic function testing including age, gender, body position, emotional state, ingested food and medicines[111], and even time of testing (morning as compared to evening)[112], [113]. Factors such as room temperature, humidity and other background noise also affect the results of the testing[86], [110], [114]. Moreover, the current techniques require a degree of dexterity or movement from the patient, which is not usually possible in patients with acute stroke and SCI, making it mandatory to develop a simpler method to assess autonomic dysfunction[15].

There is also no single test which reflects the function of the ANS, requiring a battery of tests to be run. This can be time consuming and laborious for the patient. Moreover, the interpretation of the tests is based on pre-determined thresholds which do not account for individual differences. While these thresholds inform a clinician of the dysfunction of the ANS, there is a lack of a scale which allows evaluation of the level of severity of the symptoms[65]. A scale would allow the determination of the severity of the symptoms and allow clinicians to provide customized rehabilitation plans. Clinical studies have detected the onset of AD and OH by measuring changes in physiological parameters [46], [115] including changes in BP, heart rate or abnormal sweating. However, there is currently no gold standard for measuring the severity and completeness of autonomic dysfunction. This leads to technical difficulties while administering tests to patients and can be a major concern for clinical practice.

1.6 Machine Learning Applications in Healthcare

Machine learning (ML) has been applied to various areas of healthcare and has enormous potential to improve detection of disease [116]–[119], help clinicians with making decisions (decision support system)[120]–[122] and improve the quality of life of individuals. Current

healthcare practices revolve around human expert assessments of correlations between symptoms and diagnoses. However, there is a growing trend in the medical community to use automated or semi-automated systems to monitor the well-being of individuals in their care[123]. This section will focus on applications of machine learning approaches using physiological data and not explore the advances of machine learning in domains such as imaging or natural language processing for electronic health records.

With an increase in availability of wearable sensing technologies, such as the Apple® Watch, Fitbit® , there is an increasing amount of healthcare data available to clinicians and others in the field of healthcare. ML techniques can contribute to finding patterns and trends that contribute to the knowledge about different disease states as well as help diagnose them early[124]. ML algorithms can be divided into three main categories: supervised, unsupervised and reinforcement learning. Supervised methods are among some of the most common approaches used in clinical setting due to the large amount of annotated data which is available[123]. Some applications of ML to healthcare settings include automated arrhythmia analysis tools using physiological data such as electrocardiogram (ECG) or alerts for low oxygen saturation using photoplethysmography (PPG)[125]–[128]. Additionally sensors such as electroencephalography (EEG)[129]–[131] and electromyography (EMG) [132]–[134] have also been used to develop datasets and machine learning models which enable researchers and clinicians to make better decisions about the well-being of individuals who are able-bodied as well as those with different forms of disabilities.

Supervised ML methods have three main steps [135]. The first step is extracting/collecting the n-dimensional features vector in order to reflect different aspects of the conditions (features) with a class label attached. The second step of this machine learning approach is application of the ML methods (classifier) for prediction of the class label of the features input. The third step is measuring the performance of the prediction method and its validity using approaches such cross validation technique and independent evaluation (IE) datasets. Feature extraction is the process of reducing a set of raw/preprocessed data into a smaller set of features which represent the key qualities of the data. Features are chosen so that

they possess different qualities for different classes. Feature extraction in healthcare data is often guided by physiological understanding of the mammalian system[136]–[138].

Once features have been identified from the data, various machine learning models can be trained. Classification models are commonly used when class labels are available and are discrete in nature. Several models have been used in the classification of healthcare data-particularly physiological data[137], [138]. These include logistic regression, decision trees, ensemble approaches, and deep neural networks. Each technique differs in its underlying objective function and constraints, thus requiring exploration in order to identify the best performing algorithm. Additionally, performance metrics of algorithms need to be established ahead of using particular algorithms - these include keeping in mind the clinical task of interest. These metrics allow determination of whether accuracy is sufficient for the task, or if other metrics need to be evaluated. Despite its strengths, ML cannot identify relationships that are not present in the data; therefore, data veracity plays an important role in the development of any ML model. Moreover, ML does not replace the need for standard statistical analyses or randomized, control trials[123].

In the investigation of spinal cord injuries, ML tools have been employed to investigate the changes in walking ability due to rehabilitation[139], [140], activity recognition[141], [142], pain and well-being predictions[143], [144]. However, there is a dearth in research which has been conducted in the identification of co-morbidities or secondary health conditions post-SCI.

1.7 Goal for this Project

There is currently no technique to detect dysautonomia non-intrusively in real time. Through this research, we will focus on developing a multimodal detection system which can detect changes in physiology due to dysautonomia in SCI. Particularly, we will investigate dysautonomia due to the onset of autonomic dysreflexia (AD). We propose to develop a non-invasive, multi-parametric system to detect AD using the most efficient machine learning method to differentiate sympathetic stressors. We propose to 1) develop a sensitive, non-invasive, multi-parametric approach to detect key physiological manifestations of AD, 2) develop a machine learning model that can distinguish between the onset of AD and other sympathetic

activity, and 3) test the performance of the model to optimize specificity of sympathetic activation due to different triggers.

1.8 Specific Aim 1: Characterizing unique signatures of Autonomic Dysreflexia through non-invasive sensing.

We will study the onset of AD using a rat model with high thoracic compression SCI that we have adapted. The rat models enable us to perform controlled studies and using large subject samples has previously been difficult to achieve in naturally occurring instances of dysautonomia in humans. Rat models of SCI are typically preferable in order to mimic human pathology of SCI and are most widely used to study SCI [145], [146]

1.8.1 Research Questions

1) Do readings by novel, non-invasive physiological sensors change in accordance with what is expected due to sympathetic activation as a result of the onset of AD?

An array of sensors, including skin nerve activity (skNA), ECG, blood pressure and skin temperature, were used in the development of the new AD detection system (ADDS). Rate and patterns of change in the physiological data will be correlated and mapped to the initiation and progression of AD in rats to further evaluate sympathetic activity related to AD. Different classifiers will be explored through extensive feature engineering and selection. We will determine an optimal combination of noninvasive sensors to detect the onset of AD episodes.

2) Can we characterize AD through a combination of these sensors?

Machine learning models will be built using the data collected from the rat model. These will be binary classifiers which can distinguish between AD and non-AD states. In addition to standard classifiers, feature engineering will provide strong and ideally simple relationships between new input features and the output feature for the supervised learning algorithm to model. This will enable the development of an ideal machine learning model which can detect AD and identify characteristics of the onset of AD.

1.8.2 Anticipated Outcome

We anticipated that a combination of the sensors that detect activity of a paravertebral ganglion and other non-invasive sensors would detect AD. Moreover, we anticipated that the machine learning model would be able to distinguish between the physiological parameters which are associated with AD events. The models developed with this data would enable understanding of specific features, which will provide a deeper insight into understanding the ability to identify the onset of AD.

1.9 Specific Aim 2: Distinguishing physiological signatures due to AD and other sympathetic stressors.

Having identified unique signatures of AD in Specific Aim 1, confounders to the model need to be identified. Since AD is a sympathetic response to a trigger below the level of injury, it is important to identify the difference in response between AD and other sympathetic responses. This includes triggers above and below the level of injury.

Through this aim, different stimuli are explored, and machine learning models are built to differentiate between a true AD event and other sympathetic triggers.

1.9.1 Research Questions

1) Can we distinguish between the onset of AD and other sympathetic stimuli?

Physiological responses to the onset of AD and other sympathetic stimuli will be compared. A machine learning model generated using the sensor data acquired during Aim 1 will be used to automatically detect the onset of AD and other stimuli by extracting features from the normalized physiological time-series data collected. The observation of patterns in the data is independent of the physiological differences across animals.

2) Can we optimize the developed machine learning model to distinguish between the different sympathetic stimuli?

Modifications will be made to the machine learning model developed in S.A. 1 to optimize for the detection of specific sympathetic stimuli due to different triggers. Feature selection techniques will allow for better discernment in understanding the physiological changes occurring as a result of the different sympathetic stimuli.

1.9.2 Anticipated Outcome

We anticipated an ability to discern differences in sympathetic activity as a result of different sympathetic/nociceptive triggers, as well as long-term progression of SCI on baseline sympathetic activity.

1.10 Overview of the Document's Structure

This chapter introduced the basis for the thesis and the motivation behind it as well as an overview of the literature on topics related to this research. Chapter 2 provides some more background specific to this work which has been done previously regarding AD detection research in humans. Chapter 3 provides an overall signal processing and machine learning methodology used to answer the different research questions posed in this thesis. Chapter 4 discusses the animal model used in this thesis. Chapter 5 discusses the research questions posed in Specific Aim 1 to discern the onset of AD. Chapter 6 discusses the research questions posed in Specific Aim 2 to discriminate AD from other sympathetic stressors. Finally, in Chapter 7, conclusions and future work are discussed.

2 BACKGROUND WORK

2.1 Current Gold Standards of AD detection

The standard approach for managing AD for newly injured tetraplegics is for them learn to recognize their own symptoms and triggers and how to manage them [147]. However, only 41% of persons with SCI and their family had heard of AD even though 22% of individuals with SCI reported symptoms consistent with unrecognized AD [148]. Meticulous monitoring of telltale symptoms of AD can prevent the rapid escalation of AD-induced hypertension and reduce risks to personal health if managed quickly. However, learning to recognize AD symptoms can take time and identifying the source of noxious stimuli occurring in paralyzed parts of the body may be difficult [61], [149] at the potential risk of the individual, especially for those who are newly adapting to living with paralysis. Additionally, 35-43% of individuals with SCI experience asymptomatic or 'invisible' AD [150].

Clinically, medical professionals use blood pressure monitoring to diagnose AD (at least 20 mmHg above baseline levels)[55]. However, continuously monitoring blood pressure through ambulatory blood pressure monitoring (ABPM) systems is not practical for long-term use. It restricts individuals' activities and data quality can be affected by movements such as wheeling or transferring. The tactile and sonorous stimuli to measure blood pressure can be distracting, interrupting activities of daily living (ADLs) or sleep [71]. Moreover, the sampling rate of measuring blood pressure is quite low (maximum every two minutes).

The interpretation of the ABPM data requires a trained clinician as well as an analyst who is trained with computer and data processing software. This hinders widespread adoption of ABPM in the SCI community [151]. Thus, there is a need for a sensitive yet noninvasive method of detecting the onset of AD, which can be adopted easily into clinical practice and for at home use.

2.2 Autonomic Dysreflexia Detection System Developed in Human Models

Prior work has been performed by us in human models of SCI to develop a continuous, wearable AD detection system. The initial development of the ADDS in the human model was presented in a Master's thesis titled 'A Physiological Telemetry System to Detect the Onset of Autonomic Dysreflexia in Individuals with Spinal Cord Injuries'.

We developed a proof of concept ADDS that showed that AD symptoms can be reliably detected across a sample of individuals with chronic, high-level SCI using noninvasive physiological sensors (**Error! Reference source not found.**). The system used a combination of wearable, commercially available sensors, alternative to blood pressure, to continuously monitor AD episodes for eight hours or more while the user maintains an active lifestyle. The ADDS employed a cloud-based universal classifying machine learning model to automatically recognize AD in real-time[152].

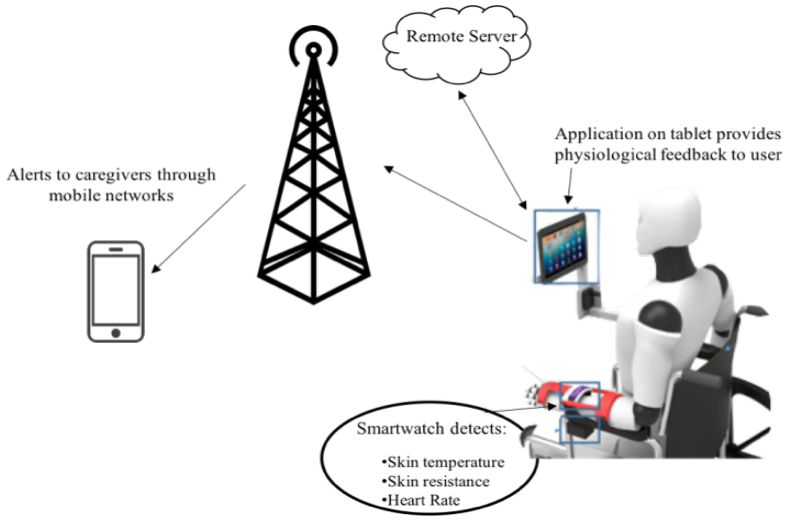

Figure 3: Overview of ADDS used to collect data and predict onset of AD symptoms in individuals with SCI

2.2.1 Development of the sensors and machine learning model

The system continuously measured skin temperature, heart rate and galvanic skin response (GSR) (sweating) through sensors available in a Microsoft Band™, a wrist-worn smartwatch (**Error! Reference source not found.**). It was chosen for its wearability, ability to

develop custom applications and controlled sampling rate [153] The physiological data whose data are wirelessly streamed to a mobile application over the internet [103], [154].

A mobile application was developed and deployed on an Android® tablet via Bluetooth, to receive data from the watch and alert the users when AD is detected. In this study, we rely on the individuals' ability to self-report symptoms of AD (**Error! Reference source not found.**a). This is supported by studies in which participants were asked to self-report AD symptoms which showed high correlation between self-reported frequency and the objectively assessed number of AD events [155]. Data was collected from eleven participants with cervical and thoracic injuries (mean age: 35.3±11.2) using the system for 8 hours a day for period of a week.

Figure 4 : The Microsoft Band and its sensors for GSR, heart rate, and skin temperature.

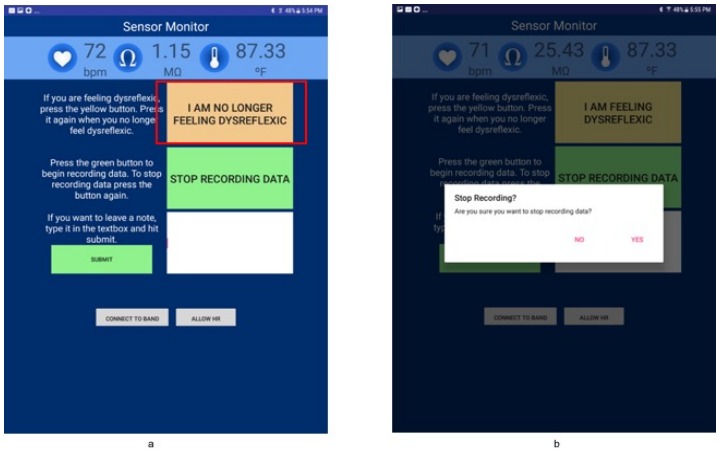

Figure 5: The Android Sensor Recorder application with features for the user to; (a) report the onset of AD, (b) stop recording data

A support vector machine (SVM) model with a radial basis function (RBF) kernel was trained using this physiological data collected from the MS Band. Four different models were trained using various combinations of physiological sensor data (GSR, skin temperature and heart rate) as features. Each model was trained and tested using a 5-fold cross validation to determine its accuracy, sensitivity and specificity of each model (**Error! Reference source not found.**). The model with the highest accuracy and lowest false negative rate was chosen as the optimal model for the detection of AD in real time. The combination of data collected from the GSR and skin temperature sensors led to the development of the most accurate and error free machine learning model. (**Error! Reference source not found.**). When tested with naïve participants whose data was not used in the training of the test model, the model detected AD with an accuracy of 94.1% and a false negative rate of 3.8% [156].

Table 1: Representation of the Confusion Matrix for AD Detection.

	Predicted AD	Predicted Non-AD
Actual AD	True Positive (TP)	False Negative (FN)
Actual Non-AD	False Positive (FP)	True Negative (TN)

Sensitivity: True positive rate; Specificity: True Negative rate

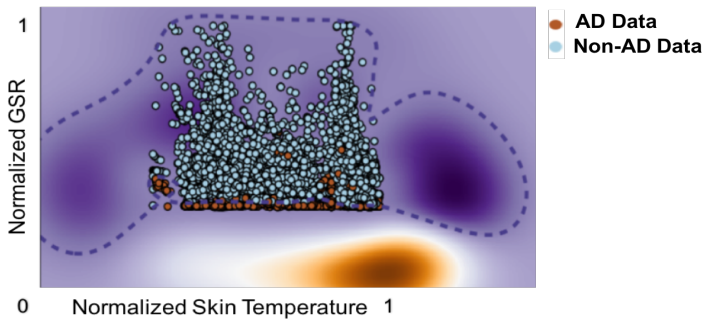

Figure 6: The optimal model developed with an RBF kernel to distinguish between AD and non-AD data

2.2.2 Developing a model with optimally weighted features

In addition to the machine learning algorithm developed to differentiate between AD and non-AD events, we investigated the impact of weighting the different parameters on the performance of the system. The data collected from the 11 participants in Section 1 were used a linear SVM for the feature weighting and classification. Each sample x_i, $i = 1,...,m$ consists an N by 3 feature vectors, where N refers to the length of the data, and two class labels $y_i \in \{+1, -1\}$ wherein +1 represents the onset of AD symptoms and -1 represents a lack of AD symptoms. Our support vector can be characterized by the following equations

$$\omega^T x_i + b \geq 1 \text{ for } x_i \text{ with class } +1$$
$$\omega^T x_i + b \leq -1 \text{ for } x_i \text{ with class } -1 \quad (1)$$

The resulting weight vector ω encodes the contributions of all features to the classifier.

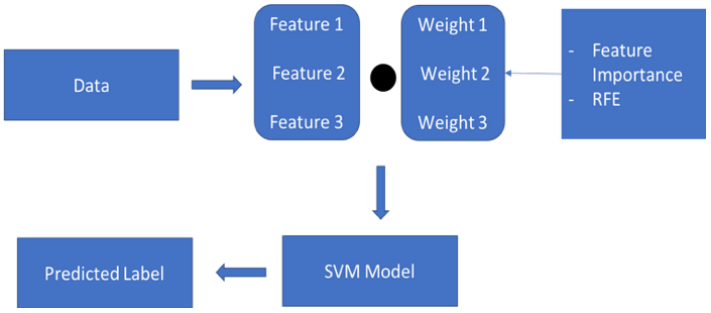

Figure 7: The process diagram of determining the optimal weights of the different features.

Two different methods were used to identify the weights of the features. An ideal set of weights with each of the methods was determined by evaluating the training accuracy of the models.

a) Feature Importance

Feature importance was estimated through bagged decision trees such as Random Forest and Extra Trees. The bagging methods reduce the variance of the base estimator and allow tuning of the parameters to maximize the performance of the algorithm. The feature weights were constructed based on the nodes of the decision tree as well as the features used to build this tree. Each node was assigned to a split point on a given feature which was then used to determine the importance of the feature[157].

b) Recursive Feature Elimination

The Recursive Feature Elimination (RFE) model works by recursively removing features and building a model with features that remain. It is a backward feature deletion method which ranks the features in the order in which the feature is removed wherein the top ranked features are removed in the last iteration and are the most important [158].We identified that the best performing model for prediction of AD was one in which GSR was given the highest importance, followed by skin temperature and the least importance given to heart rate. This is in agreement with our prior work where we developed an accurate model using a combination of GSR and skin temperature data [159]. While training the model with 100% weightage on GSR data allowed a reasonably high accuracy, distributing weights to heart rate and skin temperature led to much higher performance through an almost 6% increase in accuracy of detection, as well as 4.53% increase in the sensitivity and 12.42% increase in specificity.

The corresponding weights and training accuracies based on the two feature weighting techniques is presented in the **Error! Reference source not found.** below and the highest training accuracy was determined to be the one where all three features contributed to the model (Extra trees).

Table 2. Weights of the different parameters determined by the feature weighting strategies.

Feature Selection Strategy	GSR	HR	ST	Training Accuracy
RFE 1	1.00	0.00	0.00	94.17%
RFE 2	0.00	1.00	0.00	91.49%
RFE 3	0.00	0.00	1.00	91.24%
RFE 4	0.333	0.333	0.333	91.72%
Extra trees	**0.556**	**0.105**	**0.340**	**94.44%**
Random Forest	0.616	0.094	0.290	94.43%

When models were developed with the weights determined through the techniques, the highest sensitivity, specificity and AUC-ROC were identified for the models which were developed with the weights identified through the extra trees method. This model was built using a weighted combination of GSR, heart rate (HR) and skin temperature (ST) data with the highest importance given to GSR, followed by skin temperature. This model led to development of a linear SVM which clearly separates AD data from non-AD data (**Error! Reference source not found.**). The poorest performance was of the model that was developed using only heart rate data, which has been shown to be highly variable in persons with SCI.

Table 3. Performance measures of the Weighted linear models developed

Feature Selection Strategy	Accuracy	Sensitivity	Specificity	AUC-ROC
RFE 1	92.59%	82.25%	82.26%	0.884
RFE 2	90.85%	57.26%	52.94%	0.620
RFE 3	91.67%	64.95%	71.71%	0.700
RFE 4	91.38%	56.20%	85.50%	0.983
Extra trees	**97.38%**	**86.78%**	**94.68%**	**0.987**
Random Forest	98.39%	85.50%	92.46%	0.983

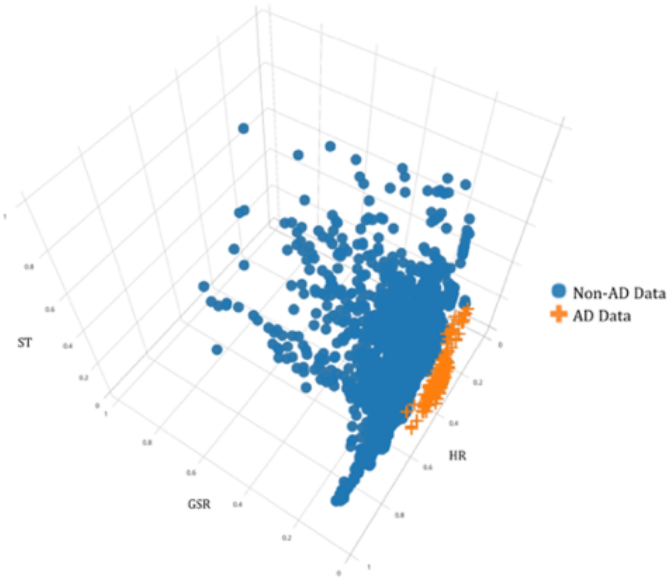

Figure 8: Linear SVM model developed using a weighted combination of features allows separation of AD and non- AD data

The choice of weights can be explained by the physiological signs of AD. AD is most commonly characterized by cold, clammy skin due to sweating above the level of injury as well as alterations in heart rate. Since GSR allows the characterization of sympathetic sudomotor function[160]–[162],which is disrupted by AD and sweating leads to an overall decrease in skin temperature, the higher weights assigned can be justified. In a prior model developed in **Error! Reference source not found.**, heart rate data was eliminated from the development of the optimal model due to variations of the data between individuals during the onset of AD. Bradycardia and tachycardia are both observed in individuals during the onset of AD symptoms [163]–[165] thereby preventing a consistent detection of AD. However, through the elimination of heart rate data, there is a possibility of discarding potentially useful data which may allow deduction of the cause of AD, such as exercise or other cardiovascular events. In the current model the low weightage given to heart rate data may be due to a consideration of the presence of change in heart rate values rather than an overall increase or decrease. Through the inclusion of heart rate data, further analysis could help us improve the detection of symptoms of AD and possibly determine the trigger.

2.2.3 Limitations of the ADDS

The ADDS model was developed with self-reported symptoms of AD as the ground truth rather than the clinical gold standard of measuring systolic blood pressure. While developing the ADDS in the human model, it was established that there were difficulties with controlling the onset of AD. The trigger of AD was not controlled, and variations in the timing of the onset of AD have led to confounders in the data. In prior studies, AD has been induced in humans through urodynamic assessments. However, it poses a risk to the individual since AD can have long term effects. Additionally, it is difficult to study the onset of AD in humans with acute SCI since there are other complications which require urgent care during the rehabilitation phase after the injury.

The rat model explored in this thesis enables a more controlled study of a specific triggers of AD. Moreover, it enables using large subject samples has previously been difficult to achieve in naturally occurring instances of AD in humans.

3 DATA ANALYSIS METHODOLOGY

In this chapter, we will discuss the various data analysis techniques used in the determination of changes in physiological data collected. The specifics of the rat model used in this thesis will be discussed in the next chapter.

3.1 Sensors for collection of Physiological Data

We collected electrocardiography (ECG), skin nerve activity (skNA), blood pressure (BP) and skin temperature data from the rodent model before and after SCI. The system uses commercially available medical research equipment (Powerlab Bioamplifier) to detect changes in cardiovascular activity. In addition to measures of cardiovascular function such as heart rate and blood pressure, we measure stellate ganglion sympathetic nerve activity through electrodes placed on the skin. skNA is a novel technique developed to estimate the stellate ganglion nerve activity and has been validated in humans[166] and canine models[167][168]. The skin nerves in the upper extremities and thorax originate in the cervical and stellate ganglia allowing measurements to estimate stellate ganglion activity[169].

ECG and skNA were measured through a pair of disposable, gel-based electrodes placed on the level of the right and left third ribs in the rats in a Lead I configuration with the electrode placed at the right leg serving as a reference electrode (Figure 9A). The electrodes were placed on the rat prior to being restrained as will be discussed in Chapter 4.2. The electrodes were connected to the bio-amplifier on the Power Lab 26T (AD Instruments, USA). The signals were digitized at a sampling rate of 10kHz with a recording bandwidth set at 10Hz to 3kHz[167].

A CODA 6-Channel High Throughput Non-Invasive Blood Pressure system (Kent Scientific, USA) was used to measure the blood pressure in the rats[170]. The Coda system provides measurements of the systolic, diastolic and mean blood pressure. The system comprises an occlusion cuff and a volume-pressure recording (VPR) cuff which are placed on the tail of the animal. Recordings of blood pressure were collected two times per minute. The blood pressure

system comprises an occlusion cuff placed at the base of the tail and a volume-pressure recording (VPR) cuff which is placed 2 inches from the base of the rat's tail (Figure 9B).

A DS18B20 waterproof digital temperature probe was used to measure skin temperature from the shaved back of the rats. The temperature probe is connected to an Arduino and provides up to 12 bits of temperature data from the onboard digital to analog controller[171]. In conjunction with the Dallas temperature control Arduino library, the temperature sensor logs data with a sampling rate of 0.03Hz (2 samples per second)[172]. The temperature probe was calibrated prior to experimentation to confirm its sensitivity using hot and iced water (temperature was validated through infrared temperature sensor).

A **B** **C**

Figure 9: A) Non-invasive ECG sensors placed in Lead I configuration B) Tail-cuff placed on rat's tail to measure blood pressure C) Temperature probe placed on the shaved back to measure skin temperature.

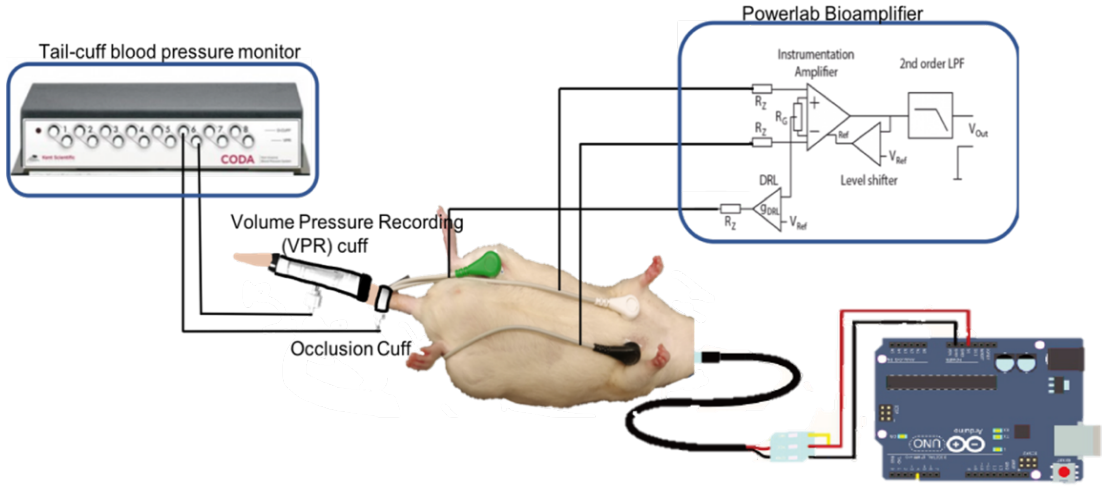

Figure 10: Schematic of the sensors. Noninvasive electrodes placed on the ventral skin surface of a rat in Lead I configuration, the Coda® Blood Pressure system with occlusion and VPR cuff and a temperature probe connected to an Arduino®.

3.2 Signal Processing and Feature Extraction

The signals collected from each sensor are processed to ensure that there are no artefacts resulting from motion or respiration of the animal. The objective of signal processing is to produce an output that can facilitate the subsequent extraction of features from the signal. Each cleaned signal was then segmented using an overlapping windowing method of fixed lengths to create sub-sections of the signal from which features could be extracted. Different window lengths were investigated, and forty-one features were extracted from the cleaned signals to allow the development of a machine learning model as well as selection of features which best resembled the stimulus. Figure 11 is a flowchart of the data collection, signal processing, feature extraction and model development.

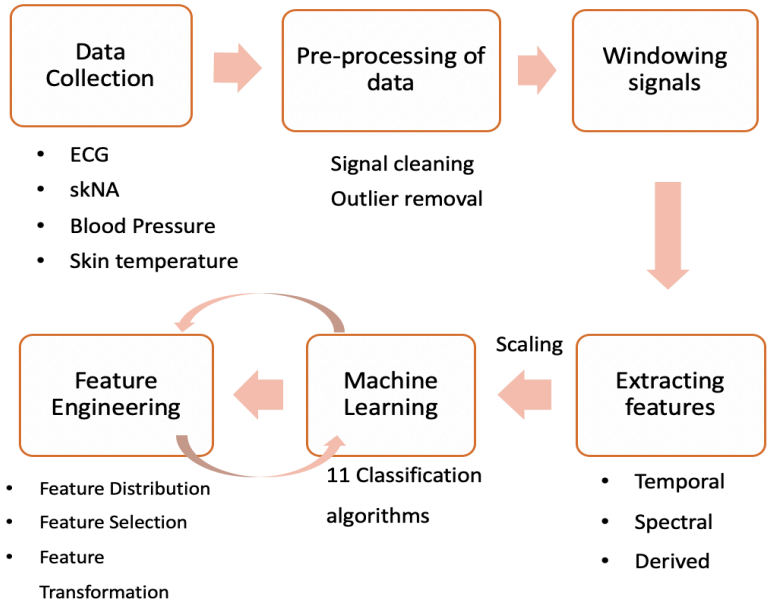

Figure 11: Pipeline of data processing approach taken for the detection of AD.

3.2.1 ECG

a) *Filtering the ECG signal*

The ECG was filtered within a bandwidth of 0.05 − 100 Hz and sampled at 10kHz. ECG data was collected from a commercially available Bioamplifier system which was shielded from the 60Hz electrical hum from other power systems in the experiment room. In addition to hardware-based filters, the ECG signal was processed using a 60Hz notch filter to remove any

power line interference. A seventh order Butterworth band-pass filter between 0.01- 30Hz was applied to remove movement artefacts [173], [174] and other high frequency noise. Smoothing plays a role in suppressing noise or interference in a signal and was done by using a moving average filter on the signal[175] (Figure 12).

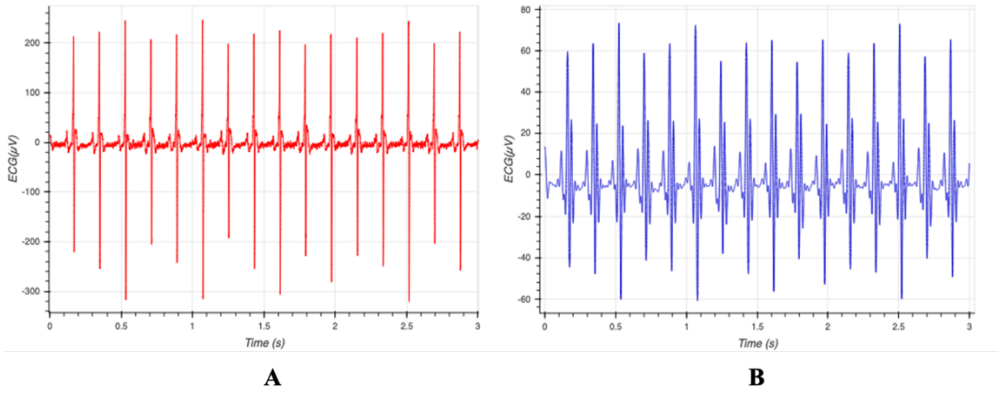

Figure 12: A) Raw ECG data collected from rats B) Processed with ECG without high frequency components and prominent R peaks.

b) *Feature Extraction*

The ECG is a recording of the electrical activity of the heart during cardiac cycles and is characterized by the recurrent sequence of the P, QRS and T segments. The detection of the QRS complexes and the R-peaks provide the fundamentals basis for various automated ECG analytics [176].

An algorithm was developed to extract the RR peaks of the ECG signal. This algorithm was based on the Pan-Tompkins algorithm – which highlights the QRS segment allowing automated retrieval of the R peaks as well as the S segments (Figure 13) [177]. To ensure detection accuracy, the derived RR peaks are further processed to ensure the minimum difference between two successive peaks is between 100-500ms (200bpm < HR <600bpm) to generate the normal to normal (NN) intervals[178]. The heart rate and medianNN are calculated from the NN intervals. The QRS interval which provides additional information about the cardiac condition was also extracted[179]. The P and T segments of the ECG were difficult to determine consistently through simple automated techniques and were not considered in this methodology.

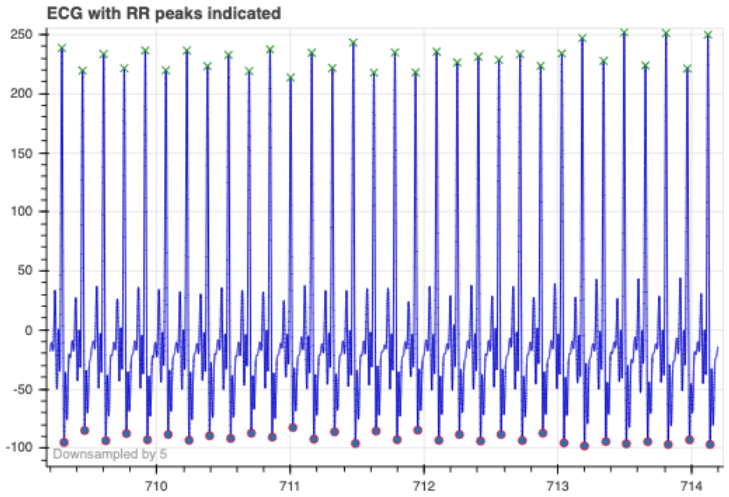

Figure 13: Cleaned ECG signal with identified R (x) and S (o) segments

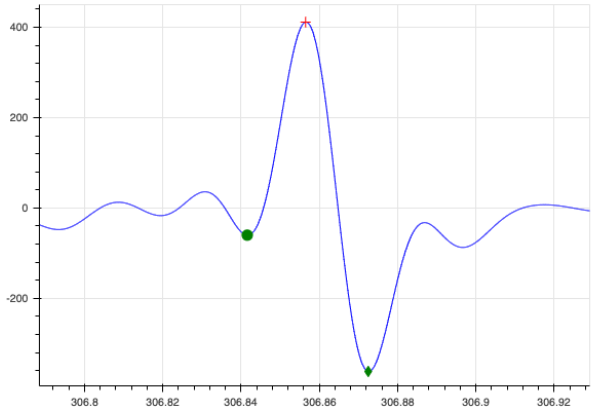

Figure 14: The automated detection of the Q (•), R (+), S (♦) segments from an individual beat of the ECG signal.

The standard deviation of NN beat intervals (SDNN), covariance of NN intervals (covNN), the square root of the mean of the squares of the successive differences between adjacent NNs (RMSSD), and the proportion of the number of pairs of successive NNs that differ by more than 5 ms (NN_5) divided by total number of NNs (pNN_5) calculated over each window were used to represent the heart rate variability (HRV) measures based on the time–domain method. Time domain analyses of HRV from ECG recordings have the widest application in routine clinical evaluation. Parameters such as the SDNN, RMSSD, and pNN_5 allow determination of the

function of the ANS [88]–[91]. The SDNN reflects overall variability but RMSSD and pNN50 predominantly reflect the parasympathetic modulation of the heart, which often decreases due to dysautonomia. However, the various time-domain based HRV parameters do not reflect the sympathetic modulation of the heart.

Frequency based analysis of the HRV through Fast Fourier transformation (FFT) separates the frequency components of the HRV into three major components: high frequency (HF) ranging from 0.15-0.4Hz, low frequency (LF) ranging from 0.04-0.15Hz, and very low frequency (VLF) which is below 0.04Hz. LF power is often interpreted as a measure of a combination of sympatho-vagal activity[91]–[93]. Other measures of sympatho-vagal balance include the LF/HF ratio[2], [81], wherein a higher ratio indicates an increased sympathetic activity, while a lower ratio indicates an increased parasympathetic activity[94], [95].For the spectral analysis, spectral power for HRV was analyzed on the windowed ECG segments. The total power (TP), VLF, LF, and HF components were extracted from an FFT performed on the ECG signal. The peak frequencies in VLF, LF, and HF components as well as the areas under these components were calculated. Additionally, the LF/HF ratio was also calculated.

3.2.2 skNA

Skin nerve activity (skNA) is the measurement of autonomic activity of the stellate ganglion which innervates the cardiovascular system[166] and can be used to estimate cardiac sympathetic tone. The skNA has a frequency range of 0-2000Hz and can be derived from ECG signals by using a bandpass filter of 500-1000Hz (Figure 15A) to account for the larger bandwidth of the skNA signals compared to the ECG and myopotential[180].

a) *Filtering skNA data*

A moving average filter is used to remove any artefacts which may occur in the skNA signal (Figure 15B). The high frequency range of the signal ensures that there are limited artefacts which commonly occur in the ECG signal. Since the skNA signal is a measurement of the sympathetic nerve which innervates the heart, the signal is contaminated with occurrences of the QRS interval of the ECG signal. In order to avoid any potential misclassification due to the QRS interference, the first step is to identify these intervals using the Pan-Tompkins algorithm[177]

(Figure 15C). Once the QRS interference is determined, the section of signal is replaced with the median value to generate a “cleaned” skNA signal (Figure 15D).

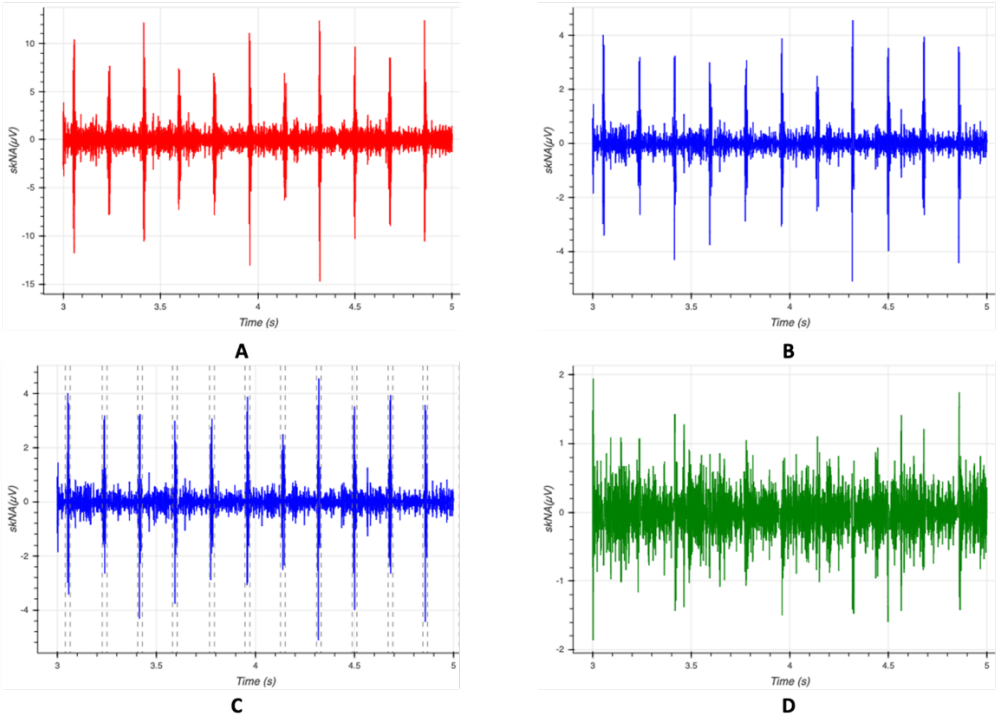

Figure 15: A) Raw skNA signal captured from performing a bandpass filter on the raw ECG signal acquired. B) The skNA after a moving average filter has been applied to remove artefacts. C) Identification of the interference caused by the QRS interval- indicated by the grey dashed lines D) Cleaned skNA signal which is used for processing. iskNA and askNA calculations.

b) *Feature Extraction*

To quantify the high-frequency discharges that are associated with nerve activity, the integrated nerve activity is calculated by integrating the amplitude of nerve activity over time. The skNA recording was also rectified and integrated (iskNA) over a 100-ms window using a leaky integrator and the results were displayed over time to simulate the display methods of microneurography (Figure 16). Additionally, we divide the absolute sum of the voltage values of the cleaned skNA signal over every window to generate the average skNA (askNA).

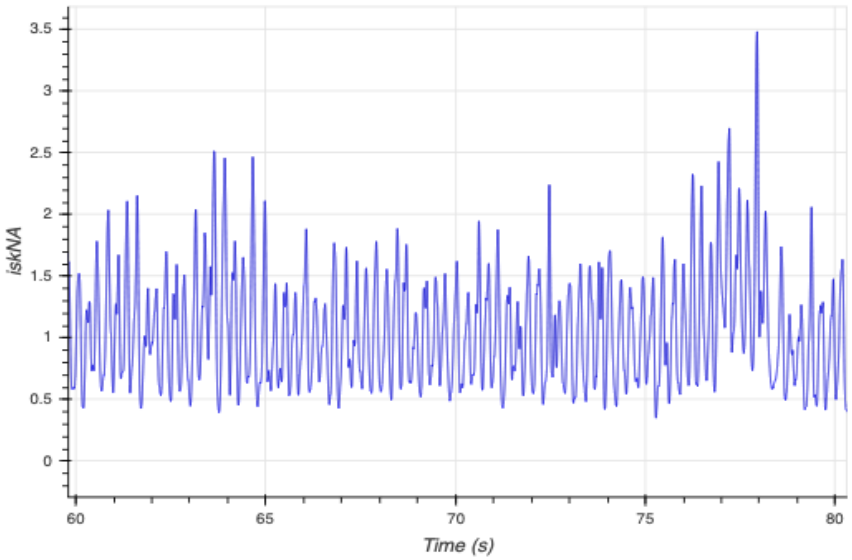

Figure 16: skNA signals are rectified and integrated over a 100ms window in order to generate the integrated skNA (iskNA) which is commonly used in microneurography.

A prominent characteristic of nervous system activity is the prevalence of single spike activity and burst activity[180]. Often in microneurography, burst analysis is performed manually due to the shorter duration. In order to automate our detection of bursts in skNA- we devised an algorithm which uses a threshold value in order to gauge if bursts were occurring. In order to compute this threshold, a baseline value was first identified. This baseline was the mean value (μ_b) of the iskNA when the animal was at rest (pink dotted line in Figure 17). The standard deviation of the iskNA values (σ_b) at rest was also calculated and the threshold was determined to the mean plus three times the standard deviation of the baseline ($\mu_b+3\sigma_b$). Values above the threshold during the processing is considered a "burst" (red dots in Figure 17). We calculate the burst frequency (bursts/window) the duration of these bursts, burst amplitude (μV) and total burst area.

In addition, in microneurography – spectral domain analyses also allow an understanding of the sympathetic nervous activity. Sympathetic neural circuits are capable of generating periodic activity patterns that range from 0.04 to 10 Hz[181]. Spectral analyses of the cleaned skNA signal were performed using a Fast Fourier transform. The total power (TP), peak power of low-frequency (LF; 0.04–2.5 Hz), high-frequency (HF; 2.5–5 Hz) and very high-frequency

(VHF; 5-10Hz) components were extracted from the FFT PSD. The peak frequencies in LF, HF and VHF components as well as the areas under these components were calculated.

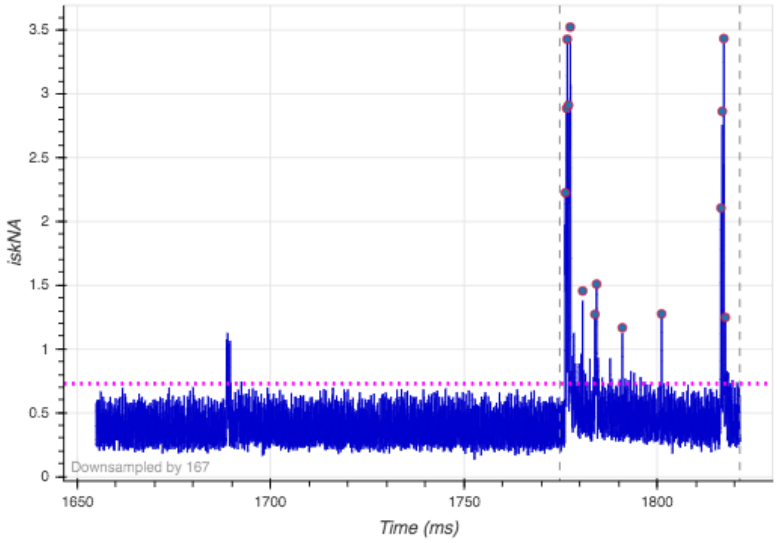

Figure 17: Bursts identified. The pink dotted line represents the mean value of the baseline iskNA(μ_b) collected from when the animal is at rest. The red dots shown represent the burst activity which are iskNA amplitudes higher than $\mu_b+3\sigma_b$. The grey dotted lines represent the onset of stimulus.

3.2.3 Skin Temperature

Skin temperature data was collected using an Arduino and due to the differences in sampling rate between the sensors, a timestamp-based approach was used in order to accurately compare the data from the temperature sensor to the changes resulting from the skNA and ECG features. A moving average was used to remove any aberrant data points from the sensor data. The data was windowed and changes in temperature during each window, as well as mean and median temperature during the windows were extracted.

3.2.4 Blood Pressure

Blood pressure was used as the gold standard in our study to identify the onset of AD due to the stimulus. In order to investigate this- the blood pressure was broken down into systolic (SBP), diastolic (DBP) and mean arterial pressure (MAP). The change in SBP, DBP and MAP during the cycles when stimulus was present as the mean values of SBP, DBP and MAP were extracted from the data.

Table 4: All features Extracted from each window of sensor data

Signal	Features	
ECG	Temporal: 1. R-R Intervals (Heart rate) 2. QRS interval 3. MedianNN 4. nn5 5. pnn5 6. stdNN 7. covNN 8. Root mean square of successive differences (RMSSD)	Spectral: 1. Peak LF & Power 2. Peak HF & Power 3. Peak VLF & Power 4. Area under low frequency bands (ALF) 5. Area under high frequency bands (AHF) 6. ALF/AHF ratio
skNA	Temporal: 1. Average skNA 2. Average iskNA 3. Burst duration 4. Frequency of bursts 5. Area under burst	Spectral: 1. Peak LF & Power 2. Peak HF & Power 3. Peak VHF & Power 4. Area under low frequency bands (ALF) 5. Area under high frequency bands (AHF) 6. ALF/AHF ratio
Skin Temperature	1. Δtemperature 2. Mean temperature 3. Median temperature	
Blood Pressure	1. ΔSBP 2. ΔDBP 3. ΔMAP 4. Mean SBP 5. Mean DBP 6. Mean MAP	

3.3 Dataset Preparation

Each feature set extracted was associated with a window, animal and trial. To minimize inter-subject variability across the different rats, the physiological features extracted were normalized using a min-max scaling method for data collected from the same trial. The scaling of data enables comparison in the patterns of change observed in the physiological data collected by sensors for AD [104]. Additionally, several of the machine learning techniques described in the next section require input scaling. Missing values, though rare were also removed from the dataset.

3.3.1 Outlier Removal

Some machine learning models are quite sensitive to outliers and removing these outliers plays a crucial role in the development of the models, as well as the understanding of the physiological changes. We used the Z-score approach [182] wherein the mean ($\bar{Y}$) and standard deviation (s) of each feature was calculated. The Z-score was determined through equation 2 below and outliers were defined as those with a score of greater than 3.

$$Z_i = \frac{Y_i - \bar{Y}}{s} \quad (2)$$

Additional care was taken that the outlier removal did not drastically reduce the size of the dataset. This was done to ensure that there was sufficient data to train, test and validate the machine learning models.

3.3.2 Dataset Augmentation

Supervised machine learning models often perform best when large amounts of labelled data are available [183], [184]. . Using simpler classifiers or ensemble methods, which will be discussed in later sections, can help improve performance of the model. An alternative is to perform data augmentation which increases the number of data points available for the development of models. This is often done through resampling the available dataset.

a) *Changing Window Lengths*

We used different window lengths to extract the various features. Datasets were created with window lengths of 5, 10, 15, 30 and 60 seconds. This was done in order to ensure sufficient data points were available. The window length of 60 seconds led to the smallest dataset which comprised 300 data points for AD detection whilst the dataset with a window length of 5 seconds comprised 2200 data points. The selection of window size also plays a role in the interpretation of the features extracted from the ECG and skNA sensors. A window size that is too small could lead to a loss of discriminative information from the data [185].

b) *Balanced and Imbalanced datasets*

Performance of the machine learning models is impacted when there is a skew in the dataset towards one of the classes, i.e., there is a higher occurrence of one class rather than the other. These datasets are "imbalanced" and can lead to misleading performance metrics with high performance. Deeper analysis of these models trained on imbalanced dataset shows that model is more likely to predict the class with higher occurrence.

In order to prevent the development of imbalanced dataset, we under sampled from the data representative of the non-AD data. Due to the longer (2x) intervals of the non-AD data, features were extracted at twice the selected window size from non-AD intervals. Features which were impacted by the window length, such as number of NN intervals greater than 5ms (nn5) and number of bursts were adjusted to account for the differences in window length.

3.4 Machine learning techniques employed

Once a balanced dataset was developed, we used machine learning techniques in order to determine the trends and patterns in the data. Eleven different classifiers were used for the initial exploration of performance of the machine learning models on the dataset we had developed. We split the data into three stratified sets- the training set (70%), the test set (15%) and the validation set (15%). 10-fold cross-validation (CV) is used to create variations of the training, test and validation sets in order to avoid trends in the features getting misinterpreted and causing overfitting of the machine learning models.

3.4.1 Metrics of Evaluation

We used various metrics to gauge the best performing algorithm for the identification of the target stimuli which will be discussed in later sections. These include accuracy, sensitivity, specificity, F-1 score and AUC-ROC which were discussed in Section 2.2.1. We developed binary and multi-class models, which will be discussed in greater detail in later chapters. For all implementations of the machine learning models, we used the scikit-learn library [186].

3.4.2 Logistic Regression

Logistic regression is one of the more popular models for analysis of healthcare data [187]. The model fits a logistic (sigmoid) function to the data in order to calculate the class membership based on a posterior distribution. The logistic regression model uses maximum likelihood estimation in order to determine the best-fit sigmoid function which predicts the probability that the data point belongs to the different classes. In our model, we use ℓ_2 regularization to reduce overfitting and minimize the cost function shown in equation 3, wherein w is the weight, y_i is the labelled class in the training set, X is the input dataset and c is a constant.

$$\min_{w,c} \frac{1}{2} w^T w + C \sum_{i=1}^{n} \log\left(\exp\left(-y_i(X_i^T w + c)\right) + 1\right) \quad (3)$$

We used the robust large scale bound constrained optimization (LBFGS) optimizer to perform the cost optimization algorithm to enable prediction of the class of the data in the test and validation set. The advantage of the logistic regression model is that it is easy to implement and makes no assumptions about the distributions. However, if there are complex/non-linear relationships between the variables and the output target (class label), logistic regression does not perform very well[188].

3.4.3 K-Nearest Neighbors (KNN)

Classification based on the k-nearest neighbors algorithm uses a pre-defined number of samples closest in distance to determine the label of the data. It is a distance-based approach wherein the adjustable parameter of the model is k which is the number of nearest neighbors to

include in the estimate of class determination. Varying the k-parameter allows changes in the flexibility. In our model, we used the Euclidean distance as the metric to determine the closest samples and a majority vote of all the neighbors to allow prediction of the label. The model we developed used a k of 5 to determine the closest class label with uniform weight distribution of all points in the neighborhood. The advantages of a kNN model are the ease of interpretation and explanation of the model. However, the model is very dependent on the data that is being presented to it and is prone to overfit.

3.4.4 Support Vector Machine (SVM)

SVM has already been extensively discussed in Section 2.2.1. In this model, we developed a linear and an RBF SVM for investigation of the functionality of the machine learning models to detect the onset of AD. The advantages of SVMs are that they are effective in high dimensional spaces and all quite versatile. However, they do not provide direct estimates of probability estimates and need to be produced through extensive-cross validation.

3.4.5 Decision Trees

A decision tree is a non-parametric method for classification which creates a model that can predict the value of a target variable by learning decision rules from the features. The decision tree begins with a root node which then uses rule-based decisions to create new internal nodes. Each leaf node then continues to create further nodes and the label of the final node known as a leaf node is the predicted class of the instance. The decision trees are inherently able to identify feature which can determines which feature allows the easiest separation between the classes. The decision tree splits the dataset which maximizes the separation of the data though decrease the level of entropy.[189]

In our model, we developed a decision tree using the Gini impurity coefficient to measure the quality of the split – allowing a determination of the features which will form our root and leaf nodes. We set the maximum depth of the tree to 10 to ensure a faster implementation of the decision tree. Additionally, as will be discussed later after feature selection, only 5 features were used. Decision trees are easy to understand and interpret requiring lesser data preparation.

Additionally, it performs well even if assumptions about normality are violated and the model can be validated using statistical tests. They can create over-complex trees which may lead to overfitting, often requiring pruning of the features which leads to better performance.

3.4.6 Naïve Bayes

The Naïve bayes algorithm applies Bayes' theorem using prior probability to determine the class of the data[189]. As shown in Equation 4, a Maximum A Posteriori (MAP) estimation is used to estimate the probability of the classified label, $P(y)$ and the probability of training data x_i given the label (posterior), $P(x_i \mid y)$. The algorithm does not affect the order of the individual rules. Naïve Bayes has high bias and low variance.

$$\begin{gathered} P(y \mid x_1, \ldots, x_n) \propto P(y) \prod_{i=1}^{n} P(x_i \mid y) \\ \Downarrow \\ \hat{y} = \arg \max_{y} P(y) \prod_{i=1}^{n} P(x_i \mid y) \end{gathered} \quad (4)$$

We use a Gaussian Naïve Bayes classifier in the development of our model which makes assumptions that the likelihood of the features is Gaussian in nature thereby affecting the calculation of the posterior as shown in Equation 5 wherein the mean (μ_y) and standard deviation (σ_y) are estimated through maximum likelihood.

$$P(x_i \mid y) = \frac{1}{\sqrt{2\pi\sigma_y^2}} \exp\left(-\frac{(x_i - \mu_y)^2}{2\sigma_y^2}\right) \quad (5)$$

Naive Bayes classifiers can be extremely fast compared to more sophisticated methods. The decoupling of the class conditional feature distributions means that each distribution can be independently estimated as a one-dimensional distribution. However, the algorithm can be affected significantly by the dataset itself, and if the dataset is not completely representative of the phenomena being studied, it can lead to misclassifications.

3.4.7 Gaussian Process

A Gaussian process is a Bayesian kernel classifier wherein the probability of belonging to a class label y_i for an input sample X_i is monotonically related to the value of some latent function f_i. There is a prior which is characterized by zero mean and a covariance matrix which is placed on the latent function. The algorithm allows interpolation of the observation, is probabilistic and versatile. Gaussian process classifier is often used because of its ability to choose hyperparameters and covariances directly from the training data However, they tend to lose efficiency in highly dimensional spaces. Additionally, they always assume that the parameters are normally distributed.

3.4.8 Neural Network

We used a feedforward neural network which learns a non-linear function approximator. As shown in Figure 18, the leftmost layer is the input layer comprising all the input features, with the rightmost layer being the output layer (predictor). Each neuron in the hidden layer transforms the values from the previous layer with weights W: $w_1x_1 + w_2x_2 + \ldots + w_mx_m$ and a non-linear activation function. The weights are adjusted through the backpropagation algorithm through continuous calculation of the gradient.

The model we developed was a 5-layer MLP with a Rectified linear unit (ReLU) activation function. The neural network uses the adaptive moment estimation (ADAM) solver to optimize and update the weights for the different layers. ADAM computes the adaptive learning rates for each parameter and uses the momentum of learning of the neural network[190]. Additionally, an ℓ_2 regularization is performed to ensure that the model is not overfit. Advantages of the neural network are that it works well with missing data and in order to train the neural network, the input data needs to be scaled appropriately. However, it is quite resource intensive and can often appear as a “black box”.

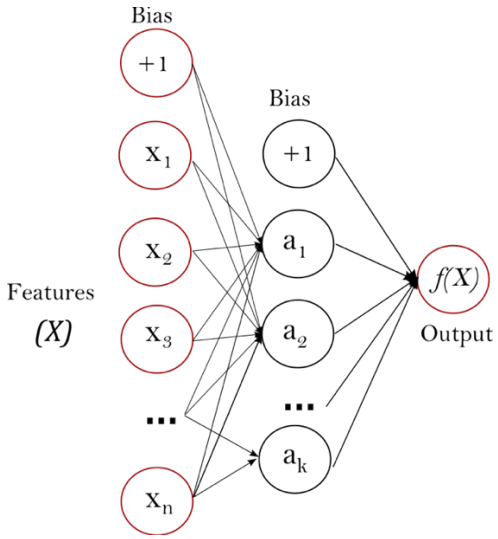

Figure 18: One hidden layer neural network [186]

3.4.9 Quadratic Discriminant Analysis

The quadratic discriminant analysis (QDA) algorithm makes an assumption that the data is Gaussian in nature and estimates the mean and variance for each feature for each class. Additionally, the QDA assumes that each class its own covariance matrix which is used to make predictions of the unknown input data. QDA uses Bayes theorem to estimate the probability of the new set of inputs it encounters and the class with the highest probability is the output class of the input data. The QDA algorithm is quick to implement but relies heavily on the training data with a tendency to overfit.

3.4.10 Ensemble Methods

Ensemble methods combine the predictions from multiple models and are able to create a method which can decrease variance (bagging), bias (boosting) or improve predictions by stacking. These improve the overall performance and robustness.

a) *Random Forest*

The random forest is an ensemble method built from decision trees and is often more flexible. Random forests build multiple decision trees through a "bootstrapped" dataset which comprises of a randomized dataset of the same size and randomly select features. Each iteration leads to a new decision tree being created from a new bootstrapped dataset and a randomly

selected set of features. When splitting each node during the construction of the tree- a best split combination is determined from all the input features.

For our random forest classifier, we built ten decision trees with a maximum depth of 5 nodes. In the model, we consider all the features instead of randomizing the feature subsets. The probabilistic decision of the predicted class label made by each tree is averaged and then a final class label is output.

b) *AdaBoost*

The Adaboost algorithm fits a sequence of weak learners on modified versions of data. The predictions from each of the weak learners is combined through a weighted majority vote to determine the final prediction. The data modifications are performed through applying different weights to each training sample. For each iteration, the weights are modified, and the learning algorithm is applied on the data. This is repeated until the weak learners perform decently well.

In our model, we use weaker decision trees and each tree only has a root node with two leaves (known as a 'stump'). The performance of each stump affects the next with some stumps having more say in the prediction ability than others. Lastly, each subsequent stump learns from the errors of the previous stump and improves itself.

Overall, ensemble methods improve the performance of the algorithms off which they are based. However, they can be less interpretable when explaining them and may be more resource intensive.

3.5 Feature Selection Techniques employed

Feature selection is a technique where we choose features in the data that contribute most to the target variable – in our case, prediction of the onset of AD. These methods are intended to reduce the number of input variables to those that are believed to be most useful to a model in order to predict the target variable[117]. The best subset contains the least number of dimensions which contribute the most to the overall performance of a chosen machine learning model. The remaining unimportant features are discarded.

Feature selection reduces overfitting allowing an improved accuracy as well as a faster training of the machine learning model, and improves the interpretability of the outcomes for the model[182]. The feature selection process results in a subset of features which produce the optimal model. All implementations of the feature selection techniques were through the scikit-learn library [186].

3.5.1 Feature Distribution and Correlation

Features extracted from the sensors can be highly correlated due to biological basis- such as the standard deviation (stdNN) and covariance (covNN) of NN intervals and RMSSD. However, when training a machine learning model, it is important to avoid training with features which are highly correlated. This is particularly applicable in the training of linear or logistic regression models which are vulnerable to multicollinearity.

In datasets with correlated features, the requirements of model sparsity and of retrieving of all predictive features are in direct competition [191]. This leads to a higher variance in the weights of a model which could cause extreme sensitivity to data, which is unwanted. Additionally, in some models such as random forests, the interaction between features can be masked if there are highly correlated features. Lastly, a simpler model performs better – by removing highly correlated features, it is possible to reduce the complexity of a model.

In our feature selection process, we calculated the Pearson correlation between each of the features which were extracted and plotted a heatmap (Figure 19). Only one of the features with very high/low correlations ($|\rho| < 0.7$) were kept in the dataset.

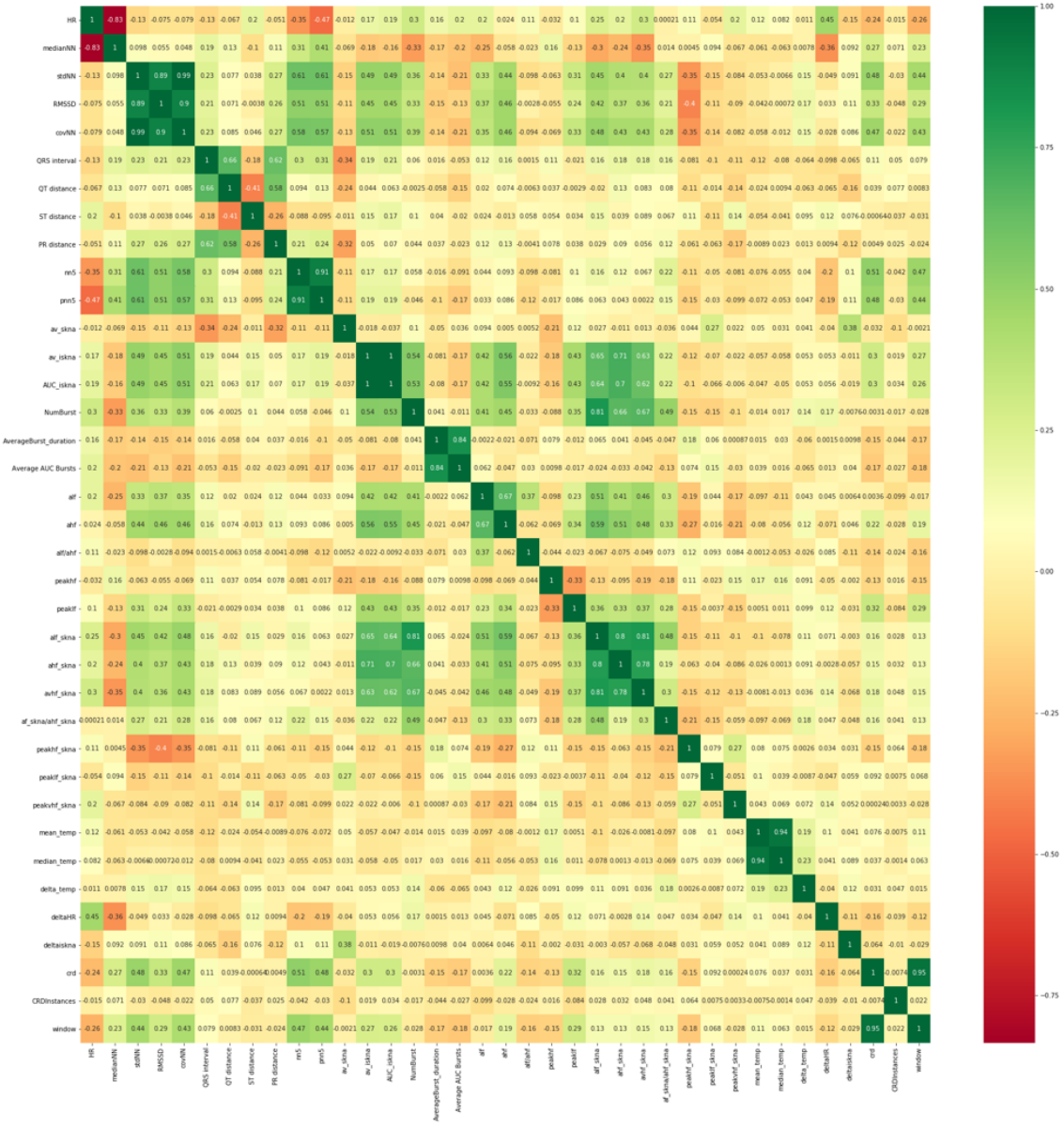

Figure 19: Heatmap of correlation of the thirty-six different features. Highly correlated features are removed and not considered in the development of the machine learning models.

3.5.2 Recursive Feature Elimination

Recursive Feature Elimination (RFE) is a wrapper feature selection method. Wrapper methods evaluate multiple models using procedures that add and/or remove predictors to find the optimal combination that maximizes model performance. The Recursive Feature Elimination (RFE) model works by recursively removing features and building a model with features that remain. It is a backward feature deletion method which ranks the features in the order in which

the feature is removed wherein the top ranked features are removed in the last iteration and are the most important [158]. This has been discussed in greater detail in Section 2.2.2b.

RFE requires that an initial model be used to perform the iterative process. We chose a logistic regression model with an LBFGS optimizer to be fit to determine the best subset of features.

3.5.3 Tree-based feature selection

Tree-based estimators use the intrinsic abilities of the decision trees and the ensemble methods discussed in Section 3.4.5 and 3.4.10. These methods compute impurity-based feature importance which can be used to discard irrelevant features. The impurity score can help rank the features and the feature with the lowest impurity is often ranked the highest. This enables an understanding of which feature enables the best separation between the classes. We used the ExtraTrees ensemble classifier to rank and determine the best performing subset of features.

The final dataset used to refine the machine learning models comprised a subset of the dataset developed in Section 3.3. The final features selected were those that were common through all the different feature selection methods and will be presented in the next few chapters of this thesis.

4 ANIMAL MODEL OF SPINAL CORD INJURY

Rodent models have been used extensively in the investigation of the pharmacology and pathophysiology in neurogenerative disorders [192]. Rat models in particular, are widely used in SCI models due to the lower cost of care, a well understood anatomy and well-established analysis techniques [145]. Measurements of the ANS play an important role in the evaluating the impact of the interventions on stress[193] as well as parameters such as the cardiovascular health of the animal or overall autonomic function[194], [195]. These physiological measurements of ANS function include measurements of ECG and derived features such as heart rate [196] or blood pressure [197], [198].

Different approaches to measurement of the rat physiology have been adopted by researchers over the years. They can be broadly divided into invasive (in-dwelling catheters, sensors, etc.) and non-invasive measurements (tail-cuff/surface electrodes). Invasive techniques often include the use of radiotelemetry- which is considered the state of the art in the monitoring of physiological functions in awake and freely moving rats[199]. However, radio telemetry often requires highly invasive surgery to be performed on the animal in order to implant the transmitters, which may lead to a higher chance of infections[197]. Moreover, the animals need to be above a minimum bod weight to be implanted with the sensors, which prevents the study of younger animals[200]. Additionally, one transmitter is dedicated to a single animal for the duration of the study. With each transmitter being quite expensive , a large amount of capital is often required for the purchase of suitable equipment[201].

Noninvasive approaches such as using tail-cuff sensors or surface-based electrodes can be accurate and consistent. Moreover, noninvasive techniques such as surface electrodes or tail-cuff manometry for BP measurement are easier when monitoring physiological parameters in conscious animals [199]. The lack of reliance on a battery allows their use for an indefinite period of time throughout the study. Additionally, these non-invasive systems can be used between different animals in a study[197]. Lastly, they are significantly less expensive than radio telemetry devices. However, non-invasive techniques often require a restraint mechanism which may lead to alterations in data due to restraint-induced stress artefacts [201], [202]. These can be

overcome through an acclimation protocol which can wane the responses in the rat elicited by a novel stimulus[203].

4.1 Justification of Rat Model

The human model of the ADDS was developed with self-reported symptoms of AD. While developing the ADDS in the human model, it was established that there were difficulties with controlling the onset of AD. The cause of the AD was not controlled, and neither was the timing of the onset of AD which may have led to confounders in the data [152]. In prior studies, AD has been induced in human studies through urodynamic assessments, but it often poses a risk to the individual since AD can have long term effects[189]. Furthermore, it is currently very difficult to study the onset of AD in humans with acute SCI since there are other complications which require urgent care during the rehabilitation phase after the injury[204]. The rat models enable us to perform controlled studies and using large subject samples has previously been difficult to achieve in naturally occurring instances of dysautonomia in humans. The rat models would enable greater investigation of the mechanisms of the onset of AD, determining its relative severity, and possible methods for intervention.

4.2 Acclimation of rats to sensors

Acclimation plays an important role in reducing the variability of behavior of the rats as it may mimic heightened anxiety, which can interfere with the measurements of the ANS [203]. Sympathetic activity is most commonly triggered in stressful situations. In order to reduce chances of confounders such as stress due to exposure to new settings, the animals were acclimated for eight weeks prior to the collection of relevant data as well as the SCI surgery. Several acclimation protocols have been created for different restraint mechanisms for varying measurement purposes. A large number of restraints are often animal holders in the form of plastic tubes produced by different companies. Some companies recommend that the animals are placed in the holder for atleast 10 to 15 minutes before non-invasive measurements[197]. Additionally, training of the animals for three consecutive days for 15 minutes prior to the beginning of measurements are recommended [205]. Mongue-Din and his colleagues include use of a simple tunnel in which the animals are placed five minutes prior to beginning of the

ECG recordings [200]. However, these techniques have not shown comparisons of the impact of long-term restraint acclimation on the physiological measurements. King et al place their animals in a “mock scanner” comprising of a plastic tube and simulated fMRI noises to acclimate the animals to the setup for up to 90 minutes per session for a week [206]. Gamaro et al restrained the animals for an hour daily for five days a week for 40 days to allow adjustment to the restraint and used a tail-flick technique to assess the habituation of the animals[207]. Similarly, Reed et al. acclimated their animals for five days prior to the fMRI experiment in an animal holder[208]. However, these techniques have only explored the impact of acclimation to a restraint using single sensors. There has not been any literature which details the acclimation protocols adopted by the different researchers in order to reduce stress experienced by animals during non-invasive measurements of ANS activity from multiple sensors.

4.2.1 Acclimation Protocol

We developed an acclimation to allow the rats to get acclimated to a restraint and a multimodal sensor. These are crucial in order to reduce the impact of stress on experiments which study the activation of the ANS. We have assessed the impact of acclimation to repeated restraint on the physiological measurements and stress levels experienced by the animals.

The rats are acclimated in plastic holders with air holes, as used for tail-cuff measurements (HLD-RL model, Kent Scientific, USA). A darkened nose cone is used to limit the animal’s view and provide a dark environment the rat is comfortable in. The nose cone is adjusted such that the rat does not move excessively, and its nose protrudes from the front of the nose cone in order to allow comfortable breathing. Additionally, the plastic restraint was placed inside a blackout box which allowed for greater darkness, which is known to reduce stress experienced by the rats (Figure 20).

Figure 20: Plexiglas container to restrain the rat. The red box allows a perception of darkness to enable the rat to feel more comfortable. The restraint is tightened sufficiently to allow the rat to breathe comfortably but also reduce movement.

The acclimation protocol developed comprises three phases which are incremental in nature. This is done in order to maximize the comfort of the animal and reduce stress as much as possible. The three phases include familiarization with the researchers, acclimation to the restraint and acclimation to the sensors used in the study.

a) *Phase One: Acclimation to Researchers and Environment*

After the rats arrive in the housing facility from the breeding facilities, they were allowed three days to adjust to their new environment. On day three the researchers introduced themselves to the rats, starting with just a hand in the cage to familiarize the rats to the scent. The rats were then introduced to the yummy foods which would later be used as a reward mechanism These yummy foods include peanut butter, apple sauce and Ensure®[209]. The researchers began to tickle the rats on day four and continued this throughout the acclimation process[210]. This enabled easy handling of the animals and ensured that there was limited stress during the interaction between the researchers and the rats.

b) *Phase Two: Acclimation to Restraint*

On day eight the rats started the familiarization process with the restraint. First the Coda® plastic holder was placed in the cage with yummy food at the end of the nose cone. The rats were allowed to explore the holder without being restrained in it. The holder was placed for a duration of 10 minutes on day eight so the rats would enter the holder without any coercion. On days nine and ten the rat was taken out of the cage and placed in the holder with a restraint inside a blackout box (Figure 2). The rat was allowed to voluntarily enter the holder and a restraining

piece was placed at the end of the holder to prevent the rat from leaving the restraint. The nose cone was adjusted to the appropriate size for each rat [197]. The rat was kept in the restraint for five minutes on day nine. This duration of time was incremented by an additional five minutes a day on days 10 and 11. While the rat was in the restraint, the researchers provided positive reinforcement through yummy foods, and disrupted the animal as minimally as possible. This included ensuring no additional sounds in the environment and keeping the baseline sound levels under 50dB. We monitored the animal was any forceful thrashing of the or any additional scurrying.

c) *Phase Three: Acclimation to Sensors*

After the establishment of comfort within the restraint, the rats were acclimated to the wearable sensors starting from day 11. First the blood pressure tail cuff was introduced. On days 11 and 12 both the occlusion and VPR cuffs were placed on the rat's tail without any inflation. On days 13 and 14 the rats were introduced to the inflation of the cuff. Days 15 through 18 the rat was introduced to the entire system of sensors. To attach the electrodes the rats were placed under anesthesia and the hair where the electrodes were placed was removed through shaving and using hair removing cream (Nair™). The shaved area was cleaned with 70% alcohol, and the electrodes were placed with additional conductive gel. The rat was then placed in the restraint and the blood pressure cuff was added to the rat's tail. All sensors were hooked up to the instrumentation and data was collected. The rat was placed in the restraint for incremental periods of time from days 15-18. After day 18, the rats were placed in the restraint for the entire duration of future studies (~30 minutes). This was continued until the rats were ready for surgery.

4.2.2 Evaluating impact of acclimation

The signal processing techniques discussed in Section 3.2 were used to extract features from each trial during Phase Three of the acclimation protocol (day 15 onward). We evaluated the changes in heart rate and blood pressure which are known measures of stress in the rodent, as well as measures of sympathetic activity (average values of skNA and Number of bursts). Significant changes over the course of acclimation were determined through an ANOVA test on the normalized feature values during each acclimation day. Heart rate and number of bursts were the only features which had statistical significance ($p<0.05$). The changes are shown in Figure

21 below. The overall decrease shown in heart rate as well as the indication of reduction in sympathetic activity suggests that there is a reduction in the level of stress experienced by the rat as it acclimates to the sensor setup over the course of the final phase of the protocol.

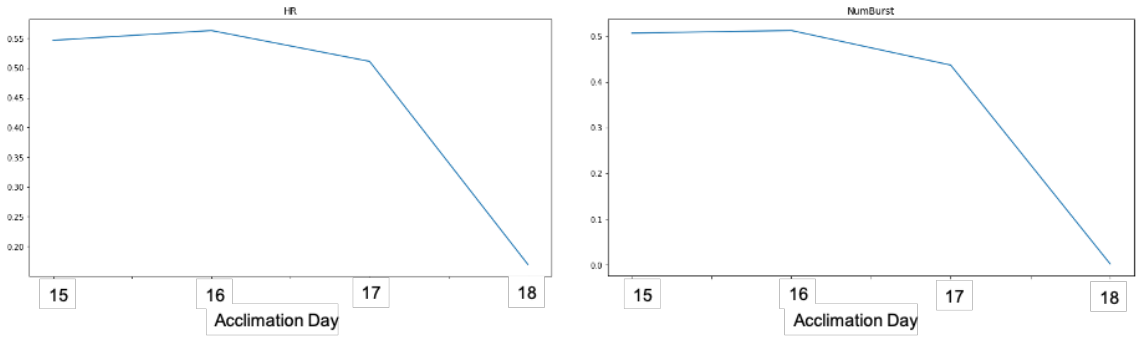

Figure 21: Decreases in normalized heart rate and the normalized number of bursts of iskNA over the course of the acclimation days suggests that there is lesser stress associated with the wearing of sensors. While this protocol does not eliminate all stress, it reduces the chances of confounders affecting the data.

4.3 Validating the use of skNA to detect sympathetic activity

An acoustic startle was used to elicit sympathetic activity in the rats [211]. A cycle of acoustic startle lasted 60 seconds. The cycle consists of three acoustic periods lasting 5 seconds each. Each period comprises three 1-second pulses of white noise. The highest values of the acoustic startle ranged from 108 to 112 dB with background noise below 50dB[212]. Three cycles were repeated on each animal on two different days. The acoustic startle was played through a loudspeaker attached to a computer and was triggered through a button press.

Five male Sprague Dawley rats aged 4 months (320-450 grams) were used in this experiment. All rats in the protocol had detectable changes a change in cardiovascular parameters and skNA in response to acoustic startle. A significant increase ($p < 0.05$) in both systolic and diastolic blood pressure was observed during the acoustic startle. On average, the rats experienced and an increase in systolic blood pressure (SBP) of 21 mmHg with an increase in diastolic blood pressure (DBP) by 22 mmHg. During acoustic startle, all the animals showed a significant increase ($p<0.05$) in both heart rate and skNA. On average, the rats showed significant tachycardia of 30.2 ± 8.8 bpm during acoustic startle. Figure 22 is a representation of the increase in skNA, represented by iskNA and the heart rate of one animal. The resting skNA can be accounted to basal nerve activity in the stellate ganglion. A 191.5% increase in iskNA

magnitudes was also observed during the acoustic startle. A positive correlation (r= 0.72) was found between skNA and heart rate in all animals due to the acoustic startle. The resting skNA can be attributed to basal nerve activity in the stellate ganglion.

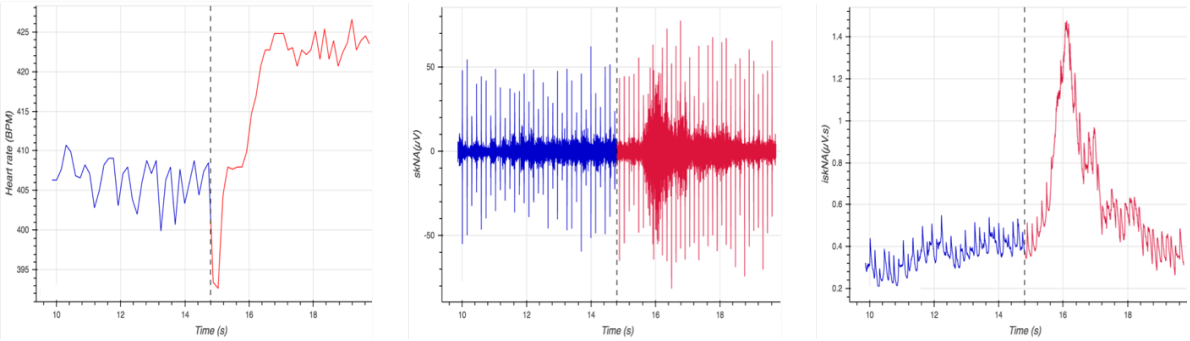

Figure 22: Representative graphs of showing A) increase in heart rate B) acceleration in raw skNA C) increase in iskNA due to acoustic startle (showed by dashed lines and different colors)

The acoustic startle response (ASR) is a common, automatic reaction to a loud stimulus, and it occurs in vertebrates ranging from zebrafish to humans[213]. While ASR is often measured as a motor response, it can be characterized through its autonomic components including cardiovascular responses[214], [215]. Studies have shown that acoustic startle often leads to tachycardia and an increase in blood pressure. This is in agreement with the observed results allowing us to validate the use of skNA as a viable option to detect sympathetic activity in rats. Prior research has shown the ability to identify skNA changes in dogs and humans. Through this work, we conclude that sympathetic activation can be detected through skNA in a rat model. skNA has been validated to be strongly correlated with the stellate ganglion nerve activity[166]. We observed a strong, positive correlation between heart rate and skNA and also observed a linear trend between the increased blood pressure, skNA and heart rate.

4.4 High Thoracic Spinal Cord Injury Surgery

Animal models play a key role in developing therapies and understanding cellular pathologies of SCI. A majority of experimental SCI research employ animal models with lower level SCIs including lower thoracic, and caudal[216](Figure 23). However, a majority of SCIs occur at higher levels and various complications, including AD are specific to higher level injuries[50], [217]. There is a relatively small group of researchers who focus on higher level

injuries due to the complications and comparatively higher mortality rate. In order to study AD effectively, we needed to develop an animal model with an injury level above T6. We developed a repeatable T3 level compression injury model which incorporates techniques presented by Ramsey et al[209], Blight[218] and Shi, Borgens [219], [220] .

4.4.1 Surgery

All SCIs were performed when the animals are approximately 4-5 months old and between 400-600 grams. The animals were firstly anesthetized using 4% isoflurane. They were then shaved closely and cleaned with Betadine. Once a plane of anesthesia was confirmed using a toe pinch reaction, the rats were moved under a dissecting microscope and draped under aseptic conditions. A plane of anesthesia was maintained using 2.5% isoflurane. The spinal cord was exposed through a midline incision (T1-T5) and a one-segment laminectomy at the T-3 level using a pair of rongeurs. A dorsal hemisection or a right lateral hemisection can be produced using a micro-dissecting knife after the dura is removed with a pair of Dumont microsurgery forceps and Vannas spring scissors. A specially designed pair of forceps was used for the compression injury. The forceps are at a thickness of 1.2 mm and the length of compression is 15 seconds. The forceps cause ischemia and mimics common clinical injuries. The injury was verified through visual observation of the damage to the spinal cord determined by the ischemia and clotting patterns seen in the spinal cord. The laminectomy and skin incision were closed with 4-0 prolene suture and the skin incision will be closed with Michel wound clips 7.5 mm.

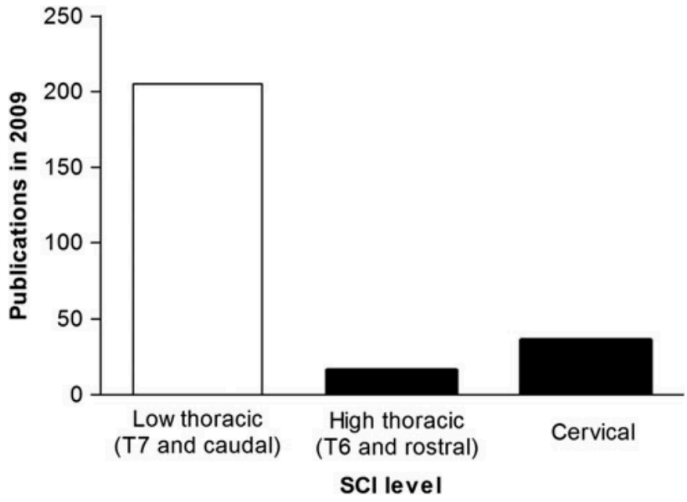

Figure 23: A breakdown of animal models for SCI from a literature search conducted by authors of [216]. High thoracic was defined as injuries between T1-T6 and low-thoracic (T7 and caudal). Studies employing models of SCI induced at levels below T7 outnumber studies of SCI at more rostral levels

To validate the SCI, motor and sensory control in the hindlimbs is evaluated. The animals were observed on an open tabletop to gauge their ability to support their weight and use their hindlimbs for movement. An uninjured animal would walk briskly with the hindlimbs beneath the body. Sensory control in the hindlimbs was evaluated through a toe pinch wherein the toes of an extended hindlimb was pinched using forceps. An uninjured animal would withdraw the limb in a flexion reflex.

4.4.2 Care of Animals post-SCI

The rats received multimodal analgesia- buprenorphine (0.1mg/kg SC) two times a day and Meloxicam (1- 2mg/kg SC) one time a day for 5 days post-surgery with regular bladder expression. Urinary Tract Infections (UTI) have been noted as a complication post-op in rats with higher level spinal cord injuries. To reduce the chances of UTIs, the bladder of the animal was manually expressed 3-4 times a day for the first week post-op. We observed for clinical signs of UTI including cloudy, discolored or foul-smelling urine in addition to difficulty in manual expression. We would also increase our monitoring of animals which are suspected of having a UTI and increase manual bladder expression. Additionally, we provided more absorbent bedding for the rat post-SCI in order to reduce chances of UTI.

Weight loss is also a consequence of an SCI. We observed the animals' weight daily post-op and while early weight loss is anticipated, we will begin oral gavage using diet gel or Ensure® nutrition powder at higher than 10% weight loss. A weight loss of greater than 20% is a humane endpoint and the animals will be euthanized immediately. In order to prevent excessive weight loss, multi-modal analgesia was provided for the first 3 post-operative days, and if there is no recovery in weight 5 days post-op, novel yummy food was introduced into the diet of the animal. Dysstasia is sometimes seen in animals with a compression injury and care was taken to replace bedding every two days post-op to prevent urine scalding.

The animals were euthanized in the event of intractable autophagic lesions, which may be expected in a small percentage of animals. Minor superficial lesions were treated with cleaning, bandaging of the affected hind limb, in addition to appropriate antibiotic treatment. We also followed a composite score [209] to determine the post-op health of the animal. If they hit a score of 20, the animals were euthanized- determined by 20% loss in weight post SCI and other factors. A detailed care manual is provided in Appendix A.

4.5 Validating Extracted Features

The impact of SCI on physiological parameters have been extensively explored in literature[204]. It is well established that sensorimotor and autonomic dysfunctions often occur after spinal cord injury. Due to reduced sympathetic activity, patients with SCI may experience hypotension as well as cardiac dysrhythmias[221], [222]. This is particularly notable in the measurement of heart rate and blood pressure. However, few researchers have combined a multitude of sensors to develop a system which can identify these changes before and after a spinal cord injury.

We compared the values of features extracted (Section 3.2) from sensor data collected on last day of acclimation prior to spinal cord injury surgery to the baseline values collected five days post-surgery. This reduced any potentially confounding effects of the analgesic drugs provided to the animals post-surgery. A t-test was used to compare significant changes in the features between the data pre-SCI and post-SCI. The decrease in heart rate and systolic blood pressure (SBP) were significantly different ($p<0.05$), but the resulting change in mean arterial

blood pressure (MAP) was not significant. Additionally, there are significant decreases in the average value of the integrated skin nerve activity (iskNA) post-SCI which represents a decrease in sympathetic nerve activity post SCI. Similarly, there is also a significant decrease in the percentage of NN intervals which are greater than 5ms, suggesting a reduction in vagal activity post-SCI.

Overall, we are able to observe an expected decrease in autonomic function post-SCI (Figure 24) which is in agreement with the extensive literature of expected changes in cardiovascular and neural function after SCI, allowing validation of the functionality and calculation of the relevant features.

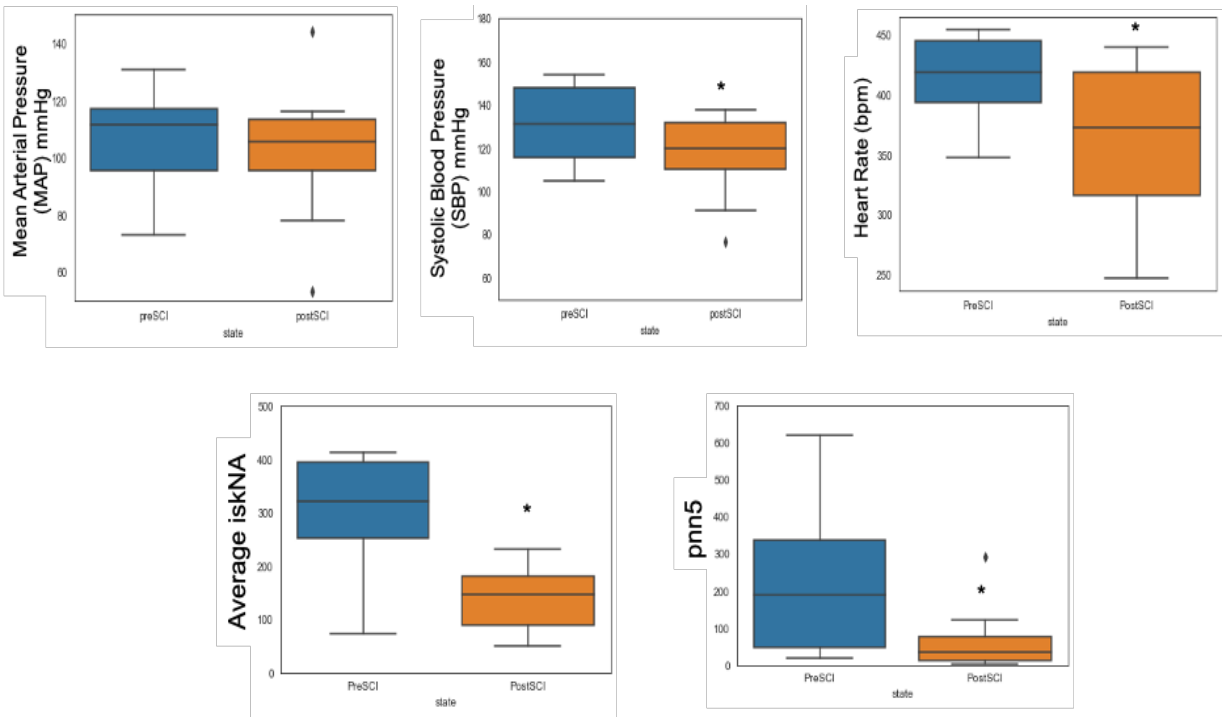

Figure 24: Expected decrease in autonomic function post-SCI represented through mean arterial pressure (MAP), systolic blood pressure (SBP), heart rate, sympathetic rate, sympathetic function (AUC iskNA) and the parasympathetic function (pnn5). * indicates significant difference ($p<0.05$).

5 CHARACTERIZING AUTONOMIC DYSREFLEXIA

Research Question: Do readings by novel, non-invasive physiological sensors change in accordance with what is expected during the onset of AD? Can we characterize AD through a combination of these sensors?

For this study, sensor data was collected from nineteen male Sprague-Dawley rats between the ages of 4-5 months (400-600g). The animals were received when they were 1 month old (~200 g) and acclimated to reduce confounding effects of stress on the characterization of AD. All animals were given dorsal laminectomies followed by an SCI due to compression at the T3 level [223] as discussed in Section 4.4.

5.1 Hypothesis

We hypothesize that the different sensors will display changes in electrophysiological signatures when AD is induced. We hypothesized these differences will be due to the individual neurophysiological and anatomical characteristics of the sympathetic outflow circuit. While the current clinical gold standard (change in blood pressure) is an indirect measure of sympathetic activation, skNA is a direct measure of the sympathetic nervous activity. We anticipate that a combination of the sensors which detect activity of a paravertebral ganglion and other non-invasive sensors will detect AD rapidly and enable characterization of AD through alternate measures.

5.2 Eliciting AD through colorectal distension

Bladder and bowel related issues are often the most commonly reported triggers of AD in individuals with SCI. We used colorectal distension (CRD) in order to control the onset of AD in the rats post-SCI [223], [224]. Seven days post-injury, the rats were anesthetized with 4% isoflurane and outfitted with the sensors discussed in Section 3.1. A Foley catheter with a balloon (Figure 25) was inserted 2cm into the rectum of the animal. The animals were then placed in the plexiglass tube discussed in Section 4.2.1 and allowed to recover and acclimate for 10 minutes. CRD was induced starting at 10 minutes by infusing 2ml of air into the catheter

causing distension of the colon and was maintained for 1 minute. CRD was repeated 3 times per trial with a minimum interval of 10 minutes between them. The CRD was performed on days 7, 9, 11, and 14 post-surgery in order to mimic the most common onset of clinical AD in humans.

Figure 25: A Foley catheter with a balloon was used for colorectal distension to induce AD.

5.3 Data Analysis

In order to ensure that the CRD trials led to the onset of AD, the corresponding change in systolic blood pressure was monitored. Only CRD trials which led to an increase of atleast 15 mmHg in SBP were considered AD events [225]. From the 130 instances of CRD that were recorded from the rats, 91 led to onset of AD (70.6%). This is in agreement with literature which supports that between 48-82% of individuals with injuries above the T6 level with SCI experience AD[55], [226].

Features were extracted from the cleaned signals collected from the selected trials through non-overlapping windows of 5-60 seconds as described in Section 3.2. The thirty-six features extracted from the time-series sensor data were normalized, and feature selection techniques described in Section 3.5 were used to narrow down features. A t-test was used to determine any significant changes in the features as a result of AD. These selected features characterize the minutia of physiological responses of sympathetic and parasympathetic activity, due to the onset of AD.

5.4 Signature Recognition through Feature Extraction

As described in Section 3.5, feature selection enabled five features to be selected from the thirty-six features extracted. These five features were determined to be highly significant and relevant in the characterization of AD. The features are representative of the sympathetic activity through changes noted in the number of bursts of sympathetic nerve activity and average value of the integrated skNA (iskNA). Vagal activity was represented through changes in the median value of the NN intervals (medianNN), the root mean square of successive differences (RMSSD), the percentage of number of NN intervals greater than 5 ms (pnn5).

5.4.1 Characteristics of AD through signature changes

AD is characterized by a hypertensive event triggered by hyperactivity of the sympathetic nervous system. This activity is centrally counteracted by baroreceptor mediated vagal activity leading to a decrease in heart rate and vasodilation above the level of the injury [227]. We were able to capture this co-activation of the sympathetic and parasympathetic branches of the ANS through statistically significant increases in features (Figure 26).

We also observed a statistically significant decrease in the heart rate over the course of the AD event (Figure 27) which has been well-established in the literature. There were also statistically significant increases in SBP by an average of 19.8 mmHg, in DBP by 13.9 mmHg and in MAP by 15.2 mmHg during the AD events.

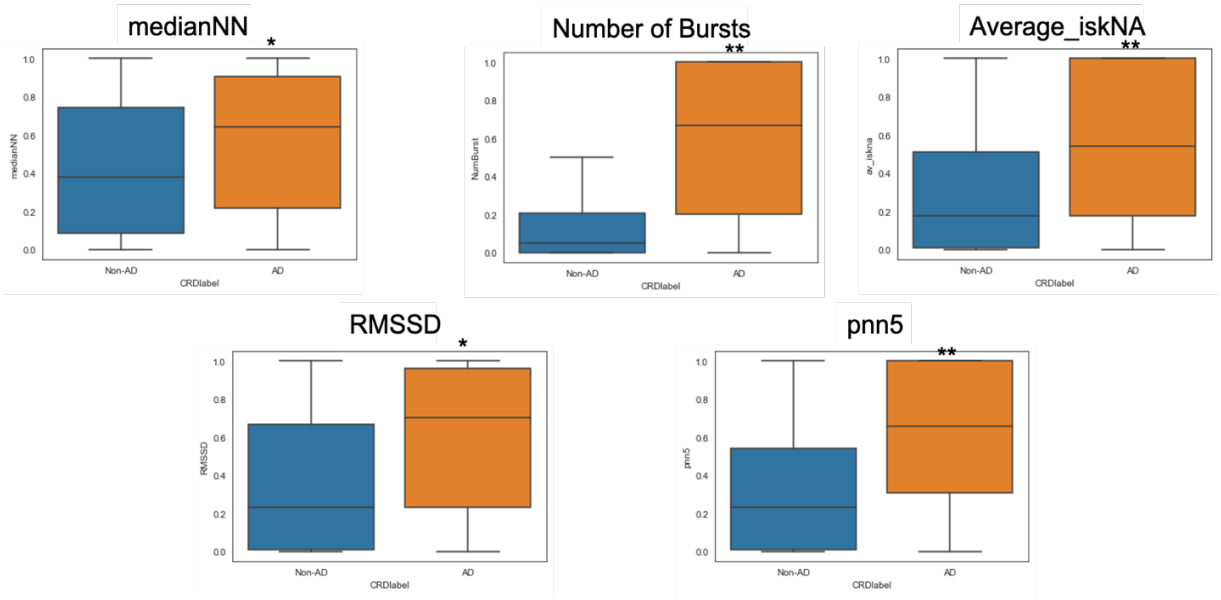

Figure 26: Significant increases observed in the five features due the onset of AD. MedianNN, Number of Bursts and Average iskNA characterize the increase in sympathetic activity whilst the RMSSD and pNN5 represent the increase in parasympathetic activity. The y-axis is the normalized units of each feature. * significant difference ($p < 0.01$), ** very significant difference ($p < 0.001$)

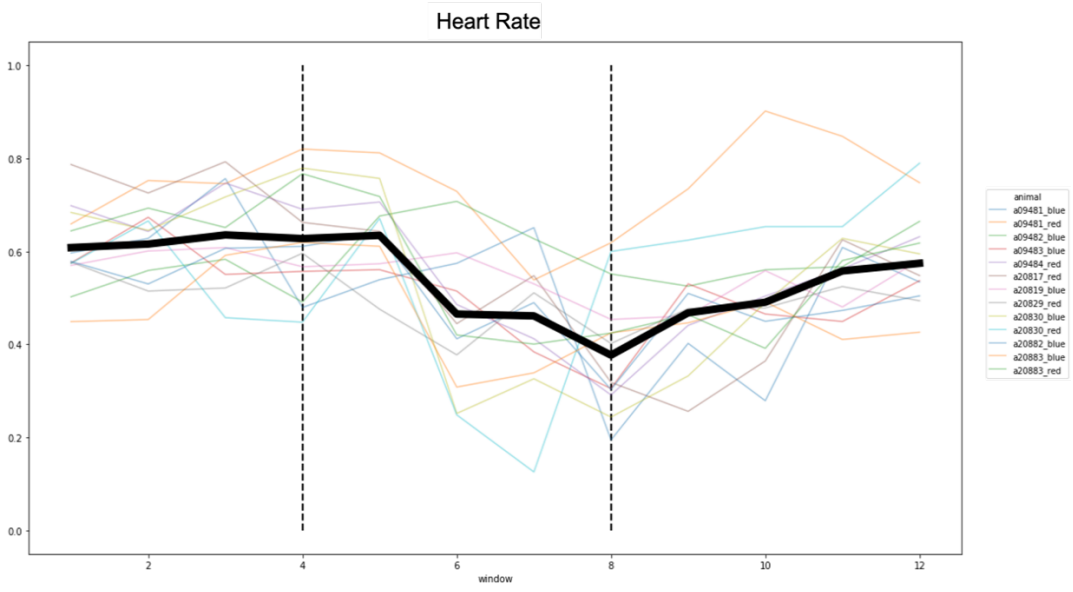

Figure 27: Significant decrease in the heart rate over the course of the AD event (indicated through the dashed lines) as a result of the vagally mediated response to the increase in the sympathetic activity. After the stimulus is removed, the heart rate returns to pre-AD levels.

In addition to these well-established metrics of AD detection, we were able to observe the cascade of sympathetic and parasympathetic activity on a higher time-scale resolution of 15 seconds (Figure 28) through our sensors. We observed an initial increase in sympathetic activity elicited by the onset of AD (dashed lines in Figure 28) characterized by the increase in values of the average iskNA and the number of bursts detected through the skNA sensors. This was followed by a subsequent increase in vagal activity characterized through the increase in the RMSSD and pnn5 features towards the end of the AD episode.

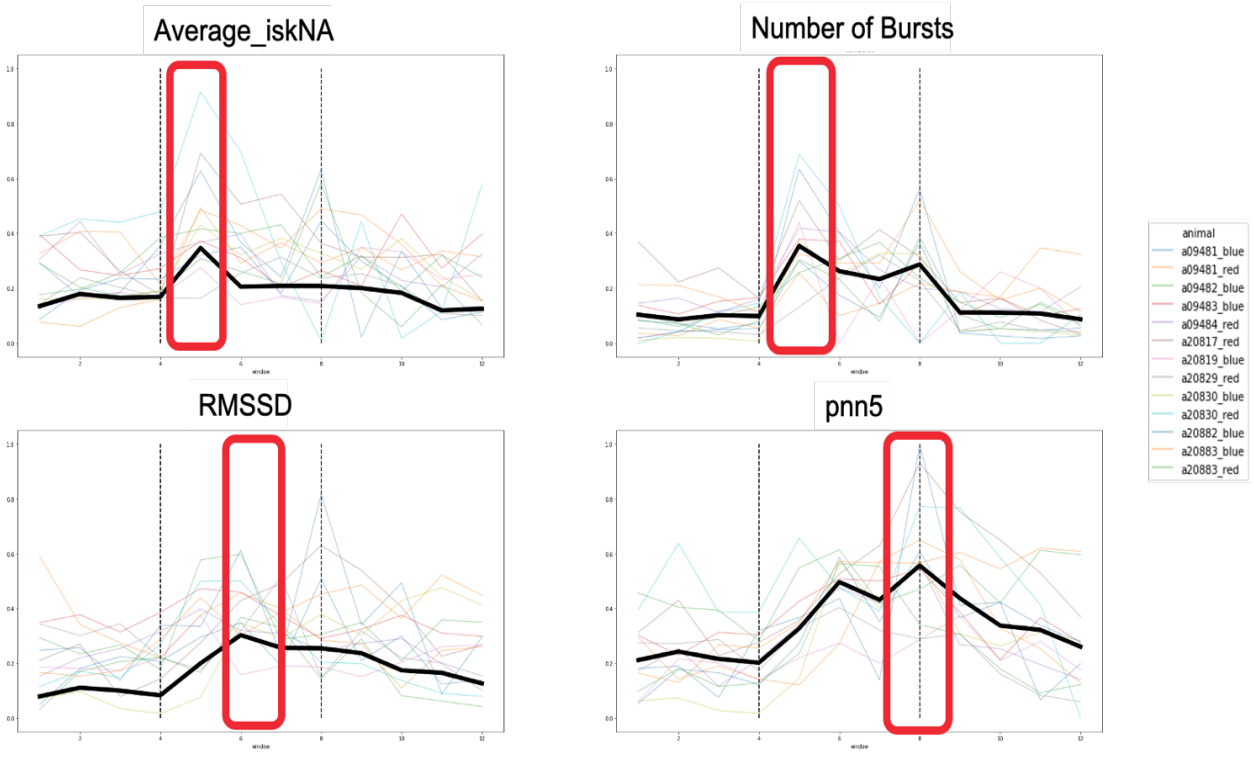

Figure 28: Increase in sympathetic activity (average iskNA and Number of bursts) detected prior to the increase in parasympathetic activity (RMSSD and pnn5). The y-axis is the normalized units of each feature while the x-axis represents windows of 15 seconds each.

5.4.2 Discriminating AD from non-AD using Machine learning

Eleven classification algorithms described in Section 0 were trained using the dataset developed using the AD and non-AD data. AD events were labelled as 1 while non-AD events will be labeled as 0. We performed a 10-fold cross validation algorithm, and evaluation of the various metrics generated by the different classifiers (Table 5). We determined that the best performing classification algorithm was a 5-layer neural network based on the accuracy as well

as specificity and sensitivity of the model. The neural network was able to distinguish AD from non-AD events with an accuracy of 93.4%, a sensitivity of 93.5% and a specificity of 93.3%. Additionally, it also had an AUC-ROC of 0.93 suggesting that the neural network was able to distinguish between the two classes with a high level of confidence.

Table 5 : Performance Metrics for the different classifiers with the AD dataset.

Name	Accuracy (%)	Sensitivity (%)	Specificity (%)	AUC-ROC
Neural Network	**93.4**	**93.5**	**93.3**	**0.93**
Adaboost	79.3	79.3	79.2	0.78
Decision Tree	86.1	83.3	89.5	0.86
Gaussian Process	91.7	88.9	94.4	0.92
K Nearest Neighbor	86.5	83.3	89.5	0.86
Linear SVM	62.2	30.1	86.7	0.61
Logistic Regression	87.4	84.3	82.5	0.87
RBF SVM	63.9	72.2	84.2	0.64
Naïve Bayes	88.9	94.4	83.3	0.89
Quadratic Discriminant Analysis	88.9	94.4	83.3	0.89
Random Forest	63.9	72.2	84.2	0.64

5.4.3 Impact of Repeated Induction of CRD on AD

CRD was repeated in the animal four times on days 7, 9, 11 and 14 post-injury to mimic onset of AD through an equivalent of 1.5 years of human years post SCI [228], [229]. While there was a statistically significant difference between the features during AD and non-AD; we observed that there was no significant difference in the AD features across the days using a one-way ANOVA (Figure 29). Similarly, there was no significant difference in the baseline (non-AD) features over the course of repeated onset of AD. This suggests that in the short-term (14 days post SCI), AD was still being triggered by CRD and its onset led to significantly different changes in ANS activity.

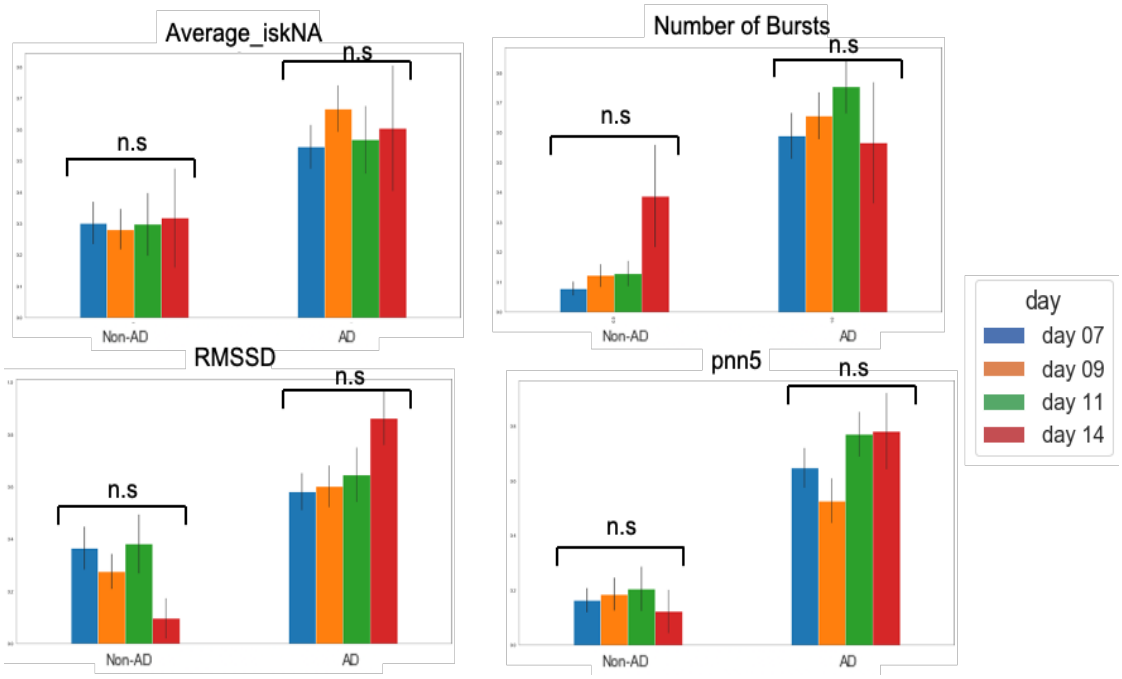

Figure 29: Repeated induction of AD over four trials caused **no** significant variation in the increase in the observed activation of the sympathetic and parasympathetic parameters over trials conducted on days 7(blue), 9(orange), 11(green) and 14(red).

5.5 Discussion

This study demonstrated the following. 1) the onset of AD is characterized by a cascade of sympatho-vagal discharge wherein we see an initial sympathetic discharge followed by a subsequent concomitant vagal discharge towards the end of the AD episode. 2) A neural network can be trained to distinguish between AD and non-AD events and can detect the onset of AD with a 93.4% accuracy. This study provides us with a non-invasive, wearable system which can clearly quantify the onset of AD and provide further insight into the temporal changes during AD.

5.5.1 Characterizing signatures of AD through non-invasive sensing

The sympatho-vagal cascade due to the onset of AD is well understood in clinical literature [51], [55], [230]. The stimulus below the level of injury triggers sympathetic hyperactivity by stimulating the neurons in the intermediolateral gray mattery of the spinal cord. This sympathetic neural outflow generates the hypertensive blood pressure response during AD. This leads to vagal activity in response to the systemic changes occurring in the body. The

hypertension leads to the activation of the carotid and aortic baroreceptors leading to a decrease in heart rate through the vagus nerve. All signs and symptoms of AD are attributed to hyperactivity of the sympathetic impulses below the level of injury and the compensatory parasympathetic activation above the level of injury[231]. However, there is no tool which characterizes the resultant physiological cascade from the onset of AD through multiple sensing modalities, which may lead to better understanding for either improved diagnosis or therapeutic intervention.

Currently AD is characterized clinically through stand-alone measurements of blood pressure through ambulatory blood pressure systems or arterial blood pressure telemetry devices[223]. However, these measurements of blood pressure do not monitor the beat-by-beat changes of other hemodynamic parameters associated with AD. Through our multimodal system, we characterized AD on a greater temporal resolution through the five ANS physiological features that we identified as most relevant to this sympatho-vagal cascade. The onset of AD was validated with traditional techniques of blood pressure measurement. AD triggered by colorectal distension led to clinically recognized increases in systolic, diastolic blood pressure, and mean arterial pressure[55] as well as the induced bradycardia (Figure 27). The features were extracted from the ECG and novel skNA sensors showed an overall increase in sympatho-vagal activity as well as an in-depth exploration of the sympatho-vagal cascade which occurs due to the onset of AD.

Sympathetic activity was characterized principally by changes detected through the skNA sensors. skNA has been extensively validated as a non-invasive surrogate for stellate ganglion nerve activity [232]. The stellate ganglion is known to be an important source of cardiac sympathetic innervation and also gives rise to sympathetic nerves which innervate blood vessels and sweat glands in the skin [233], [234]. The cardiac preganglionic sympathetic fibers (T1-T4) synapse onto postganglionic neurons in the stellate ganglia in addition to other ganglia. Sympathetic preganglionic fibers originating from T5-T9 spinal cord levels bypass the paravertebral ganglia and synapse onto postganglionic neurons in the stellate ganglion[235]. Increases in the average value of the iskNA suggest an increase in the sympathetic tone during the onset of AD. The increase in the number of spikes/bursts over the duration of the AD allow

assessment of the transient increase in synchronous firing of the stellate ganglion [236]. The sympathetic discharge occurs within 15 seconds of the introduction of the noxious trigger. However, one of the limitations of the skNA sensor is the inability to gauge parasympathetic activity[237].

Heart rate variability metrics from ECG have been extensively explored in the literature to identify changes in ANS function. While parasympathetic activity can be gauged through changes noted in the ECG data, they lack the temporal resolution to determine sympathetic tone on a second-by-second basis [238]. Towards the end of the AD episodes, a sharp increase is noted in the RMSSD and the pnn5. RMSSD is a reflection of the beat-to-beat variance in the heart rate and often estimates the vagally mediated changes reflected in the heart rate variability[239]. Similarly, pnn5 is closely related to parasympathetic activity [240]. Both these metrics are often more reliable indices for parasympathetic activity for short-term measurements and are strongly correlated with spectral components of the ECG. The LF and HF spectral component of the heart rate variability often provide insight into the sympathetic and vagal activity respectively. However, due to the low temporal resolution and extremely short duration of recording of AD (~60 seconds), there are not sufficient bins which allow conclusive evidence to be drawn from the spectral data, thereby reducing the interpretability of the extracted spectral features.

The combination of the non-invasive, wearable ECG and skNA sensors allow us to characterize the sympathetic and vagal co-activation during the onset of AD. The initial increase in sympathetic activity within seconds of introduction of the trigger is followed by parasympathetic activity towards the end of the AD episode. This signature coupled with the anticipated bradycardia and increase in blood pressure provides a quantitative understanding of the sympatho-vagal cascade which occurs during the onset of an AD episode. This unique characterization of AD has not been quantified on high temporal resolution prior to this work. This system can be used as a complementary tool to enable detection of AD earlier than the change in blood pressure, which is a result of sympathetic discharge.

5.5.2 Machine Learning as a Tool to characterize AD

The neural network created using the dataset was able to discern the differences between AD and non-AD data with an overall high-performance across all the relevant metrics. The use of blood pressure changes as the ground truth, led to a more comparable model. We prioritized the development of model which was accurate and has a high sensitivity and specificity. A balance between the sensitivity and specificity in the detection of AD ensures low false negative rates. A high false negative rate wherein the model did not detect AD when it was occurring could lead to serious medical consequences. In contrast, the incidence of false positive errors would be more of an inconvenience to users rather than not detecting episodes of AD at all. The model's high AUC-ROC (0.93) demonstrated the model's ability to detect the onset of AD symptoms with high accuracy with an inclination towards low false negative rates.

In our prior work, we used support vector machines with linear and RBF kernels to discern between AD and non-AD events[152], [159]. In the training of the SVMs we used a smaller dataset with four features. Additionally, the dataset had very limited overlapping data which allowed SVMs to perform well. The dataset developed in this study was a magnitude of order larger than the previous study. Additional feature selection also made it possible to choose the best combination of features which led to higher performance. The strong performance of the neural network as a tool to characterize AD also validates the trends observed in the temporal data collected from the sensor data. There are currently no other studies which attempt to use ML as a tool to detect the changes in physiology due to the onset of AD.

Through the neural network it is possible to translate the observed trends from a rodent model to a human analog. The model's ability to discern the differences between the two classes- AD and non-AD could enable the development of a universal detection model. Neural networks often perform well with larger training data and lead to better scaling. They have been used extensively in the field of medicine ranging from the use in stroke detection[241] to detection of cancer, as well as diagnosis of Parkinson's disease[242]. Future studies can leverage upon the dataset developed in this thesis to elicit a stronger performance from the model by introducing more data.

5.5.3 Impact and Relevance of the system

Recognition and prevention of AD related signs and symptoms plays a critical role in avoiding escalation to more dire circumstances in clinical and non-clinical environments. Currently the standard approach for managing AD is to train persons with SCI to recognize their symptoms and to promptly alleviate the AD trigger, which can be difficult to identify and frequently requires the assistance of a caregiver. There is a need for a need for a sensitive yet noninvasive method of detecting the onset of AD, which can be adopted easily into clinical practice and for at home use[151]. Additionally, there is no continuous monitoring the onset of AD before symptoms become extreme and potentially dangerous.

The major findings of this study suggest that there are alternate techniques to determining the onset of AD through non-invasive wearable sensing techniques. These could serve as complementary tools to ABPM in clinical and non-clinical settings if successfully translated to human trials. Additionally, a direct measurement of the sympathetic which leads to the increase of blood pressure, the current gold standard, could potentially lead to the ability of early detection of AD. The results presented in this research have demonstrated that skNA sensors can rapidly identify this change in sympathetic activity. The early detection of AD is critical as it mitigates shear stress on vasculature that develops during recurrent AD resulting in cardiovascular disease. A physiological-based AD detection system developed in this study can also allow the study of asymptomatic AD or 'silent AD', which can be equally harmful to cardiovascular end-organs due to a substantial rise in blood pressure without concomitant symptoms [150]

A non-invasive sensor system that can detect the onset of AD, can improve independence and quality of life of individuals with an SCI. Additionally, the implementation of the early detection system could allow individuals with more time to identify and eliminate the trigger before escalation to dangerous hypertensive levels. The innocuous nature of many precipitants of AD, often make it difficult to avoid the occurrence of AD. Tetraplegics experienced AD ranging from several times a day [243] to a few times in a month[57]. By combining the AD detection system with wireless mobile connectivity caregivers can be automatically alerted when AD is

occurring. This would enable tetraplegics greater autonomy to work, go to school, and participate in their communities knowing that if an AD episode occurs there will be emergency oversight.

5.6 Summary

We developed a system which combines non-invasive, sensing techniques with signal processing and machine learning models to detect the onset of AD in a rodent model. We were able to determine a unique signature which characterized the onset of AD through the concomitant changes in the sympathetic and parasympathetic branches of the ANS. We quantified the cascade of sympatho-vagal activity as a result of AD on a higher temporal resolution, which has not been explored in prior research.

We trained a neural network to distinguish between AD and non-AD events with high performance metrics. This machine learning model further developed in the next chapter can be translated to human models which would enable its use as a complementary tool in-clinic for the detection and management of AD in individuals with SCI.

6 DIFFERENTIATING SYMPATHETIC STIMULI

Research Question: Can we distinguish between the onset of AD and other sympathetic stimuli? Can a machine learning model learn to specifically distinguish between different triggers of AD?

For this study, data was collected from fifteen male Sprague-Dawley rats between the ages of 3-5 months (400-600g). The animals were received when they were 1 month old (~200 g) and acclimated to reduce confounding effects of stress on the characterization of AD. All animals were given dorsal laminectomies followed by an SCI due to compression at the T3 level [223] as discussed in Section 4.4.

6.1 Sympathetic Triggers

In addition to inducing AD through colorectal distension as described in Section 5.2, sympathetic responses were induced in the rats through other stimuli above and below the level of injury. The stimulus above the level of injury was induced through an acoustic startle. The acoustic startle was delivered in a similar fashion to the startle response in Section 4.3 with 1 minute of intermittent startle at 108 - 112 dB. The nociceptive stimulus below the level of injury was induced through a persistent tail pinch. The tail pinch was stimulated by a weight of 700g applied to the tail of the rat for a duration of one minute.

6.2 Hypothesis

We hypothesize that due to the different neural pathways involved, there will be a distinction in the features as a result of AD due to CRD and the sympathetic responses triggered by the acoustic startle and the persistent tail pinch. We expected these changes to be more evident in the sympathetic features rather in the parasympathetic features, as well as differences in the overall reactivity of the autonomic nervous system.

6.3 Varying Signatures due to different stimuli

The thirty-six features were extracted from the physiological data as discussed in Section 3.2. All the features were normalized by trial to ensure that changes occurring over the course of SCI did not affect the observed results. A one-way ANOVA was performed to determine any significant differences in features due to the different sympathetic stimuli.

AD led to a large increase in systolic, diastolic and the mean arterial blood pressure. The tail-pinch stimulus and startle also led to increases in observed blood pressure, but these changes were smaller compared to the hypertensive event observed due to the onset of AD ($p < 0.05$). When compared to baseline (non-stimulus) values of SBP, the AD and startle response led to significant increases while tail pinch did not lead to a statistically significant increase.

Table 6: Changes in blood pressure due to the various stimuli. Largest changes were observed due to AD. * indicates significant difference ($p < 0.01$) compared to baseline values.

Stimulus	Δ Systolic Blood Pressure (mmHg)	Δ Diastolic Blood Pressure (mmHg)	Δ Mean Arterial Pressure (mmHg)
AD	+19.8*	+13.9*	+15.2*
Tail-pinch	+5.5	+0.4	+0.9
Startle	+7.1*	+1.0	+2.1

Additionally, there was a difference in the sympathetic and parasympathetic responses observed through three features extracted from the sensor data. Changes in the number of bursts, average value of iskNA and percentage of nn5 showed that there were statistically significant differences in sympathetic and parasympathetic responses that permitted the differentiation among the different sympathetic stimuli. Startle led to tachycardia, while tail pinch did not result in significant changes in heart rate whereas AD led to bradycardia (Figure 30A).

When compared to baseline values, all three stimuli led to an increase in sympathetic activity characterized by an increase in the number of bursts (Figure 30B) with AD and startle causing significantly higher changes than tell pinch and no stimulus ($p<0.01$) (Figure 30B). However, there was a statistically significant decrease from baseline values in parasympathetic

activity due to the tail pinch characterized by a decrease in pnn5, while there was a statistically significant increase from baseline during AD and startle ($p<0.01$) (Figure 30D).

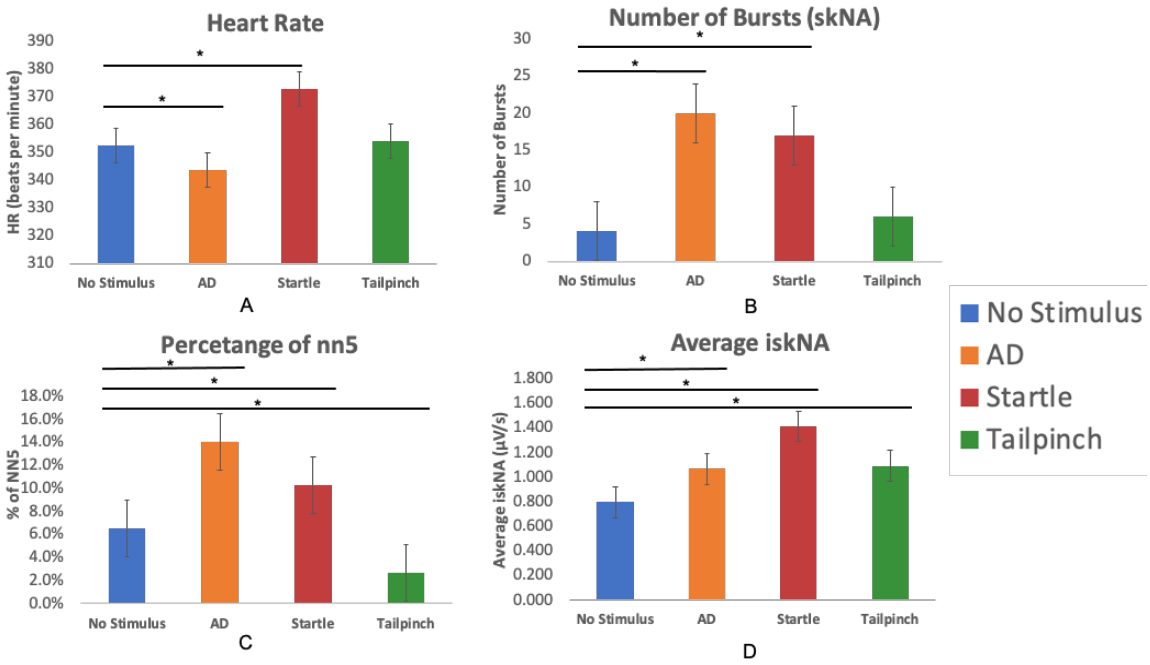

Figure 30: Changes in median values from non-stimulus of A) heart rate, B) number of bursts per minute C) pnn5 and D) average iskNA due to the different stimuli. * indicates significant difference ($p<0.01$) from baseline values

A one-way ANOVA indicated significant differences in three of the features (pnn5, average iskNA and number of bursts) across the three stimuli. There was also an observed overlap when visualizing the three stimuli on a bivariate plot shown in Figure 31, but the differences in the different distributions suggest the ability for discernment between the three stimuli as well as the absence of a stimulus.

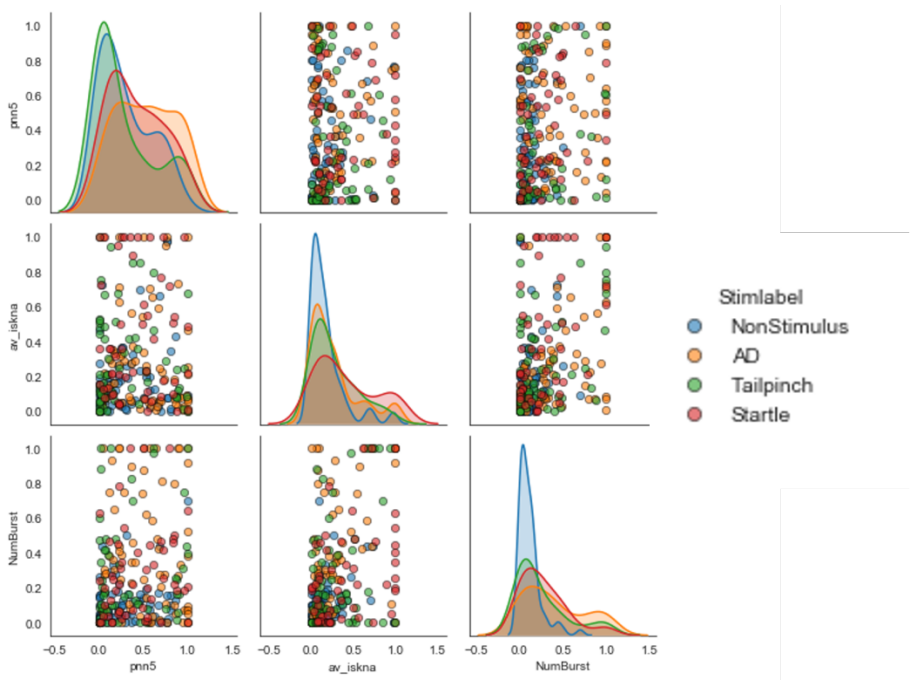

Figure 31: Bivariate plot representing the differences observed in the three statistically significantly different features due to the different stimuli. There is an observed overlap between the four classes but also some differences between the features which make them discernible. The y-axis are the normalized units of each feature.

6.4 Multi-class Machine Learning Model

We built upon the binary neural network discussed in Section 5.4.2 to develop a multi-class classifier to distinguish between AD, non-AD and other sympathetic stimuli. The features extracted from non-stimulus events were labelled 0, AD events due to CRD were labelled '1' while the features extracted during the tail pinch were labeled '2', and startle was labelled '3'.

70% of the dataset was used as training data with 15% of the dataset being used as a test set and 15% being used as a validation set. A 10-fold cross validation technique was used to test the performance of the neural network. However, unlike a binary classifier, the performance metrics gauged from the neural network were not accuracy and sensitivity. We instead reported the precision, recall and F-1 score as discussed in Section 3.4.1.

When trained on the multi-stimulus dataset with the three selected features, the neural network had a weighted average performance of 79% accuracy. However, it performed the best

on the detection of tail-pinch data with a precision of 0.91 and worst on the non-stimulus data. As can be observed in Figure 32 , this performance is likely because the non-stimulus data is falsely classified as AD data or tail pinch data. This likely leads to false positives in the model.

Table 7: Performance Metrics of a multiclass neural network built with multi-stimulus data.

	Precision	**Recall**	**F1-score**
No Stimulus	0.71	0.80	0.75
AD	0.77	0.71	0.74
Tail pinch	0.91	0.77	0.83
Startle	0.82	0.90	0.86
Accuracy			0.79
Weighted Accuracy	0.80	0.80	0.80

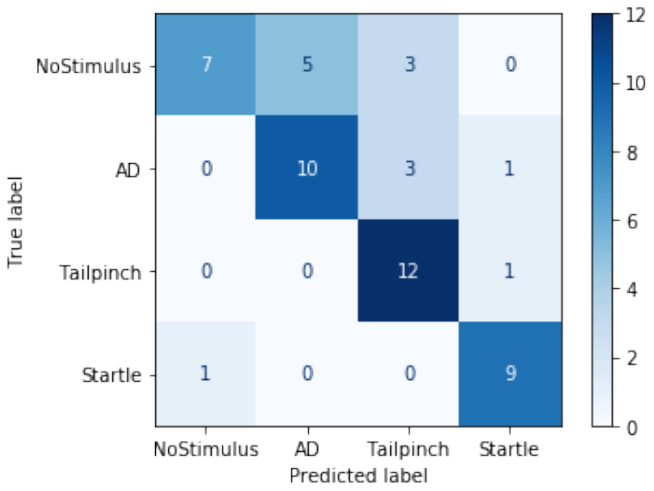

Figure 32: Confusion Matrix of the Multi-class neural network classifier trained on the data from the different triggers.

6.5 Discussion

There were differences in the physiological responses recorded from the various sympathetic stimuli above and below the level of injury. As expected, all stimuli led to an overall increase in the sympathetic activity detected by the sensors.

The startle response, a trigger above the level of injury, led to a drastically higher sympathetic activation compared to the other triggers. The observed startle response is an

expected reaction to stimuli above the level of injury [244]. This is in agreement with prior research which shows hypersensitivity to the acoustic startle reflex in individuals with spinal cord injuries [245], [246]. This is likely the result of the neuroplasticity observed post-injury wherein there is reorganization after SCI at cortical as well as brainstem levels [247]. The rats were subjected to the stimuli at least five days post-surgery allowing time for reorganization to occur in the neuronal pathways which result in the large sympathetic reflex.

Both sympathetic and vagal branches of the autonomic nervous system likely contribute to the changes in BP and HR which vary within seconds after the nociceptive stimuli were presented to the animals. The co-activation of the sympathetic and vagal system was observed as a result of both AD and the startle response. However, this co-activation was missing in the tail pinch response, which is not perceived by supraspinal centers due to paralysis.

The sympathetic surge in the tail pinch response was accompanied by a vagal inhibition. This is likely the result of a nociceptive pain response. Pain responses lead to an increase in sympathetic activity while causing a decrease in vagal activity [248]. This suggests that the rats may have regained some sensory control in their tail. Tail pinch has been used in prior research as a tool to induce AD [249]. However, we did not observe the accompanying increase in blood pressure to characterize the response as AD due to the nociceptive stimulus. While this may have been a limitation of the tail-cuff based blood pressure measurement technique used in this study it will be further explored in future studies.

While the rats did not react to the toe or tail pinch acutely after SCI, the tail pinch response was elicited after five days of recovery. During this recovery period, it is possible for the rats to have regained some motor and neural control below the level of injury [250], [251]. This pain response differs from the response seen as a result of the onset of AD from CRD, which is also a noxious stimulus below the level of injury. Additionally, it may indicate that the crush injury which induced the SCI in our rats may have led to incomplete injuries which would require further investigation in future studies.

The neural network developed with the data collected from the various stimuli was able to distinguish the responses to the different stimuli with a 76% accuracy. We ensured balance between the different classes to prevent over-representation of one class which could skew performance. The precision is a measure of the positive predicted value which is the fraction of relevant instances among the retrieved instances while recall is the sensitivity of the model. Overall, the neural network had a good weighted accuracy suggesting that there was sufficient difference between the patterns observed in the features extracted from the sensor data to different triggers to enable discernment. The overlap between the classes shown in Figure 31 could likely contribute to the poorer performance of the neural network to distinguish the non-stimulus data from the responses due to the triggers.

Additionally, the misclassification of non-stimulus data as tail pinch or AD response likely leads to false positives in the neural network leading to poorer precision and recall. These false positives could translate to alert fatigue which may cause poorer adherence when used by individuals with SCI (ref). More sympathetic stimuli response data could trigger a greater range of sympathetic responses in order to train the model better.

Distinguishing various types of sympathetic stimuli, including exercise and emotional stress, from AD could play an important role in reducing the onset of false positives as a result of sympathetic activation. This would allow an improvement in the performance of the machine learning model when it is translated to humans and could also lead to a more in-depth understanding of the impact of other sympathetic stimuli on the health of individuals with SCI. In addition, the ability to discriminate between the triggers of AD would also prove to be valuable in assisting the management of AD by providing information about possible triggers.

6.6 Summary

The system developed using non-invasive sensors was able to discern the sympathetic and vagal responses to three different stimuli above and below the level of injury. The data collected from the different triggers allowed the development of a neural network which could distinguish between AD due to CRD, nociceptive pain, and startle responses with 76% accuracy.

7 CONCLUSIONS AND FUTURE WORK

In this dissertation, we present a multi-parametric sensing system that can detect the onset of autonomic dysreflexia using an array of novel, non-invasive sensors when combined with machine learning models. This system comprises wearable ECG, skNA, blood pressure and skin temperature sensors. We used these sensors to gauge changes in physiology on rodent models of a crush T2/T3 level spinal cord injury. We stimulated AD in a controlled fashion through colorectal distension for a duration of one minute. We also induced responses to sympathetic triggers above and below the level of injury through an acoustic startle and tail pinch respectively. Physiologically relevant features were extracted and selected from windowed time-series sensor data to quantify the sympathetic and parasympathetic responses to the onset of the different triggers.

We determined five significant features that were representative of sympathetic and vagal activity, which best characterized the onset of AD. We characterized the sympatho-vagal cascade of AD through an increase in sympathetic activity determined by the skNA sensors followed by a vagal discharge determined by changes in the features extracted from the ECG sensors. After exploring eleven different binary classifiers, we were able to develop a five-layer neural network which could distinguish AD from non-AD episodes with a 93% accuracy. Additionally, when trained on data from other sympathetic triggers above and below the level of injury, the neural network was able to discern between them with an accuracy of 76%.

Current methods to detect AD are not feasible for long-term use. Through this research, we have created a tool that enables rapid detection of AD. Moreover, we were able to study the onset of AD on a higher temporal resolution allowing determination of a unique signature through changes in the sympatho-vagal branches of the ANS during AD. Lastly, the use of machine learning enables an automated detection of the onset of AD as well as the other sympathetic triggers.

The development of this system in rodent models allowed an exploration of a controlled study of AD which can be explored to a greater extent in the future.

7.1 Limitations

Although we had consistency in the physiological parameters throughout the study, there may have been cofounding factors that could have potentially impacted the data. We minimized triggers which could have caused the spontaneous development of AD such as pressure sores, proper bowel and bladder care, and urinary tract infections (UTIs). Rats were monitored after SCI and received antibiotics if UTI is observed and pressure sores were immediately treated. It is also possible that other confounding factors such as stress post-SCI or SCI-related cardiovascular/neural changes may have led to misclassifications in the machine learning algorithms

Additionally, there could have been variability in the degree of injury – crush injuries may lead to variations in paralysis. Future studies can control for these by ensuring the completeness of the injury in the animal models.

7.2 Future Studies

Collecting blood pressure data concurrently with the ECG and skNA data using an implantable telemetry system could help determine the lag between the detection of sympathetic discharge through the skNA sensors and the resultant hypertensive episode. Such an early AD detection system could help those with SCIs to detect AD before symptoms escalate. The early detection of AD is critical as it mitigates shear stress on vasculature that develops during recurrent AD resulting in cardiovascular disease [252], [253]. A physiological-based AD detection system will also allow the study of asymptomatic AD or 'silent AD', which can be equally harmful to cardiovascular end-organs due to a substantial rise in blood pressure without concomitant symptoms [150]. This could potentially reduce chances of co-morbidities.

The successful execution of this research has enabled the determination of a rat model that can be used for a multitude of research projects involving studies of AD. AD is a difficult disorder to study in human participants due to the high risks involved in inducing AD even in clinical settings. Through the development of this rat model, it would be possible to investigate even further the trigger of AD. This can be done through stimulating the onset of AD in rat

models using a variety of triggers (e.g., cutaneous nociception, exercise, bladder obstruction) and developing a pattern recognition model based on the type of trigger. This would enable the development of a system which could alert the user to the cause of AD (its trigger) and allow a quicker way to manage it.

Moreover, future investigation of this approach would also make it possible to develop a better understanding of how artificial intelligence can be applied to the understanding of other SCI complications, such as the development of pressure sores and orthostatic hypotension. This research can be also applied to further study dysautonomia detection in different disease models such as Parkinson's disease or diabetes.

REFERENCES

[1] J. E. Hall and M. E. Hall, *Guyton and Hall: Textbook of Medical Physiology*, vol. 8, no. 1. Elsevier, 2017.

[2] R. M. Buijs, "The autonomic nervous system : a balancing act," *Auton. Nerv. Syst.*, vol. 117, pp. 1–11, 2013.

[3] J. N. Langley, "The autonomic nervous system," *Brain*, vol. 26, no. 1, pp. 1–26, Jan. 1903.

[4] W. R. Lovallo and J. J. Sollers, "The Enlarged Autonomic Nervous System," in *Autonomic Nervous System*, Cham: Springer International Publishing, 2018, pp. 1–17.

[5] D. P. Cardinali, "First Level: Peripheral Sympathetic and Parasympathetic Nervous System," in *Autonomic Nervous System*, Cham: Springer International Publishing, 2018, pp. 57–111.

[6] R. C. Drew and L. I. Sinoway, "Autonomic Control of the Heart," in *Primer on the Autonomic Nervous System*, Elsevier, 2012, pp. 177–180.

[7] D. S. Goldstein, "Differential responses of components of the autonomic nervous system," *Handb. Clin. Neurol.*, vol. 117, pp. 13–22, 2013.

[8] J. G. McLeod and R. R. Tuck, "Disorders of the autonomic nervous system: Part 1. Pathophysiology and clinical features," *Ann. Neurol.*, vol. 21, no. 5, pp. 419–430, May 1987.

[9] M. D. S. Goldstein, D. D. Robertson, M. Esler, and S. E. Straus, "NIH Conference Dysautonomias : Clinical Disorders of the Autonomic Nervous System," *Ann. Intern. Med.*, vol. 137, no. May 2000, pp. 753–764, Nov. 2002.

[10] K. Thornton and M. O. Mitchell, "Autonomic dysfunction: A guide for FPs," *J. Fam. Pract.*, vol. 66, no. 9, 2017.

[11] M. Walter *et al.*, "Prediction of autonomic dysreflexia during urodynamics: a prospective cohort study," *BMC Med.*, vol. 16, no. 1, p. 53, Dec. 2018.

[12] M. A. Pfeifer *et al.*, "Autonomic neural dysfunction in recently diagnosed diabetic subjects.," *Diabetes Care*, vol. 7, no. 5, pp. 447–53, Sep. 1984.

[13] A. I. Vinik, T. Erbas, and C. M. Casellini, "Diabetic cardiac autonomic neuropathy, inflammation and cardiovascular disease.," *J. Diabetes Investig.*, vol. 4, no. 1, pp. 4–18, Jan. 2013.

[14] Dysautonomia International, "Dysautonomia international - What is Dysautonomia?," 2012. [Online]. Available: http://www.dysautonomiainternational.org/page.php?ID=34. [Accessed: 04-Mar-2018].

[15] H. Chidambaram, "Assessment of Autonomic Dysfunction in Acute Stroke Patients at a Tertiary Care Hospital," *J. Clin. Diagnostic Res.*, vol. 11, no. 2, pp. OC28–OC31, Feb. 2017.

[16] J. Parkinson *et al.*, "An Essay on the Shaking Palsy," *The Journal of Neuropsychiatry and Clinical Neurosciences*, vol. 14, no. 2. pp. 223–236, May-2002.

[17] R. C. Roges, H. Kita, L. L. Butcher, and D. Novin, "Afferent projections to the dorsal motor nucleus of the vagus," *Brain Res. Bull.*, vol. 5, no. 4, pp. 365–373, 1980.

[18] C. Singer, W. J. Weiner, and J. R. Sanchez-Ramos, "Autonomic dysfunction in men with Parkinson's disease.," *Eur. Neurol.*, vol. 32, no. 3, pp. 134–40, 1992.

[19] K. Kujawa, S. Leurgans, R. Raman, L. Blasucci, and C. G. Goetz, “Acute Orthostatic Hypotension When Starting Dopamine Agonists in Parkinson’s Disease,” *Arch. Neurol.*, vol. 57, no. 10, pp. 1461–1463, Oct. 2000.
[20] R. D. Abbott *et al.*, “Frequency of bowel movements and the future risk of Parkinson’s disease.,” *Neurology*, vol. 57, no. 3, pp. 456–62, Aug. 2001.
[21] D. S. Goldstein, “Dysautonomia in Parkinson disease,” *Compr. Physiol.*, vol. 4, no. 2, pp. 805–826, 2014.
[22] K. R. Chaudhuri, D. G. Healy, and A. H. Schapira, “Non-motor symptoms of Parkinson’s disease: diagnosis and management,” *Lancet Neurol.*, vol. 5, no. 3, pp. 235–245, Mar. 2006.
[23] S. Sveinbjornsdottir, “The clinical symptoms of Parkinson’s disease,” *J. Neurochem.*, vol. 139, pp. 318–324, Oct. 2016.
[24] H. Kaufmann and D. S. Goldstein, “Autonomic dysfunction in Parkinson disease,” *Handb. Clin. Neurol.*, vol. 117, pp. 259–278, Jan. 2013.
[25] A. Krassioukov, D. E. Warburton, R. Teasell, and J. J. Eng, “A Systematic Review of the Management of Autonomic Dysreflexia After Spinal Cord Injury,” *Arch. Phys. Med. Rehabil.*, vol. 90, no. 4, pp. 682–695, 2009.
[26] J. T. Korpelainen, K. A. Sotaniemi, and V. V. Myllylä, “Autonomic nervous system disorders in stroke.,” *Clin. Auton. Res.*, vol. 9, no. 6, pp. 325–333, Dec. 1999.
[27] World Health Organization, “What are neurological disorders?,” World Health Organization, 2007.
[28] A. I. Vinik and T. Erbas, “Recognizing and treating diabetic autonomic neuropathy,” *Cleve. Clin. J. Med.*, vol. 68, no. 11, p. 929, 2001.
[29] A. I. Vinik and D. Ziegler, “Diabetic cardiovascular autonomic neuropathy.,” *Circulation*, vol. 115, no. 3, pp. 387–97, Jan. 2007.
[30] R. E. Maser, J. M. Lenhard, and S. G. DeCherney, “Cardiovascular Autonomic Neuropathy,” *Endocrinologist*, vol. 10, no. 1, pp. 27–33, Jan. 2000.
[31] S. Wheeler, N. Singh, and E. J. Boyko, “The Epidemiology of Diabetic Neuropathy,” in *Diabetic Neuropathy*, Totowa, NJ: Humana Press, 2007, pp. 7–30.
[32] A. Veves and G. L. King, “Can VEGF reverse diabetic neuropathy in human subjects?,” *J. Clin. Invest.*, vol. 107, no. 10, pp. 1215–8, May 2001.
[33] R. D. Hoeldtke *et al.*, “Nitrosative stress, uric Acid, and peripheral nerve function in early type 1 diabetes.,” *Diabetes*, vol. 51, no. 9, pp. 2817–25, Sep. 2002.
[34] S. L. Tokgözoglu, M. K. Batur, M. A. Topçuoglu, O. Saribas, S. Kes, and A. Oto, “Effects of stroke localization on cardiac autonomic balance and sudden death,” *Stroke*, vol. 30, no. 7, pp. 1307–1311, 1999.
[35] J. P. Casanova, M. Contreras, E. A. Moya, F. Torrealba, and R. Iturriaga, “Effect of insular cortex inactivation on autonomic and behavioral responses to acute hypoxia in conscious rats,” *Behav. Brain Res.*, vol. 253, pp. 60–67, Sep. 2013.
[36] S. Oppenheimer, “The anatomy and physiology of cortical mechanisms of cardiac control.,” *Stroke*, vol. 24, no. 12 Suppl, pp. I3-5, Dec. 1993.
[37] S. M. Oppenheimer and D. F. Cechetto, “Cardiac chronotropic organization of the rat insular cortex,” *Brain Res.*, vol. 533, no. 1, pp. 66–72, Nov. 1990.

[38] J. G. van Dijk, J. Haan, K. Zwinderman, B. Kremer, B. J. van Hilten, and R. A. Roos, "Autonomic nervous system dysfunction in Parkinson's disease: relationships with age, medication, duration, and severity.," *J. Neurol. Neurosurg. Psychiatry*, vol. 56, no. 10, pp. 1090–5, Oct. 1993.
[39] G. Micieli, P. Tosi, S. Marcheselli, and A. Cavallini, "Autonomic dysfunction in Parkinson's disease," *Neurol. Sci.*, vol. 24, no. SUPPL. 1, pp. s32–s34, May 2003.
[40] R. F. Pfeiffer, "Autonomic dysfunction in Parkinson's disease," *Expert Rev. Neurother.*, vol. 12, no. 6, pp. 697–706, Jun. 2012.
[41] P. Kempler *et al.*, "Management strategies for gastrointestinal, erectile, bladder, and sudomotor dysfunction in patients with diabetes," *Diabetes. Metab. Res. Rev.*, vol. 27, no. 7, pp. 665–677, Oct. 2011.
[42] A. I. Vinik, R. E. Maser, B. D. Mitchell, and R. Freeman, "Diabetic autonomic neuropathy," *Diabetes Care*, vol. 26, no. 5. pp. 1553–1579, 2003.
[43] National Spinal Cord Injury Statistical Center (NSCISC), "Spinal cord injury facts and figures at a glance.," 2017.
[44] D. S. Tulsky *et al.*, "Developing a contemporary patient-reported outcomes measure for spinal cord injury," *Arch. Phys. Med. Rehabil.*, vol. 92, no. 10, pp. S44--S51, 2011.
[45] M. J. DeVivo, "Causes and costs of spinal cord injury in the United States," *Spinal Cord*, vol. 35, no. 12, pp. 809–813, 1997.
[46] J. J. E. Adriaansen *et al.*, "Secondary health conditions in persons with spinal cord injury: a longitudinal study from one to five years post-discharge," *J. Rehabil. Med.*, vol. 45, no. 10, pp. 1016–1022, 2013.
[47] P. V. of America, *Acute management of autonomic dysreflexia: individuals with spinal cord injury presenting to health-care facilities*. Paralyzed Veterans of America, 2001.
[48] N. Sezer, "Chronic complications of spinal cord injury," *World J. Orthop.*, vol. 6, no. 1, p. 24, 2015.
[49] K. G. Lehmann, J. G. Lane, J. M. Piepmeier, and W. P. Batsford, "Cardiovascular abnormalities accompanying acute spinal cord injury in humans: Incidence, time course and severity," *J. Am. Coll. Cardiol.*, vol. 10, no. 1, pp. 46–52, Jul. 1987.
[50] R. W. Teasell, J. M. O. Arnold, A. Krassioukov, and G. A. Delaney, "Cardiovascular consequences of loss of supraspinal control of the sympathetic nervous system after spinal cord injury," *Archives of Physical Medicine and Rehabilitation*, vol. 81, no. 4. W.B. Saunders, pp. 506–516, 01-Apr-2000.
[51] A. Krassioukov, D. E. Warburton, R. Teasell, and J. J. Eng, "A Systematic Review of the Management of Autonomic Dysreflexia After Spinal Cord Injury," *Archives of Physical Medicine and Rehabilitation*, vol. 90, no. 4. pp. 682–695, 2009.
[52] a K. Karlsson, "Autonomic dysreflexia.," *Spinal Cord*, vol. 37, no. 6, pp. 383–91, 1999.
[53] A. Giannantoni *et al.*, "Autonomic dysreflexia during urodynamics," *Spinal Cord*, 1998.
[54] A. Krassioukov, D. E. Warburton, R. Teasell, and J. J. Eng, "A Systematic Review of the Management of Autonomic Dysreflexia After Spinal Cord Injury," *Arch. Phys. Med. Rehabil.*, vol. 90, no. 4, pp. 682–695, 2009.
[55] H.-Y. Ko, "Autonomic Dysreflexia," in *Management and Rehabilitation of Spinal Cord Injuries*, Singapore: Springer Singapore, 2019, pp. 265–273.
[56] R. W. Teasell, J. M. O. M. O. Arnold, A. Krassioukov, and G. A. Delaney, *Cardiovascular consequences of loss of supraspinal control of the sympathetic nervous system after spinal cord injury*, vol. 81, no. 4. W.B. Saunders, 2000, pp. 506–516.

[57] C. K. Flack and M. J. Mellon, “Current Management Strategies for Autonomic Dysreflexia,” *Curr. Bladder Dysfunct. Rep.*, pp. 1–6, Sep. 2018.
[58] J. Cragg and A. Krassioukov, “Autonomic dysreflexia.,” *CMAJ*, vol. 184, no. 1, p. 66, Jan. 2012.
[59] S. Canon *et al.*, “Autonomic dysreflexia during urodynamics in children and adolescents with spinal cord injury or severe neurologic disease,” *J. Pediatr. Urol.*, vol. 11, no. 1, pp. 32.e1--32.e4, 2015.
[60] D. Caruso, D. Gater, and C. Harnish, “Prevention of recurrent autonomic dysreflexia: a survey of current practice,” *Clin. Auton. Res.*, vol. 25, no. 5, pp. 293–300, 2015.
[61] D. Wan and A. V. Krassioukov, “Life-threatening outcomes associated with autonomic dysreflexia: A clinical review,” *J. Spinal Cord Med.*, vol. 37, no. 1, pp. 2–10, Jan. 2014.
[62] T. G. Robinson, S. L. Dawson, P. J. Eames, R. B. Panerai, and J. F. Potter, “Cardiac baroreceptor sensitivity predicts long-term outcome after acute ischemic stroke.,” *Stroke*, vol. 34, no. 3, pp. 705–12, Mar. 2003.
[63] S. Nayani, S. E. Sreedharan, N. Namboodiri, P. S. Sarma, and P. N. Sylaja, “Autonomic dysfunction in first ever ischemic stroke: Prevalence, predictors and short term neurovascular outcome,” *Clin. Neurol. Neurosurg.*, vol. 150, pp. 54–58, Nov. 2016.
[64] M. Sykora, J. Diedler, A. Rupp, P. Turcani, and T. Steiner, “Impaired baroreceptor reflex sensitivity in acute stroke is associated with insular involvement, but not with carotid atherosclerosis,” *Stroke*, vol. 40, no. 3, pp. 737–742, Mar. 2009.
[65] S. De Raedt, A. De Vos, and J. De Keyser, “Autonomic dysfunction in acute ischemic stroke: an underexplored therapeutic area?,” *J Neurol Sci*, vol. 348, no. 1–2, pp. 24–34, Jan. 2015.
[66] A. M. Mäkikallio, T. H. Mäkikallio, J. T. Korpelainen, K. A. Sotaniemi, H. V Huikuri, and V. V Myllylä, “Heart rate dynamics predict poststroke mortality.,” *Neurology*, vol. 62, no. 10, pp. 1822–6, May 2004.
[67] M. I. Chimowitz, R. M. Poole, M. R. Starling, M. Schwaiger, and M. D. Gross, “Frequency and severity of asymptomatic coronary disease in patients with different causes of stroke.,” *Stroke*, vol. 28, no. 5, pp. 941–5, May 1997.
[68] H. S. Jørgensen, H. Nakayama, J. Reith, H. O. Raaschou, and T. S. Olsen, “Stroke recurrence: predictors, severity, and prognosis. The Copenhagen Stroke Study.,” *Neurology*, vol. 48, no. 4, pp. 891–5, Apr. 1997.
[69] L. Xiong *et al.*, “Preliminary findings of the effects of autonomic dysfunction on functional outcome after acute ischemic stroke,” *Clin. Neurol. Neurosurg.*, vol. 114, no. 4, pp. 316–320, May 2012.
[70] M. I. Chimowitz, R. M. Poole, M. R. Starling, M. Schwaiger, and M. D. Gross, “Frequency and severity of asymptomatic coronary disease in patients with different causes of stroke.,” *Stroke*, vol. 28, no. 5, pp. 941–5, May 1997.
[71] A. I. Vinik and T. Erbas, “Diabetic autonomic neuropathy,” *Handb. Clin. Neurol.*, vol. 117, pp. 27–294, Jan. 2013.
[72] A. Minguez-Castellanos *et al.*, “Do alpha-synuclein aggregates in autonomic plexuses predate Lewy body disorders?: a cohort study.,” *Neurology*, vol. 68, no. 23, pp. 2012–8, Jun. 2007.
[73] H. Kaufmann, K. Nahm, D. Purohit, and D. Wolfe, “Autonomic failure as the initial presentation of Parkinson disease and dementia with Lewy bodies.,” *Neurology*, vol. 63, no. 6, pp. 1093–5, Sep. 2004.

[74] H. Braak, M. Sastre, J. R. E. Bohl, R. A. I. de Vos, and K. Del Tredici, “Parkinson’s disease: lesions in dorsal horn layer I, involvement of parasympathetic and sympathetic pre- and postganglionic neurons,” *Acta Neuropathol.*, vol. 113, no. 4, pp. 421–429, Apr. 2007.
[75] J. A. Palma and H. Kaufmann, “Autonomic disorders predicting Parkinson’s disease,” *Park. Relat. Disord.*, vol. 20, no. SUPPL.1, 2014.
[76] C. J. Winstein *et al.*, “Guidelines for Adult Stroke Rehabilitation and Recovery: A Guideline for Healthcare Professionals from the American Heart Association/American Stroke Association,” *Stroke*, vol. 47, no. 6. American Heart Association, Inc., pp. e98–e169, 04-Jun-2016.
[77] M. Wirz *et al.*, “Effectiveness of automated locomotor training in patients with chronic incomplete spinal cord injury: A multicenter trial,” *Arch. Phys. Med. Rehabil.*, vol. 86, no. 4, pp. 672–680, Apr. 2005.
[78] A. McLaren *et al.*, “Autonomic Function Is Impaired in Elderly Stroke Survivors.”
[79] L. Muslumanoglu, G. Akyuz, S. Aki, S. Karsidag, and O. Us, “Evaluation of autonomic nervous system functions in post-stroke patients,” *Am. J. Phys. Med. Rehabil.*, vol. 81, no. 10, pp. 721–725, 2002.
[80] D. J. Ewing, C. N. Martyn, R. J. Young, and B. F. Clarke, “The value of cardiovascular autonomic function tests: 10 years experience in diabetes.,” *Diabetes Care*, vol. 8, no. 5, pp. 491–8, Sep. 1985.
[81] M. J. Hilz and M. Dütsch, “Quantitative studies of autonomic function,” *Muscle and Nerve*, vol. 33, no. 1. Wiley-Blackwell, pp. 6–20, Jan-2006.
[82] J. G. Mcleod and R. R. Tuck, “Disorders of the Autonomic Nervous System: Part 2. Investigation and Treatment’,” *Ann Neurol*, vol. 2, no. 1, pp. 5–19, 1987.
[83] T. K. Rasmussen *et al.*, “Autonomic function testing: Compliance and consequences,” *Auton. Neurosci. Basic Clin.*, vol. 208, pp. 150–155, Dec. 2017.
[84] R. Freeman and M. W. Chapleau, “Testing the autonomic nervous system,” *Handb. Clin. Neurol.*, vol. 115, pp. 115–136, Jan. 2013.
[85] S. S. Jaradeh and T. E. Prieto, “Evaluation of the autonomic nervous system.,” *Phys. Med. Rehabil. Clin. N. Am.*, vol. 14, no. 2, pp. 287–305, May 2003.
[86] A. Zygmunt and J. Stanczyk, “Methods of evaluation of autonomic nervous system function,” *Arch. Med. Sci.*, vol. 6, no. 1, pp. 11–18, 2010.
[87] I. Cygankiewicz and W. Zareba, “Heart rate variability,” *Handb. Clin. Neurol.*, vol. 117, pp. 379–393, Jan. 2013.
[88] P. K. Stein, M. S. Bosner, R. E. Kleiger, and B. M. Conger, “Heart rate variability: a measure of cardiac autonomic tone.,” *Am. Heart J.*, vol. 127, no. 5, pp. 1376–81, May 1994.
[89] C. M. A. van Ravenswaaij-Arts, “Heart Rate Variability,” *Ann. Intern. Med.*, vol. 118, no. 6, p. 436, Mar. 1993.
[90] J. D. Guieu *et al.*, “Heart rate variability and Parkinson?s disease severity,” *J. Neural Transm.*, vol. 110, no. 9, pp. 997–1011, Sep. 2003.
[91] B. Pomeranz *et al.*, “Assessment of autonomic function in humans by heart rate spectral analysis.,” *Am. J. Physiol.*, vol. 248, no. 1 Pt 2, pp. H151-3, Jan. 1985.
[92] A. Malliani, F. Lombardi, and M. Pagani, “Power spectrum analysis of heart rate variability: a tool to explore neural regulatory mechanisms.,” *Br. Heart J.*, vol. 71, no. 1, pp. 1–2, Jan. 1994.

[93] A. Malliani, M. Pagani, F. Lombardi, and S. Cerutti, “Cardiovascular neural regulation explored in the frequency domain.,” *Circulation*, vol. 84, no. 2, pp. 482–492, 1991.
[94] A. MALLIANI, F. LOMBARDI, M. PAGANI, and S. CERUTTI, “Power Spectral Analysis of Cardiovascular Variability in Patients at Risk for Sudden Cardiac Death,” *Journal of Cardiovascular Electrophysiology*, vol. 5, no. 3. Wiley/Blackwell (10.1111), pp. 274–286, Mar-1994.
[95] M. Malik and A. J. Camm, “Components of heart rate variability — what they really mean and what we really measure,” *Am. J. Cardiol.*, vol. 72, no. 11, pp. 821–822, Oct. 1993.
[96] E. S. of Cardiology, “Heart rate variability: standards of measurement, physiological interpretation and clinical use. Task Force of the European Society of Cardiology and the North American Society of Pacing and Electrophysiology.,” *Circulation*, vol. 93, no. 5, pp. 1043–1065, 1996.
[97] W. F. Brown, C. F. Bolton, and M. J. Aminoff, *Neuromuscular function and disease: basic, clinical, and electrodiagnostic aspects*, vol. 1. Gulf Professional Publishing, 2002.
[98] J. T. Bigger, J. L. Fleiss, R. C. Steinman, L. M. Rolnitzky, R. E. Kleiger, and J. N. Rottman, “Correlations among time and frequency domain measures of heart period variability two weeks after acute myocardial infarction.,” *Am. J. Cardiol.*, vol. 69, no. 9, pp. 891–8, Apr. 1992.
[99] J. Sztajzel, “Heart rate variability: a noninvasive electrocardiographic method to measure the autonomic nervous system,” 2004.
[100] A. J. McDougall and J. G. McLeod, “Autonomic neuropathy, I. Clinical features, investigation, pathophysiology, and treatment,” *Journal of the Neurological Sciences*, vol. 137, no. 2. Elsevier, pp. 79–88, 01-May-1996.
[101] B. M. W. Illigens and C. H. Gibbons, “Sweat testing to evaluate autonomic function,” *Clinical Autonomic Research*, vol. 19, no. 2. Steinkopff-Verlag, pp. 79–87, 06-Apr-2009.
[102] T. Yokota *et al.*, “Sympathetic skin response in patients with multiple sclerosis compared with patients with spinal cord transection and normal controls,” *Brain*, vol. 114, no. 3, pp. 1381–1394, Jun. 1991.
[103] S. Suresh, R. Brendan, and B. Duerstock, “Wearable Physiological Telemetry for Individuals with Spinal Cord Injuries to Self-Monitor Secondary Health Complications,” in *RESNA/NCART 2016*, 2016.
[104] S. Suresh, H. Duerstock, and B. Duerstock, “Skin Resistance as a Physiological Indicator for Quadriplegics with Spinal Cord Injuries During Activities of Daily Living,” in *International Conference on Smart Health*, 2015, pp. 157–168.
[105] A. Mori *et al.*, “Autonomic nervous function in upper gastrointestinal endoscopy: A prospective randomized comparison between transnasal and oral procedures,” *J. Gastroenterol.*, vol. 43, no. 1, pp. 38–44, Jan. 2008.
[106] A. E. Bharucha, M. Camilleri, P. A. Low, and A. R. Zinsmeister, “Autonomic dysfunction in gastrointestinal motility disorders.,” *Gut*, vol. 34, no. 3, pp. 397–401, Mar. 1993.
[107] K. L. Jones, A. Russo, M. K. Berry, J. E. Stevens, J. M. Wishart, and M. Horowitz, “A longitudinal study of gastric emptying and upper gastrointestinal symptoms in patients with diabetes mellitus,” *Am. J. Med.*, vol. 113, no. 6, pp. 449–455, Oct. 2002.
[108] D. Ziegler *et al.*, “Octanoic acid breath test for non-invasive assessment of gastric emptying in diabetic patients: Validation and relationship to gastric symptoms and cardiovascular autonomic function,” *Diabetologia*, vol. 39, no. 7, pp. 823–830, Jul. 1996.

[109] M. S. Alexander *et al.*, "International standards to document remaining autonomic function after spinal cord injury," *Spinal Cord*, vol. 47, no. 1, pp. 36–43, Jan. 2009.
[110] P. A. Low, V. A. Tomalia, and K.-J. Park, "Autonomic function tests: some clinical applications.," *J. Clin. Neurol.*, vol. 9, no. 1, pp. 1–8, Jan. 2013.
[111] A. J. Moss, *Moss and Adams' heart disease in infants, children, and adolescents: including the fetus and young adult*, vol. 1. Lippincott Williams & Wilkins, 2007.
[112] R. Mosqueda-Garcia, "Evaluation of autonomic failure.," in *Disorders of the Autonomic Nervous System.*, Harwood Academic Press, 1995, pp. 25–59.
[113] M. J. Hilz, "Quantitative autonomic functional testing in clinical trials," *Neuromuscul. Funct. Dis. Philadelphia WB Saunders Co.*, pp. 1899–1929, 2002.
[114] B. M. W. Illigens and C. H. Gibbons, "Sweat testing to evaluate autonomic function," *Clin. Auton. Res.*, vol. 19, no. 2, pp. 79–87, Apr. 2009.
[115] T. A. Linsenmeyer, D. I. Campagnolo, and I. H. Chou, "Silent autonomic dysreflexia during voiding in men with spinal cord injuries.," *J. Urol.*, vol. 155, no. 2, pp. 519–22, Feb. 1996.
[116] S. Saria, A. K. Rajani, J. Gould, D. Koller, and A. A. Penn, "Integration of early physiological responses predicts later illness severity in preterm infants," *Sci. Transl. Med.*, vol. 2, no. 48, pp. 48ra65-48ra65, 2010.
[117] M. Kuhn and K. Johnson, *Applied predictive modeling*, vol. 26. Springer, 2013.
[118] T. Mishra *et al.*, "Early Detection Of COVID-19 Using A Smartwatch," *medRxiv*, 2020.
[119] A. Alimadadi, S. Aryal, I. Manandhar, P. B. Munroe, B. Joe, and X. Cheng, "Artificial intelligence and machine learning to fight covid-19," *Physiological Genomics*. 2020.
[120] A. Esteva *et al.*, "Dermatologist-level classification of skin cancer with deep neural networks," *Nature*, vol. 542, no. 7639, pp. 115–118, 2017.
[121] J. Roski, G. W. Bo-Linn, and T. A. Andrews, "Creating value in health care through big data: opportunities and policy implications," *Health Aff.*, vol. 33, no. 7, pp. 1115–1122, 2014.
[122] A. Rumshisky *et al.*, "Predicting early psychiatric readmission with natural language processing of narrative discharge summaries," *Transl. Psychiatry*, vol. 6, no. 10, pp. e921–e921, 2016.
[123] J. Wiens and E. S. Shenoy, "Machine Learning for Healthcare: On the Verge of a Major Shift in Healthcare Epidemiology," *Clin. Infect. Dis.*, vol. 66, no. 1, pp. 149–153, Jan. 2018.
[124] M. Chen, Y. Hao, K. Hwang, L. Wang, and L. Wang, "Disease Prediction by Machine Learning over Big Data from Healthcare Communities," *IEEE Access*, vol. 5, pp. 8869–8879, 2017.
[125] K. Polat and S. Güneş, "Detection of ECG Arrhythmia using a differential expert system approach based on principal component analysis and least square support vector machine," *Appl. Math. Comput.*, vol. 186, no. 1, pp. 898–906, Mar. 2007.
[126] M. Alfaras, M. C. Soriano, and S. Ortín, "A fast machine learning model for ECG-based heartbeat classification and arrhythmia detection," *Front. Phys.*, 2019.
[127] M. Radha *et al.*, "Estimating blood pressure trends and the nocturnal dip from photoplethysmography," *Physiol. Meas.*, 2019.
[128] M. K. Uçar, M. R. Bozkurt, C. Bilgin, and K. Polat, "Automatic detection of respiratory arrests in OSA patients using PPG and machine learning techniques," *Neural Comput. Appl.*, 2017.

[129] F. Lotte *et al.*, "A review of classification algorithms for EEG-based brain-computer interfaces: A 10 year update," *Journal of Neural Engineering*. 2018.
[130] X. W. Wang, D. Nie, and B. L. Lu, "Emotional state classification from EEG data using machine learning approach," *Neurocomputing*, 2014.
[131] A. Craik, Y. He, and J. L. Contreras-Vidal, "Deep learning for electroencephalogram (EEG) classification tasks: A review," *Journal of Neural Engineering*. 2019.
[132] J. Yousefi and A. Hamilton-Wright, "Characterizing EMG data using machine-learning tools," *Computers in Biology and Medicine*. 2014.
[133] B. Karlık, "Machine Learning Algorithms for Characterization of EMG Signals," *Int. J. Inf. Electron. Eng.*, 2014.
[134] S. S. Nair, R. M. French, D. Laroche, and E. Thomas, "The application of machine learning algorithms to the analysis of electromyographic patterns from arthritic patients," *IEEE Trans. Neural Syst. Rehabil. Eng.*, 2010.
[135] S. Badillo *et al.*, "An Introduction to Machine Learning," *Clin. Pharmacol. Ther.*, 2020.
[136] C.-T. Su, P.-C. Wang, Y.-C. Chen, and L.-F. Chen, "Data mining techniques for assisting the diagnosis of pressure ulcer development in surgical patients," *J. Med. Syst.*, vol. 36, no. 4, pp. 2387–2399, 2012.
[137] C.-H. Jen, C.-C. Wang, B. C. Jiang, Y.-H. Chu, and M.-S. Chen, "Application of classification techniques on development an early-warning system for chronic illnesses," *Expert Syst. Appl.*, vol. 39, no. 10, pp. 8852–8858, 2012.
[138] N. Jothi and W. Husain, "Data mining in healthcare–a review," *Procedia Comput. Sci.*, vol. 72, pp. 306–313, 2015.
[139] A. Kostov, B. J. Andrews, D. B. Popovic, R. B. Stein, and W. W. Armstrong, "Machine learning in control of functional electrical stimulation systems for locomotion," *IEEE Trans. Biomed. Eng.*, vol. 42, no. 6, pp. 541–551, 1995.
[140] A. Kostov, "Machine learning techniques for the control of FES-assisted locomotion after spinal cord injury," 1995.
[141] P. Sok, T. Xiao, Y. Azeze, A. Jayaraman, and M. V Albert, "Activity recognition for incomplete spinal cord injury subjects using hidden Markov models," *IEEE Sens. J.*, vol. 18, no. 15, pp. 6369–6374, 2018.
[142] M. V Albert, Y. Azeze, M. Courtois, and A. Jayaraman, "In-lab versus at-home activity recognition in ambulatory subjects with incomplete spinal cord injury," *J. Neuroeng. Rehabil.*, vol. 14, no. 1, p. 10, 2017.
[143] O. Khan, J. H. Badhiwala, C. D. Witiw, J. R. Wilson, and M. G. Fehlings, "Machine learning algorithms for prediction of health-related quality-of-life after surgery for mild degenerative cervical myelopathy," *Spine J.*, 2020.
[144] N. N. HeidarAbadi, L. Hakemi, P. Kolivand, R. Safdari, and M. G. Saeidi, "Comparing performances of intelligent classifier algorithms for predicting type of pain in patients with spinal cord injury," *Electron. physician*, vol. 9, no. 7, p. 4847, 2017.
[145] M. Sharif-Alhoseini *et al.*, "Animal models of spinal cord injury: A systematic review," *Spinal Cord*, vol. 55, no. 8. pp. 714–721, 2017.
[146] N. Zhang, M. R. Fang, H. H. Chen, F. M. Gou, and M. X. Ding, "Evaluation of spinal cord injury animal models," *Neural Regen. Res.*, vol. 9, no. 22, pp. 2008–2012, Nov. 2014.
[147] M. Kupfer, B. T. Kucer, H. Kupfer, and C. S. Formal, "Persons With Chronic Spinal Cord Injuries in the Emergency Department: a Review of a Unique Population," *J. Emerg. Med.*, vol. 55, no. 2, pp. 206–212, Aug. 2018.

[148] C. F. McGillivray, S. L. Hitzig, B. C. Craven, M. I. Tonack, and A. V Krassioukov, "Evaluating knowledge of autonomic dysreflexia among individuals with spinal cord injury and their families.," *J. Spinal Cord Med.*, vol. 32, no. 1, pp. 54–62, 2009.
[149] V. E. Claydon, S. L. Elliott, A. W. Sheel, and A. Krassioukov, "Cardiovascular responses to vibrostimulation for sperm retrieval in men with spinal cord injury," *J. Spinal Cord Med.*, 2006.
[150] Y. H. Huang, L. I. Bih, J. M. Liao, S. L. Chen, L. W. Chou, and P. H. Lin, "Blood pressure and age associated with silent autonomic dysreflexia during urodynamic examinations in patients with spinal cord injury," *Spinal Cord*, vol. 51, no. 5, pp. 401–405, May 2013.
[151] M. Hubli and A. V Krassioukov, "Ambulatory Blood Pressure Monitoring in Spinal Cord Injury: Clinical Practicability," *J. Neurotrauma*, vol. 31, no. 9, pp. 789–797, 2014.
[152] S. Suresh and B. S. Duerstock, "Automated detection of symptomatic autonomic dysreflexia through multimodal sensing," *IEEE J. Transl. Eng. Heal. Med.*, 2020.
[153] J. Gaskin, J. Jenkins, T. Meservy, J. Steffen, and K. Payne, "Using Wearable Devices for Non-invasive, Inexpensive Physiological Data Collection," in *Proceedings of the 50th Hawaii International Conference on System Sciences*, 2017.
[154] S. Suresh and B. S. Duerstock, "Continuous Real-Time Detection of Autonomic Dysreflexia in Persons with Spinal Cord Injuries Using a Wearable Physiological Telemetry System," *Ann. Biomed. Eng.*, vol. Submitted.
[155] M. Hubli, C. M. Gee, and A. V. Krassioukov, "Refined assessment of blood pressure instability after spinal cord injury," *Am. J. Hypertens.*, vol. 28, no. 2, pp. 173–181, Feb. 2015.
[156] S. Suresh, B. Raftery, and B. Duerstock, "Detection of Autonomic Dysreflexia in persons with Cervical Spinal Cord Injuries through a Support Vector Machine," in *Resna 2017*, 2017.
[157] A. E. Sarabadani Tafreshi, A. S. Tafreshi, and A. L. Ralescu, "Ranking Based on Collaborative Feature- Weighting Applied to the Recommednation of Research Papers," *Int. J. Artif. Intell. Appl. (IJAIA)*, vol. 9, no. 2, 2018.
[158] X. Lin, C. Li, Y. Zhang, B. Su, M. Fan, and H. Wei, "Selecting feature subsets based on SVM-RFE and the overlapping ratio with applications in bioinformatics," *Molecules*, vol. 23, no. 1, p. 52, Dec. 2018.
[159] S. Suresh and B. S. Duerstock, "Optimal Feature Selection for the Detection of Autonomic Dysreflexia in Individuals with Tetraplegia," in *2018 IEEE International Symposium on Signal Processing and Information Technology (ISSPIT)*, 2019, pp. 480–485.
[160] J. T. Korpelainen, U. Tolonen, K. A. Sotaniemi, and V. V Myllylä, "Suppressed sympathetic skin response in brain infarction.," *Stroke*, vol. 24, no. 9, pp. 1389–92, Sep. 1993.
[161] B. Elie and J. P. Loubo'Jtin, "Sympathetic skin response (SSR) is abnormal in multiple sclerosis," *Muscle Nerve*, vol. 18, no. 2, pp. 185–189, Feb. 1995.
[162] C. Dettmers, D. Fatepour, H. Faust, and F. Jerusalem, "Sympathetic skin response abnormalities in amyotrophic lateral sclerosis," *Muscle Nerve*, vol. 16, no. 9, pp. 930–934, Sep. 1993.
[163] Y.-D. Cai, X.-J. Liu, X. Xu, and G.-P. Zhou, "Support vector machines for predicting protein structural class," *BMC Bioinformatics*, vol. 2, no. 1, p. 3, 2001.

[164] Y. Bhambhani, “Physiology of wheelchair racing in athletes with spinal cord injury,” *Sport. Med.*, vol. 32, no. 1, pp. 23–51, 2002.
[165] J. Blackmer, “Rehabilitation medicine: 1. Autonomic dysreflexia,” *Can. Med. Assoc. J.*, vol. 169, no. 9, pp. 931–935, 2003.
[166] T. H. Everett, A. Doytchinova, Y. M. Cha, and P. S. Chen, “Recording sympathetic nerve activity from the skin,” *Trends in Cardiovascular Medicine*, vol. 27, no. 7. Elsevier, pp. 463–472, 01-Oct-2017.
[167] Z. Jiang *et al.*, “Using skin sympathetic nerve activity to estimate stellate ganglion nerve activity in dogs,” *Hear. Rhythm*, vol. 12, no. 6, pp. 1324–1332, 2015.
[168] A. Doytchinova *et al.*, “Simultaneous noninvasive recording of skin sympathetic nerve activity and electrocardiogram,” *Hear. Rhythm*, vol. 14, no. 1, pp. 25–33, Jan. 2017.
[169] G. Lenis, N. Pilia, A. Loewe, W. H. W. Schulze, and O. Dössel, “Comparison of Baseline Wander Removal Techniques considering the Preservation of ST Changes in the Ischemic ECG: A Simulation Study,” *Comput. Math. Methods Med.*, vol. 2017, pp. 1–13, Mar. 2017.
[170] A. Daugherty, D. Rateri, L. Hong, and A. Balakrishnan, “Measuring Blood Pressure in Mice using Volume Pressure Recording, a Tail-cuff Method,” *J. Vis. Exp.*, no. 27, May 2009.
[171] Maxim, “Maxim DS18B20 thermometer datasheet,” 2008. [Online]. Available: https://cdn-shop.adafruit.com/datasheets/DS18B20.pdf. [Accessed: 09-Sep-2020].
[172] Z. Y. LI Gang, “Principle and Application of 1Wire Bus Digital Thermometer DS18B20,” in *Modern Electronic Techniques*, 2005, p. 21.
[173] Y. Zhong, K.-M. Jan, K. H. Ju, and K. H. Chon, “Quantifying cardiac sympathetic and parasympathetic nervous activities using principal dynamic modes analysis of heart rate variability,” *Am. J. Physiol. Circ. Physiol.*, vol. 291, no. 3, pp. H1475–H1483, Sep. 2006.
[174] P. P. Pereira-Junior, M. Marocolo, F. P. Rodrigues, E. Medei, and J. H. M. Nascimento, “Noninvasive method for electrocardiogram recording in conscious rats: Feasibility for heart rate variability analysis,” *Ann. Brazilian Acad. Sci.*, vol. 82, no. 2, pp. 431–437, 2010.
[175] A. Gacek and W. Pedrycz, *ECG signal processing, classification and interpretation: A comprehensive framework of computational intelligence*, vol. 9780857298. 2014.
[176] D. Sadhukhan and M. Mitra, “R-Peak Detection Algorithm for Ecg using Double Difference And RR Interval Processing,” *Procedia Technol.*, vol. 4, pp. 873–877, Jan. 2012.
[177] J. Pan and W. J. Tompkins, “A Real-Time QRS Detection Algorithm,” *IEEE Trans. Biomed. Eng.*, 1985.
[178] H. L. Chan, W. S. Chou, S. W. Chen, S. C. Fang, C. S. Liou, and Y. S. Hwang, “Continuous and online analysis of heart rate variability,” *J. Med. Eng. Technol.*, vol. 29, no. 5, pp. 227–234, Sep. 2005.
[179] L. Schamroth, “An introduction to electrocardiography 7th ed.” Blackwell Scientific Pub, Oxford, 1990.
[180] T. Kusayama *et al.*, “Simultaneous noninvasive recording of electrocardiogram and skin sympathetic nerve activity (neuECG),” *Nat. Protoc.*, 2020.
[181] S. M. Barman, “2019 Ludwig Lecture: Rhythms in sympathetic nerve activity are a key to understanding neural control of the cardiovascular system,” *Am. J. Physiol. Regul. Integr. Comp. Physiol.*, vol. 318, no. 2, pp. R191–R205, Feb. 2020.

[182] W. E. Pentland and L. T. Twomey, “Upper limb function in persons with long term paraplegia and implications for independence: Part II.,” *Paraplegia*, vol. 32, no. 4, pp. 219–224, 1994.
[183] G. Dong and H. Liu, *Feature engineering for machine learning and data analytics*. CRC Press, 2018.
[184] J. Friedman, T. Hastie, and R. Tibshirani, *The elements of statistical learning*, vol. 1, no. 10. Springer series in statistics New York, 2001.
[185] Q. Pan, X. Li, and L. Fang, “Data Augmentation for Deep Learning-Based ECG Analysis,” in *Feature Engineering and Computational Intelligence in ECG Monitoring*, Springer, 2020, pp. 91–111.
[186] F. Pedregosa *et al.*, “Scikit-learn: Machine Learning in Python,” 2011.
[187] S. Dreiseitl and L. Ohno-Machado, “Logistic regression and artificial neural network classification models: A methodology review,” *J. Biomed. Inform.*, vol. 35, no. 5–6, pp. 352–359, Oct. 2002.
[188] S. Sperandei, “Understanding logistic regression analysis,” *Biochem. Medica*, vol. 24, no. 1, pp. 12–18, 2014.
[189] N. Liu, R. Fougere, M.-W. Zhou, M. K. Nigro, and a V Krassioukov, “Autonomic dysreflexia severity during urodynamics and cystoscopy in individuals with spinal cord injury.,” *Spinal Cord*, vol. 51, no. 11, 2013.
[190] D. P. Kingma and J. L. Ba, “Adam: A method for stochastic optimization,” in *3rd International Conference on Learning Representations, ICLR 2015 - Conference Track Proceedings*, 2015.
[191] L. Toloşi and T. Lengauer, “Classification with correlated features: Unreliability of feature ranking and solutions,” *Bioinformatics*, vol. 27, no. 14, pp. 1986–1994, Jul. 2011.
[192] B. Ellenbroek and J. Youn, “Rodent models in neuroscience research: Is it a rat race?,” *DMM Dis. Model. Mech.*, vol. 9, no. 10, pp. 1079–1087, 2016.
[193] A. Sgoifo *et al.*, “Social stress, autonomic neural activation, and cardiac activity in rats,” *Neurosci. Biobehav. Rev.*, vol. 23, no. 7, pp. 915–923, Nov. 1999.
[194] S. A. Doggrell and L. Brown, “Rat models of hypertension, cardiac hypertrophy and failure,” *Cardiovascular Research*, vol. 39, no. 1. Oxford Academic, pp. 89–105, 01-Jul-1998.
[195] M. J. Janse, T. Opthof, and A. G. Kléber, “Animal models of cardiac arrhythmias,” *Cardiovascular Research*, vol. 39, no. 1. Oxford Academic, pp. 165–177, 01-Jul-1998.
[196] P. Konopelski and M. Ufnal, “Electrocardiography in rats: a comparison to human.,” *Physiol. Res.*, vol. 65, no. 5, pp. 717–725, Nov. 2016.
[197] J. Malkoff, “Non-invasive blood pressure for mice and rats,” *Anim. Lab News, Kent Sci. Corp.*, pp. 1–12, 2005.
[198] C. R. E. F. Id, M. L. Ipl, and M. Library, “Telemetric Blood Pressure Monitoring in Conscious Rats,” vol. 1968, 2019.
[199] K. Kramer and L. B. Kinter, “Evaluation and applications of radiotelemetry in small laboratory animals,” in *Physiological Genomics*, 2003, vol. 13, pp. 197–205.
[200] H. Mongue-Din, A. Salmon, M. Y. Fiszman, and Y. Fromes, “Non-invasive restrained ECG recording in conscious small rodents: A new tool for cardiac electrical activity investigation,” *Pflugers Arch. Eur. J. Physiol.*, vol. 454, no. 1, pp. 165–171, Mar. 2007.

[201] K. Kramer, L. Kinter, B. P. Brockway, H. P. Voss, R. Remie, and B. L. M. Van Zutphen, "The Use of Radiotelemetry in Small Laboratory Animals: Recent Advances," *Contemp. Top. Lab. Anim. Sci.*, vol. 40, no. 1, pp. 8–16, 2001.
[202] E. Nalivaiko, "Animal models of psychogenic cardiovascular disorders: what we can learn from them and what we cannot," *Clin. Exp. Pharmacol. Physiol.*, vol. 38, no. 2, pp. 115–125, Feb. 2011.
[203] M. P. Leussis and V. J. Bolivar, "Habituation in rodents: A review of behavior, neurobiology, and genetics," *Neuroscience and Biobehavioral Reviews*, vol. 30, no. 7. Pergamon, pp. 1045–1064, 01-Jan-2006.
[204] V. T. Grigorean *et al.*, "Cardiac dysfunctions following spinal cord injury.," *Journal of medicine and life*. 2009.
[205] A. Daugherty, D. Rateri, L. Hong, and A. Balakrishnan, "Measuring blood pressure in mice using volume pressure recording, a tail-cuff method," *J. Vis. Exp.*, no. 27, May 2009.
[206] J. A. King *et al.*, "Procedure for minimizing stress for fMRI studies in conscious rats," *J. Neurosci. Methods*, vol. 148, no. 2, pp. 154–160, Oct. 2005.
[207] G. D. Gamaro *et al.*, "The effects of acute and repeated restraint stress on the nociceptive response in rats," *Physiol. Behav.*, vol. 63, no. 4, pp. 693–697, Feb. 1998.
[208] M. D. Reed, A. S. Pira, and M. Febo, "Behavioral effects of acclimatization to restraint protocol used for awake animal imaging," *J. Neurosci. Methods*, vol. 217, no. 1–2, pp. 63–66, Jul. 2013.
[209] J. B. G. Ramsey, L. M. Ramer, J. A. Inskip, N. Alan, M. S. Ramer, and A. V. Krassioukov, "Care of Rats with Complete High-Thoracic Spinal Cord Injury," *J. Neurotrauma*, vol. 27, no. 9, pp. 1709–1722, 2010.
[210] M. R. LaFollette, M. E. O'Haire, S. Cloutier, and B. N. Gaskill, "Practical rat tickling: Determining an efficient and effective dosage of heterospecific play," *Appl. Anim. Behav. Sci.*, 2018.
[211] M. Davis, D. S. Gendelman, M. D. Tischler, and P. M. Gendelman, "A primary acoustic startle circuit: lesion and stimulation studies.," *J. Neurosci.*, 1982.
[212] V. Baudrie, H. M. Tulen, J. Blanc, and J. L. Elghozi, "Autonomic components of the cardiovascular responses to an acoustic startle stimulus in rats," *J. Auton. Pharmacol.*, vol. 17, no. 5, pp. 303–309, Oct. 1997.
[213] L. Hantsoo, C. E. M. Golden, S. Kornfield, C. Grillon, and C. N. Epperson, "Startling Differences: Using the Acoustic Startle Response to Study Sex Differences and Neurosteroids in Affective Disorders," *Curr. Psychiatry Rep.*, vol. 20, no. 6, p. 40, Jun. 2018.
[214] B. J. Young and R. N. Leaton, "Fear potentiation of acoustic startle stimulus-evoked heart rate changes in rats," *Behav. Neurosci.*, 1994.
[215] R. Casto, T. Nguyen, and M. P. Printz, "Characterization of cardiovascular and behavioral responses to alerting stimuli in rats," *Am. J. Physiol. Integr. Comp. Physiol.*, 1989.
[216] J. B. G. Ramsey, L. M. Ramer, J. A. Inskip, N. Alan, M. S. Ramer, and A. V. Krassioukov, "Care of rats with complete high-thoracic spinal cord injury," *J. Neurotrauma*, vol. 27, no. 9, pp. 1709–1722, 2010.
[217] National Spinal Cord Injury Statistical Center (NSCISC), "Spinal Cord Injury Facts and Figures at a Glance," 2018.

[218] A. R. Blight, “Morphometric analysis of a model of spinal cord injury in guinea pigs, with behavioral evidence of delayed secondary pathology,” *J. Neurol. Sci.*, vol. 103, no. 2, pp. 156–171, Jun. 1991.
[219] R. Shi and R. B. Borgens, “Anatomical repair of nerve membranes in crushed mammalian spinal cord with polyethylene glycol,” *J. Neurocytol.*, vol. 29, no. 9, pp. 633–643, 2000.
[220] R. Shi and R. B. Borgens, “Acute Repair of Crushed Guinea Pig Spinal Cord by Polyethylene Glycol,” *J. Neurophysiol.*, vol. 81, no. 5, pp. 2406–2414, May 1999.
[221] E. Partida, E. Mironets, S. Hou, and V. J. Tom, “Cardiovascular dysfunction following spinal cord injury,” *Neural Regeneration Research*, vol. 11, no. 2. Editorial Board of Neural Regeneration Research, pp. 189–194, 01-Feb-2016.
[222] J. C. Furlan, F. Verocai, X. Palmares, and M. G. Fehlings, “Electrocardiographic abnormalities in the early stage following traumatic spinal cord injury,” *Spinal Cord*, vol. 54, no. 10, pp. 872–877, Oct. 2016.
[223] D. N. Mayorov, M. A. Adams, and A. V. Krassioukov, “Telemetric Blood Pressure Monitoring in Conscious Rats Before and After Compression Injury of Spinal Cord,” *J. Neurotrauma*, vol. 18, no. 7, pp. 727–736, Jul. 2002.
[224] S. M. O’ Mahony, M. Tramullas, P. Fitzgerald, and J. F. Cryan, “Rodent models of colorectal distension,” *Curr. Protoc. Neurosci.*, no. SUPPL.61, pp. 1–13, 2012.
[225] B. P. Grubb, “Pathophysiology and differential diagnosis of neurocardiogenic syncope.,” *Am. J. Cardiol.*, vol. 84, no. 8A, pp. 3Q-9Q, Oct. 1999.
[226] M. B. Ekland, A. V. Krassioukov, K. E. McBride, and S. L. Elliott, “Incidence of autonomic dysreflexia and silent autonomic dysreflexia in men with spinal cord injury undergoing sperm retrieval: implications for clinical practice.,” *J. Spinal Cord Med.*, vol. 31, no. 1, pp. 33–9, Jan. 2008.
[227] a K. Karlsson, “Autonomic dysreflexia.,” *Spinal Cord*, vol. 37, no. 6, pp. 383–91, Jun. 1999.
[228] Pallav Sengupta, “The Laboratory Rat : Relating its Age with Human’s,” *Int. J. Prev. Med.*, vol. 4, no. 6, pp. 624–630, 2013.
[229] P. Sengupta, “The laboratory rat: Relating its age with human’s,” *International Journal of Preventive Medicine*. 2013.
[230] S. Hou and A. G. Rabchevsky, “Autonomic consequences of spinal cord injury,” *Compr. Physiol.*, 2014.
[231] A. Krassioukov, D. E. Warburton, R. Teasell, and J. J. Eng, “A Systematic Review of the Management of Autonomic Dysreflexia After Spinal Cord Injury,” *Archives of Physical Medicine and Rehabilitation*, vol. 90, no. 4. pp. 682–695, 2009.
[232] T. Kusayama *et al.*, “Simultaneous noninvasive recording of electrocardiogram and skin sympathetic nerve activity (neuECG),” *Nat. Protoc.*, vol. 15, no. 5, pp. 1853–1877, May 2020.
[233] J. A. Armour, “Functional anatomy of intrathoracic neurons innervating the atria and ventricles,” *Hear. Rhythm*, vol. 7, no. 7, pp. 994–996, 2010.
[234] T. Taniguchi, M. Morimoto, Y. Taniguchi, M. Takasaka, and T. Totoki, “Cutaneous distribution of sympathetic postganglionic fibers from stellate ganglion: A retrograde axonal tracing study using wheat germ agglutinin conjugated with horseradish peroxidase,” *J. Anesth.*, 1994.
[235] A. K. Karlsson, “Autonomic dysfunction in spinal cord injury: Clinical presentation of symptoms and signs,” in *Progress in Brain Research*, 2005, vol. 152, pp. 1–8.

[236] N. Montano, R. Furlan, S. Guzzetti, R. M. Mcallen, and C. Julien, "Analysis of sympathetic Neural discharge in rats and humans," *Philos. Trans. R. Soc. A Math. Phys. Eng. Sci.*, vol. 367, no. 1892, pp. 1265–1282, Apr. 2009.
[237] A. Kumar *et al.*, "Skin sympathetic nerve activity as a biomarker for syncopal episodes during a tilt table test," *Hear. Rhythm*, vol. 17, pp. 804–812, 2020.
[238] F. Shaffer and J. P. Ginsberg, "An Overview of Heart Rate Variability Metrics and Norms," *Front. Public Heal.*, vol. 5, Sep. 2017.
[239] F. Shaffer, R. McCraty, and C. L. Zerr, "A healthy heart is not a metronome: an integrative review of the heart's anatomy and heart rate variability," *Front. Psychol.*, 2014.
[240] K. Umetani, D. H. Singer, R. McCraty, and M. Atkinson, "Twenty-four hour time domain heart rate variability and heart rate: Relations to age and gender over nine decades," *J. Am. Coll. Cardiol.*, 1998.
[241] D. Shanthi, G. Sahoo, and N. Saravanan, "Designing an artificial neural network model for the prediction of thrombo-embolic stroke," *Int. Journals Biometric Bioinforma.*, vol. 3, no. 1, pp. 10–18, 2009.
[242] T. J. Hirschauer, H. Adeli, and J. A. Buford, "Computer-aided diagnosis of Parkinson's disease using enhanced probabilistic neural network," *J. Med. Syst.*, vol. 39, no. 11, p. 179, 2015.
[243] E. S. Lee and M. C. Joo, "Prevalence of autonomic dysreflexia in patients with spinal cord injury above T6," *Biomed Res. Int.*, vol. 2017, 2017.
[244] H. Kumru, J. Vidal, M. Perez, P. Schestatsky, and J. Valls-Solé, "Sympathetic skin responses evoked by different stimuli modalities in spinal cord injury patients," *Neurorehabil. Neural Repair*, vol. 23, no. 6, pp. 553–558, 2009.
[245] M. E. Kiziltan, M. Sohtaoglu, A. Gunduz, M. Bozluolçay, and N. Uzun, "Somatosensory and auditory startle reflex in patients with stroke and spinal cord injury," *Clin. Neurophysiol.*, vol. 127, no. 3, p. e4, 2016.
[246] H. Kumru, J. Vidal, M. Kofler, J. Benito, A. Garcia, and J. Valls-Solé, "Exaggerated auditory startle responses in patients with spinal cord injury," *J. Neurol.*, vol. 255, no. 5, pp. 703–709, 2008.
[247] H. Topka, L. G. Cohen, R. A. Cole, and M. Hallett, "Reorganization of corticospinal pathways following spinal cord injury," *Neurology*, vol. 41, no. 8, p. 1276, 1991.
[248] D. Hallman and E. Lyskov, "Autonomic regulation in musculoskeletal pain," 2012.
[249] J. E. Jacob, A. Pniak, L. C. Weaver, and A. Brown, "Autonomic dysreflexia in a mouse model of spinal cord injury," *Neuroscience*, vol. 108, no. 4, pp. 687–693, 2001.
[250] D. N. Loy *et al.*, "Functional redundancy of ventral spinal locomotor pathways," *J. Neurosci.*, vol. 22, no. 1, pp. 315–323, 2002.
[251] A. A. Webb and G. D. Muir, "Course of motor recovery following ventrolateral spinal cord injury in the rat," *Behav. Brain Res.*, vol. 155, no. 1, pp. 55–65, 2004.
[252] J. Milligan, J. Lee, C. McMillan, and H. Klassen, "Autonomic dysreflexia: recognizing a common serious condition in patients with spinal cord injury.," *Can. Fam. physician Médecin Fam. Can.*, vol. 58, no. 8, pp. 831–5, Aug. 2012.
[253] D. Wan and A. V Krassioukov, "Life-threatening outcomes associated with autonomic dysreflexia: a clinical review.," *J. Spinal Cord Med.*, vol. 37, no. 1, pp. 2–10, 2014.

VITA

Shruthi Suresh

Weldon School of Biomedical Engineering, Purdue University

Education

B.Eng., Electrical Engineering, 2013, National University of Singapore, Singapore

M.S, Biomedical Engineering, 2017, Purdue University, West Lafayette, IN, US
Topic: A Physiological Telemetry System to Detect the Onset of Autonomic Dysreflexia in Individuals with Spinal Cord Injuries

PhD, Biomedical Engineering, 2020, Purdue University, West Lafayette, IN, US
Topic: Detection of Dysautonomia in Spinal Cord Injury through Non-invasive Multi-modal Sensing and Machine Learning

Research Interests

Quantified Self, Machine Learning, Assistive Technologies, Digital Signal Processing

PUBLICATIONS

Palaniappan, SM, **Suresh, S,** Haddad, J.M, & Duerstock, B. S. (2020). Adaptive Virtual Reality Exergame for Individualized Rehabilitation for Persons with Spinal Cord Injury. In Proceedings of the European Conference on Computer Vision (ECCV) Workshops.

Suresh, S., & Duerstock, B. S. (2020). Automated Detection of Symptomatic Autonomic Dysreflexia through Multimodal Sensing, In *IEEE Journal of Translational Engineering in Health and Medicine*

Suresh, S., Everett, T. H. , Li, J. , Walls E. K. , Duerstock, B.S. (2019). Sensing Sympathetic Activation Using Novel Non-Invasive Techniques in Rats. In *2019 IEEE Sensors*. (IEEE)

Suresh, S., & Duerstock, B. S. (2018). Optimal Feature Selection for the Detection of Autonomic Dysreflexia in Individuals with Tetraplegia. In *2018 IEEE International Symposium on Signal Processing and Information Technology (ISSPIT)* (pp. 480-485). IEEE.

Suresh, S.; Manda S., Marrero C., Jacob L. & Duerstock B. (2017). Multi-functional Wrist Orthotic with Universal Gesture Recognition System. In *Proceedings of the Rehabilitation Engineering Society of North America Annual Conference 2017*.

Suresh, S; Raftery, B.; Duerstock, B. (2017). Detection of Autonomic Dysreflexia in persons with Cervical Spinal Cord Injuries through a Support Vector Machine. In *Proceedings of the Rehabilitation Engineering Society of North America Annual Conference 2017*.

Suresh S., Raftery B. & Duerstock B. (2016)**.** Wearable Physiological Telemetry for Individuals with Spinal Cord Injuries to Self-Monitor Secondary Health Complications. In *Proceedings of the Rehabilitation Engineering Society of North America Annual Conference 2016*.

Suresh S., Chiquito DFM., Manda S., Jacob L. & Duerstock B. (2016)**.** Motor Activated Multi-Functional Wrist Orthotic to Assist Individuals with Cervical Spinal Cord Injuries with Activities of Daily Living. In *Proceedings of the Rehabilitation Engineering Society of North America Annual Conference 2016*.

Suresh S., Duerstock H., & Duerstock B. (2015). Skin Resistance as a Physiological Indicator for Quadriplegics with Spinal Cord Injuries During Activities of Daily Living. In *Smart Health* (pp. 157-168). Springer International Publishing.

Suresh S, Liu Y, Yeow CH (2015). Development of a Wearable Electroencephalographic Device for Anxiety Monitoring. ASME Journal of Medical Devices.

Suresh, S, & Yeow, CH. (2014). Detection of anxiety through analysis of occipital EEG. In *Proceedings of the International Convention on Rehabilitation Engineering & Assistive Technology* (p. 3). Singapore Therapeutic, Assistive & Rehabilitative Technologies (START) Centre.

Cabibihan, J. J., Chauhan, S. S., & **Suresh, S**. (2014). Effects of the artificial skin's thickness on the subsurface pressure profiles of flat, curved, and Braille surfaces. *IEEE Sensors Journal*, *14*(7), 2118-2128.

APPENDIX A

Rat care post T2/T3 SCI: Things that can go wrong and how to fix it

Recommended antibiotic: Baytril (10mg/kg SC)

Recommended gavage max: 20ml/kg

Problem	Proposed Solution
Gastrointestinal failure	Remove Ketamine+ Xylazine from surgery protocol, use only isoflurane. K+X seems to have a combinatorial effect on the GI tract which led to several animals' untimely death.
Blood in urine	Will likely occur 2-4 days post-surgery. This is often due to hematuria which is common post-SCI. Usually clears up within first 6 days post-op. If doesn't clear out, make sure to check if it is a UTI- and if so, start antibiotic treatment.
Porphyrin around eyes and nose	Some porphyrin is expected around the eyes and nose due to painful surgery. If the porphyrin doesn't clear up and is showing signs of increasing, rat may be in pain. Would be good to check with vet, but can start antibiotics if there is no decrease within 7 days post-op.
Lethargy (excessive)	Some lethargy is common post-SCI, but if rat is not moving a lot, it is often the result of an infection/ other issue. Check to make sure the rat is hydrated. If the rat is also not eating and losing weight day 6 post-op, start antibiotics.
Inappetence (loss of appetite)	Weight loss will occur for the first 5-7 days post-op. If no weight gain or stabilization occurs, try bottle-feeding the rat Ensure. If the rat reaches > 10% weight loss, begin oral gavage of food to prevent further complications. This also likely occurs with excessive lethargy, so would be good to start antibiotics.
Continued weight loss past day 5 post-op	Start the antibiotics and gavaging on day 6 post-op. Can use a little bit of iso to knock them out a bit to help with gavage process.

Cold to touch	Place hand warmers under cage, immediately after observation of cold to touch. Often a sign of deterioration and needs immediate care- might be good to give lactate ringers and warm the animal as much as possible.
Skin doesn't snap back after being pinched.	This is usually a sign of dehydration- begin offering the rats more lactated ringers and saline. Increase frequency rather than amount.
Unable to feel a bladder for expression.	This happens once in a while, where the bladder is too small to express. Check the cage for wetness in the bedding. It's possible that the rat might have enough neural control for urinary function. If not, give ringers and check in a few hours. Worst case, it might be a burst bladder.
Eye turning cloudy	This has occurred in the first few animals SCI was performed on. Not sure why this occurred but can often lead to an infection. Apply some ophthalmic antibiotic for 3 days 2 times daily. If it doesn't clear out, reach out to vet- might need to be extracted.